

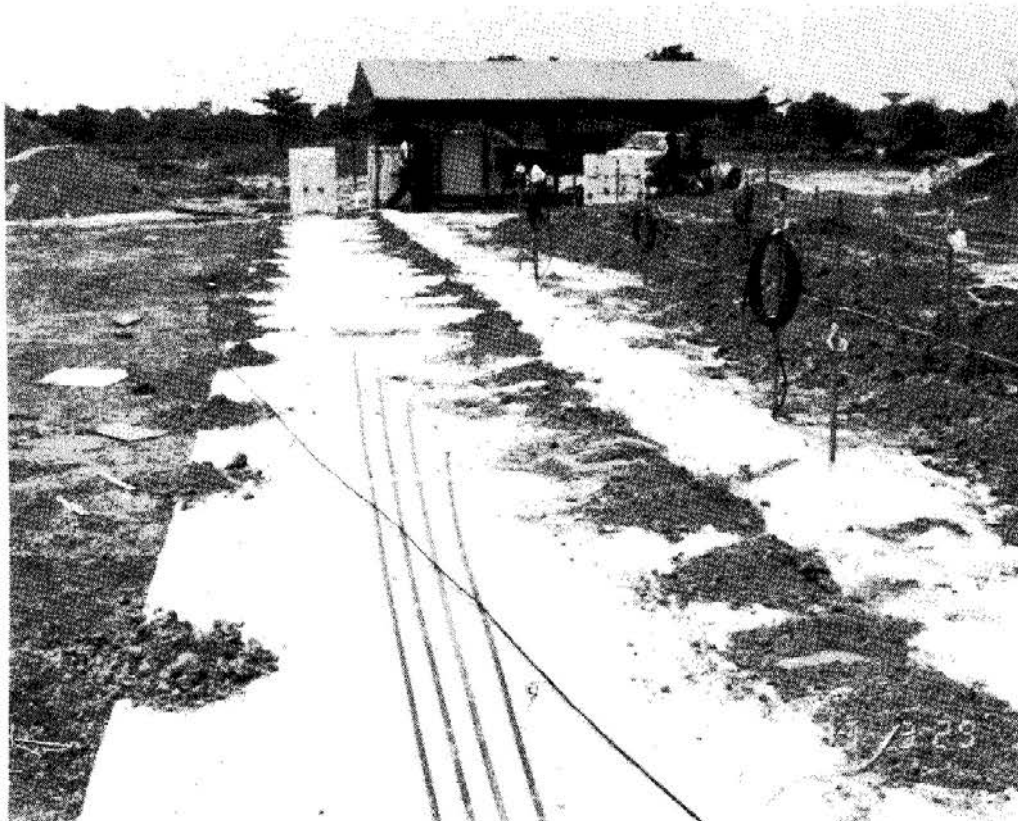
Volume 25    Number 1    June 1994

ISSN 0046-5828

# GEO TECHNICAL ENGINEERING

*Journal of*  
SOUTHEAST ASIAN GEOTECHNICAL SOCIETY

*Sponsored by*  
ASIAN INSTITUTE OF TECHNOLOGY



# GEOTECHNICAL ENGINEERING

## CONTENTS

### Photographic Feature:

<b>Laboratory Testing of Prefabricated Vertical Drains (PVD)</b> by D.T. BERGADO and A.S. BALASUBRAMANIAM .....	1
--	---

### Main Papers:

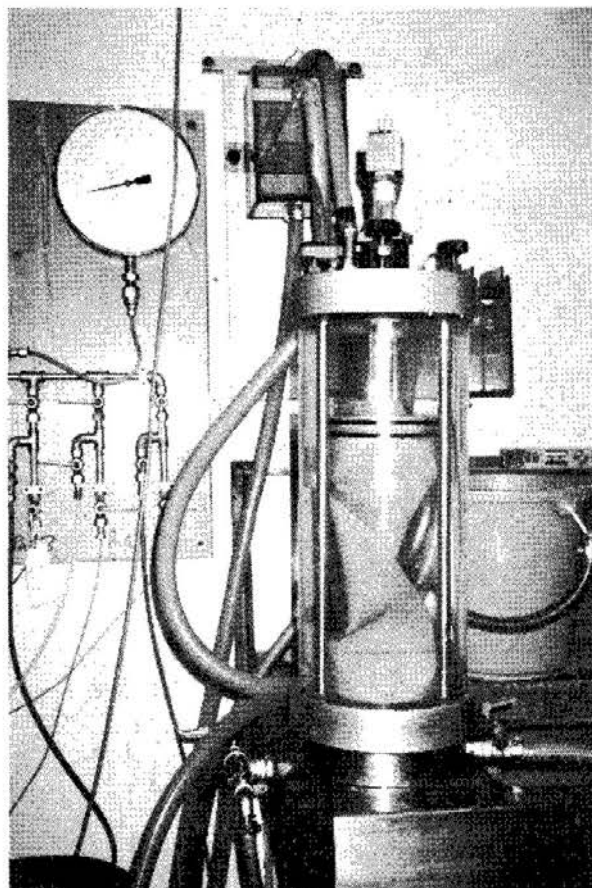
<b>Treatment of Expansive Soils to Control Swelling</b> by A.A. BASMA and M. AL-SHARIF .....	3
<b>A Parametric Study of the Bearing Capacity Equation</b> by N.S. PANDIAN, A. SRIDHARAN and U. SATHIDEVI .....	21
<b>Performance of Polypropylene-Strip-Reinforced Soil Retaining Structure</b> by Y.H. WANG and M.C. WANG .....	39
<b>Preliminary Groundwater Modelling of Mae Moh Lignite Mine in Thailand with Reference to Floor Heave</b> by Y. HONJO and P.H. GIAO .....	55
<b>Hyperbolic Method for Evaluation of Settlement of Ground Pretreated by Drains and Surcharge</b> by S.A. TAN .....	75
<b>Technical Note:</b>	
<b>Uniaxial Compressive Strengths of Marble from the Kuala Lumpur Limestone Abstracted and/or Indexed in Geotechnical Abstracts</b> by J.K. RAJ .....	91

**PHOTOGRAPHIC FEATURE**

**LABORATORY TESTING OF PREFABRICATED  
VERTICAL DRAINS (PVD)**

D.T. Bergado<sup>1</sup> and A.S. Balasubramaniam<sup>1</sup>

Due to the consolidation and the possible lateral movement in the subsoil, the PVD may be subjected up to 20% compression. To simulate the actual performance of PVD in the field, the PVD types were tested in straight, bent, twisted, and clamped conditions, in a modified triaxial test. In this test, the PVD is wrapped by rubber membrane surrounded by de-aired water under pressure as shown in the figure below. This apparatus together with other equipments are now available at the Soil Engineering Laboratory of A.I.T. Thus, A.I.T. is now capable of quality control and performance tests for PVD, geotextiles, and other geosynthetic materials.



---

<sup>1</sup>School of Civil Engineering, Asian Institute of Technology, P.O. Box 2754, Bangkok, Thailand

# TREATMENT OF EXPANSIVE SOILS TO CONTROL SWELLING

A.A. Basma<sup>1</sup> and M. Al-Sharif<sup>2</sup>

## SYNOPSIS

Swelling of expansive soils and the associated movement of foundations causes serious distress to many structures. With the existing expansive clays in Irbid, many buildings along with roads and highways have shown severe damage resulting in considerably higher maintenance costs. This paper reports the findings of an experimental investigation to reduce swelling properties of clays. Several stabilization techniques were assessed. These include compacting the soils at various water contents and unit weights, remolding the soils with different proportions of sand, lime and cement and finally using different proportions of salt in the pore fluid. The results of the study show that all the techniques are effective in reducing the expansive behavior of the tested soils to various degrees. However, lime addition and prewetting are best suited to improve swelling behavior whereas salt solution had relatively little effect.

## INTRODUCTION

Geotechnical engineers have long recognized that swelling of expansive soils caused by moisture variation may result in considerable distress and consequently in severe damage to overlying structures. In the past three decades or more many researchers have conducted extensive studies to assess soil properties that affect swelling. These studies provide helpful information which may be applicable to engineering practice. Furthermore, many investigators have proposed several techniques to reduce or even eliminate swelling of expansive clays (Basma and Tuncer, 1991; Chen, 1989; Kennedy et. al., 1989; Mowafy et. al., 1985).

Based on the information provided by earlier researchers (Tuncer et. al. 1990), the clays in Irbid (a city in Northern Jordan) are classified as medium to highly plastic expansive clay. Experimental investigations of the swelling properties of these clays were carried out by a number of researchers namely, the Royal Scientific Society (1982) and Abu El-sha'r (1986). The latter conducted an investigation to develop a rational approach for the design of light structures founded on the expansive clay in Irbid area. However, these studies were done on a very limited region in Irbid city and a small number of samples were used. Another more extensive investigation was

---

<sup>1</sup> Associate Professor, Department of Civil Engineering, Jordan University of Science and Technology, Irbid - Jordan.

<sup>2</sup> Assistant Professor, Department of Civil Engineering, Jordan University of Science and Technology, Irbid - Jordan.

carried out by a group of researchers from Jordan University of Science and Technology (Tuncer, et. al. 1990) to collect a more detailed information about the physical and geotechnical properties of Irbid expansive clays, based on a large number samples extracted from an area of ten square kilometers from the eastern part of Irbid, at various depths. However, this study did not suggest any possible solution(s) to the problem of expansion. Furthermore, this study did not investigate the effect of initial water content and unit weight of the soil on the swelling properties. The main objective of the aforementioned study was to quantify the swelling characteristics of selected Irbid soils, and, no technique to control swelling of this soil was suggested. Furthermore, no researcher has yet attempted to study possible method(s) of controlling the expansive problem in Irbid.

### **OBJECTIVES OF THE STUDY**

Due to the lack of information concerning methods to stabilize Irbid expansive clays, this study was carried. The specific objective of this study was to suggest alternative economic and practical techniques that can be used to reduce and control the swelling behavior of such clays. The techniques investigated are:

- (a) Remolding the expansive soil at different unit weights and water contents.
- (b) Mixing the expansive soil with various proportions of local sand to study the effect on the swelling potential.
- (c) Use of various salt concentrations of the pore fluid to show their effectiveness in reducing the overall swelling properties.
- (d) Mixing the expansive soil with different percentages of lime or cement to evaluate their effectiveness on the swelling characteristics.

Both undisturbed and remolded samples are utilized in this work. The samples were obtained from two boreholes selected from a group of eighteen boreholes drilled in the eastern part of Irbid. The reason for selecting these soils is discussed in a later section.

### **MECHANISM OF SWELL**

Swelling of clays takes place upon changing the environment of the expansive soil. Environmental changes consist of pressure release due to excavation, desiccation caused by temperature increase and volume increase associated with the introduction of water. However, the most important environmental factor which affects the swelling of expansive soils is water. With the introduction of water, volumetric expansion takes place. If pressure is applied to prevent swelling and to maintain the initial volume of the specimen, then this pressure is called the swelling pressure.

Generally speaking the swelling potential of an expansive clay can be minimized or even completely eliminated by several methods, such as, pre-wetting of the swelling soils to achieve high soil moisture content. Another method is the compaction control required to reach a certain decreased dry unit weight at which the swell

## *TREATMENT OF EXPANSIVE SOILS*

potential is minimum. Chemical methods of stabilization can also be used using lime, cement, fly ash, sodium chloride, calcium chloride, and phosphoric acid to stabilize expansive soils. Chemical stabilization methods are usually more effective than other methods. The final technique is the isolation of the expansive soil so that no moisture change occurs. This is usually achieved by using horizontal and vertical isolating systems to prevent moisture transfer from and into the expansive soil.

Engineers in Jordan and, in Irbid in particular, do not pay much attention to the treatment of expansive clays to control swelling potential. Rather they tend to overcome the swelling problem through structural design. However, many of the previously mentioned techniques to control swelling can be conducted on the expansive soils of Irbid using local materials which are available in large quantities and at reasonable prices in Jordan. These materials include sand, lime, cement, sodium chloride and others.

### **OVERVIEW OF IRBID SOILS**

Expensive clays are susceptible to volume change due to the variation of the moisture content. This usually results in considerable damage to overlying structures. In Irbid many incidents of structural damage have been reported in different locations. Generally speaking, the soil in Irbid is classified as medium to highly expansive clay consisting of superficial brown clays to a depth of about 3.0 meters followed by calcarious brown clay, calcarious red clay and red clay successively. These deposits are derived mainly from the weathering of marl, limestone and chert parent rocks. The superficial clay is laterally uniform in character and calcarious throughout with the percentage of calcium carbonate increasing with depth. This formation is typical for Jordanian clays.

Previous investigations of Irbid soil (Tuncer et. al. 1990) indicated that it consists of 50 to 80% clay, 10 to 45% silt, and 6 to 15% sand. About 80% of the clay fraction is smectite-illite, the rest is kaolinite. In General, Irbid clays have a Liquid Limit ranging from 65% to 85%, Plastic Limit from 25% to 40% and shrinkage limit from 10% to 25% with a specific gravity of about 2.67. The insitu moisture content at the surface varies from about 15% in summer to around 40% in winter. This moisture content variation is only found in the near surface (3 to 4 meters) soil as below 4 meters moisture content is constant. Consequently, the active expansive zone in Irbid ranges from 3 to 4 meters.

### **EXPERIMENTAL PROGRAM**

#### **Treatment Techniques Considered**

In selecting suitable techniques to reduce the swell properties, it was important to consider the availability of the material used, especially, in sufficient and economic quantities. As far as stabilization materials are concerned, the following are known to reduce swell and indeed are abundant in Jordan: lime, cement, salt, and sand.

Other economical methods such as compacting the soil at different dry unit weights and water content are also considered. All of these methods were found to reduce swelling of expansive clays by various degrees and, except in few cases, were found to be suitable.

### Selection of Spils For This Study

Due to the wide variation in the physical properties of Irbid soils and in order for the soil to be representative of the general formation of Irbid clays, a careful selection process was required. The criteria that the soils must satisfy to be selected for testing are:

- (a) The water content of the soils must cover the widest possible range.
- (b) The dry unit weight of the soil must also be the extremes,
- (c) The soil must have a clay content that is representative of the natural soil deposit in Irbid.

From the eighteen boreholes drilled (symbolized by BH) the two soils satisfying the above criteria were obtained from BH8 and BH22. Their location relative to Irbid city can be seen in Fig. 1. Furthermore, a general soil profile is provided for

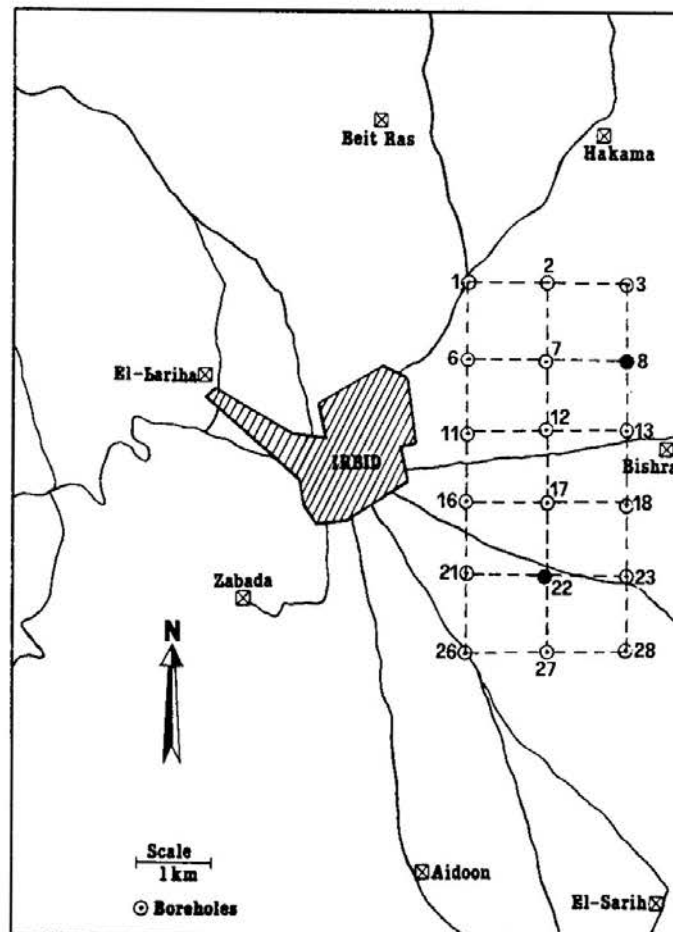
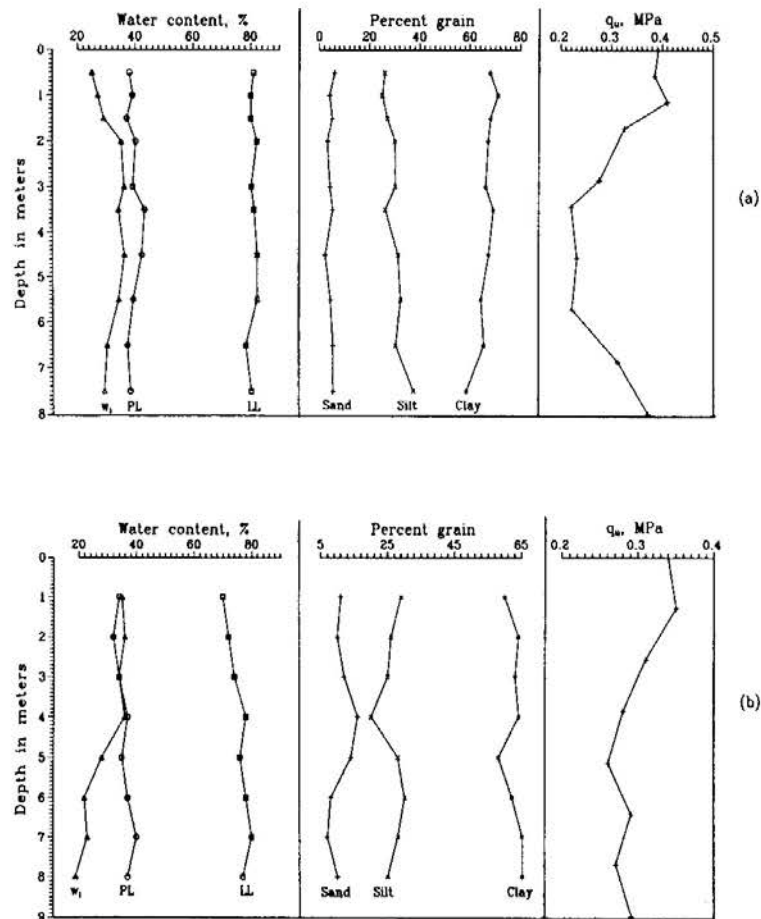


Fig. 1 Location of Investigated Site and Boreholes

## TREATMENT OF EXPANSIVE SOILS

both boreholes in Fig. 2. Fig. 3 presents the grain size distribution of the selected soils.

Before testing and in order to preserve the samples at their natural state at the time of boring, the selected specimens were tightly wrapped in aluminum foil and then placed in tightly sealed plastic bags. This was done to ensure that no moisture loss occurs.

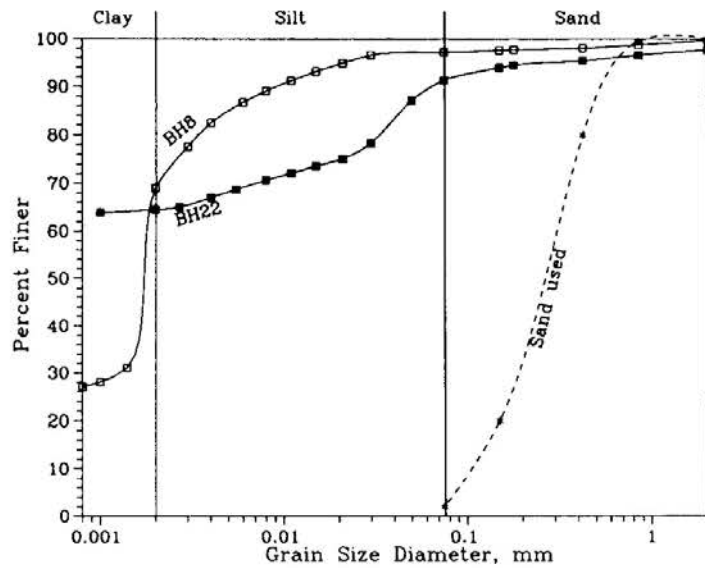


**Fig. 2 Results of Boring for a) BH8 and b) BH22**

### Physical Properties of Selected Soils

To assess the swelling behavior of the selected soils (BH8 and BH22), it was first necessary to evaluate their general physical properties such as consistency limits, specific gravity and the grain size characteristics. These properties were obtained by using the ASTM and AASHTO standard procedures. A summary of the physical properties of the soils is given in Table 1. Generally speaking, BH22 samples have higher dry unit weight and lower natural water content than BH8. In considering the consistency limits and using Casagrande's plasticity chart, the soils from both boreholes can be classified as inorganic clays or silts of high plasticity. This fact is very





**Fig. 3 Grain Size Distribution of Original Soils and Sand Used in Testing Program**

typical of Irbid clays. It should reiterated that these samples were selected to have different natural water content and dry unit weight in order to show the effect of these two important parameters on the different techniques used to control swelling.

### **Selection of Standard Conditions for Testing**

In order to compare the swelling behavior of the two selected soils under different conditions of stabilization, it is clearly necessary to compare the swelling potential and swelling pressure under some condition of placement and testing. It should not matter greatly what the selected conditions are so long as it is adopted and maintained throughout the testing program. However, it is desirable that the selected standard conditions be, to some extent, representative of the manner in which the soils might be compacted in engineering practice.

In general, compaction unit weights in the field vary widely depending on the purpose for which the soils are used. In airfield construction, for instance, the required degree of compaction is 100% based on the standard AASHTO compaction test. For highway subgrades, the degree of compaction ranges between 92% to 100%. Therefore, a degree of compaction,  $D_c$ , of 95% would be considered as a reasonable average for all tested specimens. Furthermore, and for maximum economy, placement would require that the soils be compacted at this unit weight at about the optimum water content. However, since these values ( $D_c = 95\%$  and optimum water content) were close to the natural state of the soils (Table 1), it was decided to compact the soils to their natural dry unit weight and water content. Finally, it could be noted that the swelling behavior of expensive soils is greatly affected by the initial surcharge pressure.

*TREATMENT OF EXPANSIVE SOILS*

**Table 1 Physical Properties of Tested Soils**

Property	Unit	Value for	
		BH8	BH22
Depth of sampling	m	3.5	7.0
Natural water content	%	33.8	19.2
Natural dry unit weight	kN/m <sup>3</sup>	15.0	18.0
Specific gravity	-	2.66	2.75
Initial void ratio	-	0.75	0.52
Percent sand	%	5.0	10.0
Percent silt	%	26.0	24.5
Percent clay	%	69.0	65.5
Liquid limit	%	80.5	77.3
Plastic limit	%	37.9	36.9
Plasticity index	%	42.6	40.4
Clay activity	-	0.62	0.62
Optimum water content	%	29.2	20.8
Maximum dry unit weight	kN/m <sup>3</sup>	14.2	14.5
Unconfined compressive strength	kPa	218.7	289.4
Undrained cohesion	kPa	73.6	24.5
Undrained angle of internal friction	degrees	15.0	34.2
Overconsolidation ratio	-	4.9	1.7
Soil Classification	-	CH	CH

In the field this will vary widely. Consequently, no single value could be considered as representative of all conditions. Generally speaking, many researchers consider a surcharge load of 1-psi (6.9 kPa) as a representative value for soils used in highway construction. For the purposes of this work, however, and because the soils used herein are highly over-consolidated with the overconsolidation ratio ranging from 10-40 at about 1 to 2 meters below the surface, this load was considered very low. Consequently, an alternative surcharge was sought. The most reasonable value in this case would be the effective stress. At 1 to 2 below the surface, the effective stress ranges from 15 to 30 kPa. Thus, as a representative value, a 25 kPa initial seating load was selected for the testing program.

**Samples Preparation for Swell Test**

To maintain accuracy in the results great care was taken in preparing the soil samples. For undisturbed specimens, a section of the soil about 50 mm thick was cut from the cylindrical soil sample using a sharp knife then trimmed to fit the cutting ring having diameter of 76 mm. Both the top and bottom of the soil was then leveled to bring it flush with the cutting ring and, therefore, a constant initial volume is maintained.

The preparation of remolded sample needed the construction of a special mold arrangement. The basic units for this mold were the consolidation cell (including the ring) and an upper piston of mild steel. To prepare remolded samples, the soil was first cut into small pieces and air dried for twenty four hours, then it was pulverized using a plastic hammer. The soil was then placed in the oven at 105°C for twenty four hours. The dry soil was further pulverized to very small pieces. At this stage the soil is ready for remolding.

The remolding procedure for each method is as follows:

- (a) Remolding at different water contents: An amount of soil required for a specific dry unit weight, was first weighed and the water needed for a specific water content was also weighed. The soil and water were mixed thoroughly till a homogeneous mixture was achieved. The wet soil was then placed into the mold and compacted to exactly fit the cutting ring. At this stage the mold was dismantled and the remolded specimen was extracted.
- (b) Remolding at various dry unit weights: An amount of soil required for each selected dry unit weight was weighed and the water needed for the natural water content was added to the dry soil. The procedure was then continued as in (a).
- (c) Remolding with various proportions of sand, lime or cement: A specific weight of additive required for a predetermined percentage of the dry weight of the soil was added to the dry soil. Water was then added to the mixture and the previous compaction procedure was carried out to produce specimens at the natural water content and dry unit weight.
- (d) Use of salt in the pore fluid: specimens are prepared in the same fashion as in (a) and (b) to give the natural water content and dry unit weight. The test is commenced by inundating the remolded samples with water containing a prescribed salt content.

All remolded specimens were left in a desiccator for 24 hours before testing. This process allowed the water to redistribute itself uniformly within the sample without any moisture loss.

## **General Description of Tests Performed**

### ***I-Swell Test***

This test was carried out on both remolded and undisturbed samples, using a standard one dimensional odometer. Samples were placed in the consolidation frame and an initial seating load creating a vertical stress of 25 kPa was applied. This load was maintained until full settlement was ensured. Samples were then fully saturated and allowed to swell under the seating load. Deformation readings were recorded at 0.1, 0.25, 0.5, 1.0, 2.0, 4.0, 8.0, 15.0, 30.0, 60.0, 120.0, and 1440.0 minutes. If appreciable deformation was still taking place, then readings were continued to 48 hours, 72 hours, etc. until full swell was ensured. The swell percent is, thus, defined as the ratio of the maximum deformation to the sample's initial height (20 mm).

## *TREATMENT OF EXPANSIVE SOILS*

The swell pressure was determined through carrying out the standard consolidation test on the swollen samples. Loads were added to create a vertical stress of 50, 100, 200, 400, 800, 1600, and 3200 kPa on the specimen. The equilibrium deformation of the sample was recorded for each stress level using the same time intervals as that for the swelling part of this test. The final deformation reading for each stress level was used to evaluate the void ratio at the end of each loading. The results were presented (not shown in this paper) in the form of a plot of the void ratio versus logarithm of stress. The swell pressure, in this case, is obtained from such a plot as the pressure required to bring the sample to its initial void ratio.

### ***II-Zero Swell Test***

Zero swell test was carried out on both undisturbed and remolded samples. Only one sample from each borehole was tested in order to compare the swell pressure data obtained by this method with that previously found in the swell test. Here samples were placed in the consolidation frame and a seating pressure of 25 kPa was applied, then samples were given excess water. Vertical deformation was prevented and the samples were kept at their initial void ratio by continuous addition of loads at every vertical expansion of the tested samples. Loads were applied using sand added to a plastic bag hanging off the loading arm. The addition of loads was continued until deformation ceased. The swell pressure is then calculated as the load required to maintain zero swell divided by the specimen area.

## **ANALYSIS OF RESULTS**

### **Results of Swell and Zero Swell Tests**

As indicated previously, both swell and zero swell tests were performed to determine the swell potential and swell pressure for both undisturbed and remolded. Table 2 lists the results for both BH8 and BH22. As can be seen, remolding of the soil has an effect on the results, especially for BH8. This could be related to the high plasticity of the soil from this borehole. Consequently, one may deduce that higher soil plasticity may indicate greater sensitivity to remolding as far as swelling is concerned. Additionally, results of the swell pressure obtained by the swell test are higher than that obtained by the zero swell test. This may be because after swelling has fully developed in the specimen a higher force is needed to expel water from the voids since low permeability is encountered. Furthermore, a new arrangement of soil particles is reached, and this might cause the increase in the swell pressure. For the purpose of this work, however, the swell test was used on remolded samples to determine both the swell potential and swell pressure for the following reasons:

- (a) The experimental data will be used for comparative purposes.
- (b) The swell percent and swell pressure can be obtained using a single remolded sample while two samples are needed for the same purpose when the zero swell test is performed.

**Table 2 Effect of Sample State and Testing Method on Results**

Soil	Swell Potential, %		Swell Pressure, kPa			
			Zero Swell Test		Swell Test	
	UD	RD*	UD	RD*	UD	RD*
BH8	9.34	4.68	325	192	1450	390
BH22	11.77	12.78	1538	1373	2700	2500

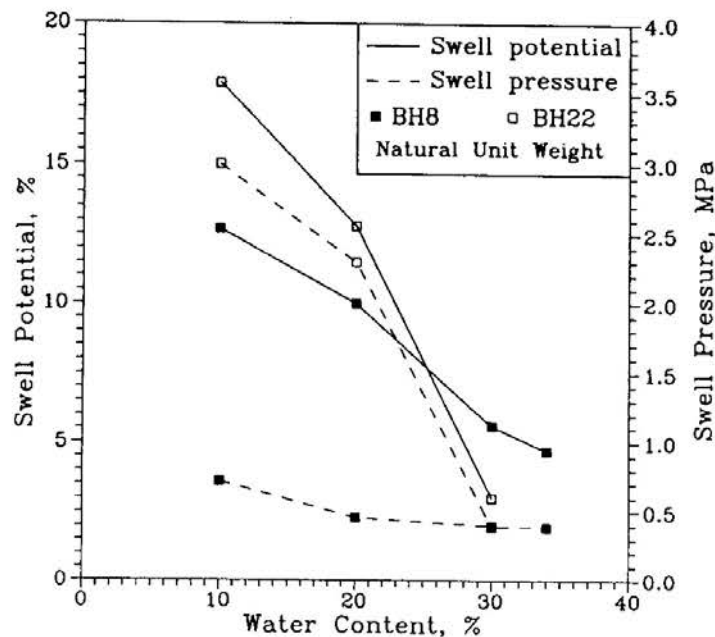
UD = Undisturbed samples; RD = Remolded samples

\*Note: Samples remolded at natural water content and unit weight.

**Effect of Stabilization Techniques on Swelling Behavior**

**Effect of Water Content Variation**

Specimens were prepared and compacted to their natural dry unit weight with varying water contents. Fig. 4 shows the effect of water content variation on the swell percent (solid lines) and swell pressure (dashed lines). For the two soils tested, it is clear that as the water content increases both swelling percent and pressure decrease. Furthermore, the curves developed for the two soils are descending nearly in the same manner with a rate of decrease in the swelling percent of BH22 slightly higher than that for BH8. This might be attributed to the fact that BH22 has a higher sand content, 10%, compared with 5% for BH8. Furthermore, the dry unit weight of soil from BH22 is higher than that of BH8 which in turn can be an important factor. For the swell pressure, on the other hand, BH22 shows a higher rate of decrease



**Fig. 4 Effect of Water Content on Swell Potential and Swell Pressure**

## TREATMENT OF EXPANSIVE SOILS

in swell pressure with increasing water content than BH8. This may be explained by the same reasons as before.

Fig. 4 shows that for an increase from 10% to 30% in water content, the soil from BH22 shows a swelling percent reduction from 17.87% to 3.15% and a swell pressure decrease from 3.0 MPa to 0.4 MPa. For BH8 the decrease is from 12.67% for swell percent, and from 0.75 MPa to 0.4 MPa for swell pressure for the same range of water content variation.

Komornik and David (1969) and, Mowafy and Bauer (1985) have reported similar behavior in expansive soil upon increasing their water content. However, their reported curves were linear in nature.

### Effect of Dry Unit Weight Variation

The samples from BH22 were remolded at the dry unit weights of 15, 17, 17.5 and 18 kN/m<sup>3</sup>, while BH8 samples were remolded at 13, 14, 15 and 15.2 kN/m<sup>3</sup>. All samples were remolded at their natural water content. A wider range of dry unit weights for soils from both boreholes was initially planned. However, it was difficult to remold and/or handle samples below the minimum or above the maximum selected values.

The variation of the swell percent with the dry unit weight are shown in Fig. 5 for both boreholes. The variation of swell pressure with dry unit weight is shown in the same figure. This figure illustrates that for both boreholes, the swelling percent and the swell pressure increase with an increase in the initial remolding dry unit weight of the specimen. For BH22 the rate of increase in the swelling percent and the

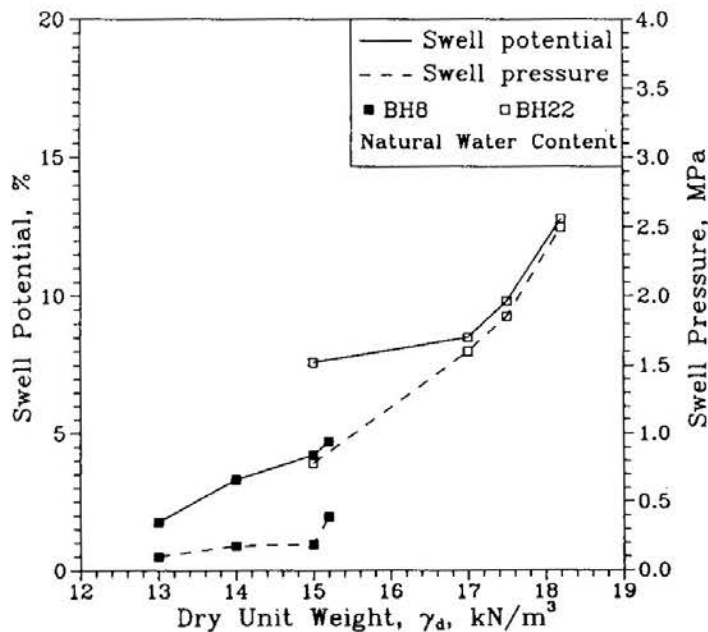
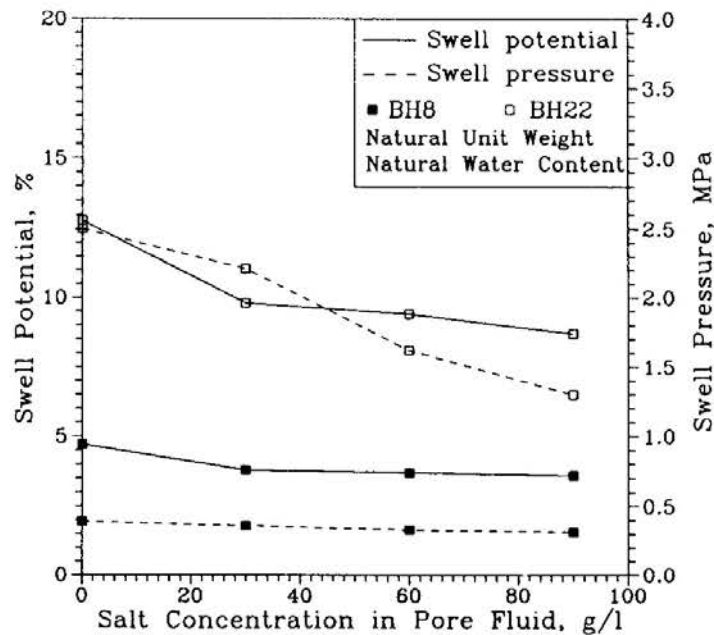


Fig. 5 Effect of Dry Unit Weight on Swell Potential and Swell Pressure



**Fig. 6 Effect of Salt in Pore Fluid on Swell Potential and Swell Pressure**

swell pressure was higher than that for BH8. However, it should be noted that the range over which the specimens were compacted was different for the two boreholes.

For BH22 an increase in the dry unit weight from 15 to 18 kN/m<sup>3</sup> resulted in an increase in the swelling percent from 7.62 to 12.77% and the swell pressure from 0.8 MPa to 2.5 MPa, respectively. For BH8, on the other hand, an increase from 13 to 15.2 kN/m<sup>3</sup> resulted in an increase from 1.74% to 4.68% for swell percent and from 0.1 to 0.4 MPa for swell pressure, respectively.

***Effect of Salt Concentration in Pore Fluid***

Remolded soil samples from both boreholes were flooded with water having salt concentrations of 3, 6, and 9% by wight of the water. The effect of salt concentration of the pore fluid on the swelling percent and the swell pressure are shown in Fig. 6. It can be seen from this figure that as the concentration of sodium chloride in the pore water increases, the swelling percent and the swelling pressure decrease for the same conditions of initial water content, initial dry unit weight, and clay content. However, the effect of salt concentration on the swelling properties tends to decrease beyond a certain value. For BH8 both swelling pressure and swelling percent tend to remain almost constant at 3.5% and 0.3 MPa, respectively, as the salt concentration varies from 6 to 9% whereas for BH22 these values appear to remain constant beyond a point slightly higher than 9%.

Mowafy et. al. (1985) suggested that the decrease of swell percent may be due to changes in the clay particles surfaces in the presence of a small concentration of electrolytes. The addition of sodium chloride produces a large amount of electrolytes

## TREATMENT OF EXPANSIVE SOILS

that precipitate in the colloids with the effect of rapidly flocculating them. The increase in the size of particles leads to a decrease in the total surface area, hence, the amount of absorbed water decreases and, in turn, swelling decreases. Furthermore, for calcium montmorillonite (such as the case with Irbid clays) treated with sodium chloride a cation exchange between the sodium and the calcium ions occurs while the chloride ions are absorbed between the sheets of montmorillonite forming calcium chloride. This prevents water from entering between the sheets and thus decreases the swelling ability.

### Effect of Lime and Cement Addition

Samples were remolded at their natural water contents and dry unit weights, with various proportions of lime or cement added to the dry soil. The percentages, by dry weight of the soil, used for stabilization were 3%, 6%, and 9% for both boreholes. After remolding, the samples were cured for 28 days at 20°C and 75% humidity.

Fig. 7 shows that for a variation of lime percent from 0% to 6% results in a decrease in swelling from 4.68% to zero and a reduction in swell pressure from 0.4 MPa to zero for BH8. For BH22 the variation is from 12.77% to 4.40% for swelling percent and from 2.5 MPa to 2.2 MPa for swell pressure for the same range of lime percent increase. The behavior of the soils in both boreholes is the same for the swelling percent and swell pressure versus lime percentage. In addition, there is a limiting value of the lime proportion added to the soil which will result in zero swell pressure.

The ability of lime to reduce swelling potential comes from its ability to reduce soil plasticity. The chemical reaction occurring between lime and soil is very complex.

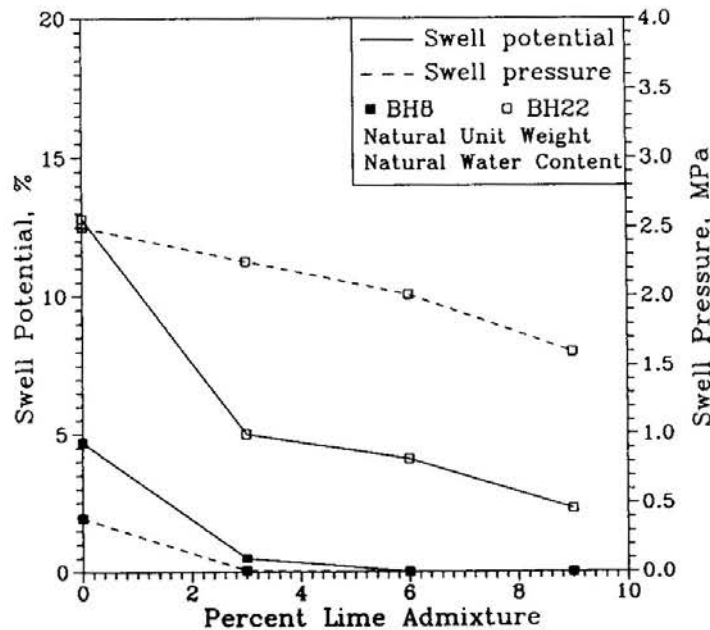


Fig. 7 Effect of Percent Lime Admixture on Swell Potential and Swell Pressure

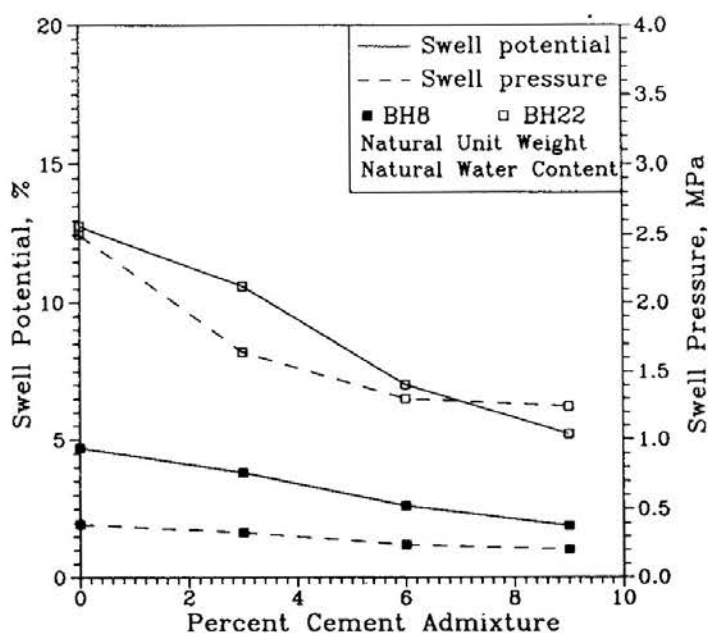


However, the stabilization process can be described as resulting mainly through two processes. In one process, a base exchange occurs with the strong calcium ions of the lime replacing the weaker ions such as sodium on the surface of the clay particles. Additional non-exchanged calcium ions may be adsorbed so that the total ion unit weight increases. The net result is a low base-exchange capacity for the particle with a resulting lower volume change potential. In the other process, a change of soil texture through flocculation of the clay particles takes place when lime is mixed with clays. As the concentration of lime is increased, there is an artificial reduction in clay content and a corresponding reduction in shrinkage and thus swell. Basma and Tuncer (1991) found that lime drastically reduces the plasticity index and raises the shrinkage limit on montmorillonitic clays.

Fig. 8 shows the effect of cement addition on both swell potential and swell pressure. As the cement content increases the swelling characteristics decrease. Such a reduction may be explained in a similar fashion as for lime. However, cement, in general, generates a greater pozzolanic effect. This effect transforms the soil into a more granular soil, thus, reducing the swelling behavior. In addition, the pozzolanic reaction caused by cement addition creates increased bonding between the clay layers. Such a bonding resists the swelling forces resulting in a more stable state. Kennedy et. al. (1987) and Basma and Al-Sulieman (1992) observed similar behavior. In general, though, for the tested soils, lime was more effective than cement in reducing swelling (compare values in Figs. 7 and 8).

**Effect of Sand Addition**

The effect of sand addition to the expansive soil was studied by mixing the soils with different proportions of local Swaileh sand (see grain size distribution in Fig. 1).



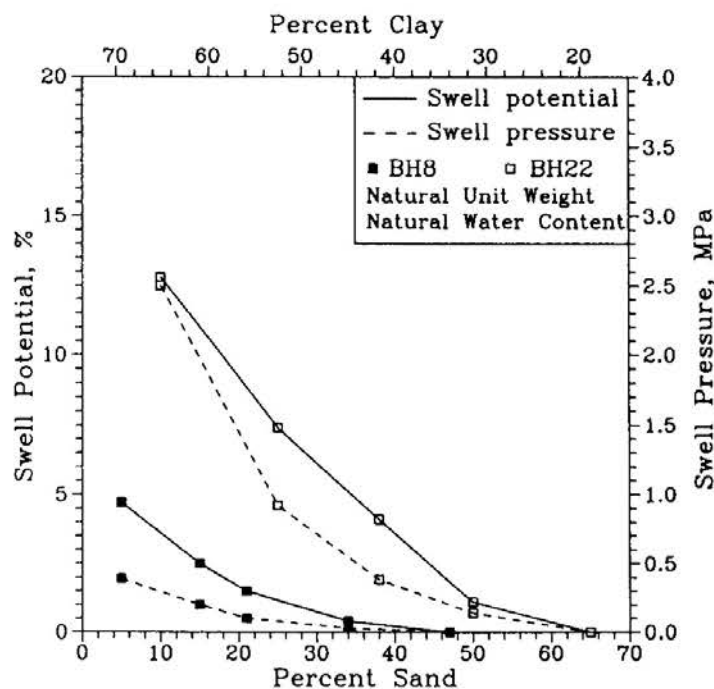
**Fig. 8 Effect of Percent Cement Admixture on Swell Potential and Swell Pressure**

## TREATMENT OF EXPANSIVE SOILS

Samples from BH8 were remolded in such a manner that they have sand contents of 15%, 21%, 34%, and 47% while BH22 samples were remolded having sand contents of 25%, 37.5%, 50%, and 65%. All samples were remolded at their natural water content and dry unit weight.

Fig. 9 shows the effect of sand addition to the swell-susceptible soils. Since a given sand percentage corresponds to a certain clay content value, then as the percent sand in the soil increases the clay content of that soil decreases. In this respect, Fig. 9 clearly demonstrates that the sand percent by dry weight of the soil and consequently, the corresponding clay content, has a great influence on the magnitude of both swelling percent and swell pressure. As the sand percentage increases, the swelling potential decreases. For BH8, an increase in sand percent from 15% to around 47% results in a decrease from 2.53% to zero percent whereas for BH22 an increase from 25% to 65% results in a decrease from 7.41% to a negative value (compression) of 0.26% for the swelling percent. Within the same range of sand percentage, the swell pressure decreased from 0.92 MPa to zero for BH8 and from 0.2 MPa to zero for BH22. This result indicates that for a given initial water content and dry unit weight, there is a sand contents beyond which the soil will not be susceptible to swelling. For BH8 the critical sand percent is around 47%, while for BH22 it is around 61%.

The effect of sand addition to the soil on the swelling properties is attributed to the larger capillary canals in the soil pores and the corresponding reduction in soil suction. Similar results were reported by Mowafy et. al. (1985).



**Fig. 9 Effect on Sand Percentage on Swell Potential and Swell Pressure**

## CONCLUSIONS

Tests were carried out on samples from two boreholes at different depths compacted at different dry unit weights and water contents and with various agents added to the soil or in the pore fluid. The following conclusions have been reached.

1. The particle size distribution indicates that the soils used were mostly composed of fine particles. Ninety to ninety five percent of the soil was in the silt to clay particle size range, with the clay fraction being the most dominant forming more than 70% of the fines.

2. The soils from both boreholes can be classified according to the Casagrande's plasticity chart as inorganic silts and clays with high plasticity. The high plasticity index and the high clay fraction of the soil indicated that they are highly expansive in nature. This was to some extent typical of Irbid clays.

3. The techniques used for controlling the swelling properties were: molding the soil at various water contents and dry unit weights, using different concentrations of salt in the pore fluid, increasing the proportions of sand content and, adding different lime and cement percentages to the dry soil. All techniques were found effective in reducing the swelling behavior of Irbid expansive soil to various degrees.

4. Initial water content of the soil has a great influence on the amount of both swelling and swelling pressure of the soil. The swelling properties are reduced drastically when increasing the initial compaction water content of the soils.

5. The dry unit weight of the specimen is a very important parameter affecting the swelling properties. It is evident from the results that a decrease in the initial dry unit weight of the specimen resulted in a decrease in the swelling properties of the tested soils.

6. It is clear that an increase in water content and decrease in dry unit weight means lower swell behavior. However, this usually results in a lower strength whereas the opposite means higher strength and higher swell. Therefore, one must select a water content and a dry unit weight for compaction purposes which will result in reasonable values for both strength and swelling.

7. The reduction of the clay content, i.e. the increase in the coarser fractions of the soil, resulted in the reduction in both the amount of swelling and swell pressure. This is achieved through increasing the proportion of sand in the soil samples.

8. The presence of salt in the pore fluid resulted in some reduction in the amount of swelling and swell pressure of the tested soils. However, it is also obvious that after reaching a certain salt concentration within the pore fluid, no reduction in the swelling characteristics is recorded.

9. The addition of lime or cement in small percentages (3% - 9%) of the dry weight of the soil resulted in a decrease in the swelling characteristics. However, lime

## TREATMENT OF EXPANSIVE SOILS

was found to be a better stabilizing agent than cement as far as swelling is concerned.

### ACKNOWLEDGEMENTS

This investigation was performed in the Soil Mechanics Laboratory of the Civil Engineering Department at Jordan University of Science and Technology (JUST). The authors are grateful for the generous financial support of the Deanship of Scientific Research at JUST without which this study would not have been a reality. Much thanks is extended to Ms. Nisreen Naji Ma'ya for typing this manuscript. The work herein is part of the second author's Thesis submitted in partial fulfillment for the degree of Masters of Science in Civil Engineering at JUST.

### REFERENCES

- ABU EL-SHA'R W. (1985). Analysis of Shallow Foundations on Expansive Clays of Irbid, Masters Thesis, Dept. of Civil Engineering, Yarmouk University, Irbid-Jordan (unpublished).
- BASMA, A. A. and TUNCER, E. R. (1991). "Effect of Lime on the Volume Change and Compressibility of Expansive Clays", Transportation Research Board, Washington, D.C., TRR No. 1296, pp. 54-61.
- BASMA A. A. and AL-SULEIMAN, T. (1992). "Economic Feasibility of Lime and Cement Stabilization of Jordanian Soil", *Proceeding of the Jordanian Civil Engineering Conference*, Jordan University, Amman-Jordan, June 1992.
- CHEN, F. H. (1989). Foundations on Expansive Clays, 2nd. Ed., Elsevier Science Publishers Company, Amsterdam.
- KENNEDY, T. W., SMITH, R., HOLMGREEN, R.J. and TAHMORESSI, M. (1987). "An Evaluation of Lime and Cement Stabilization", Transportation Research Board, Washington, D.C., TRR No. 1119, pp. 11-25.
- KOMORMIK, A. and DAVID, D. (1969). "Prediction of Swelling of Clays", *Journal of Soil Mechanics and Foundation Engineering*, ASCE, Vol. 1, No. 3, pp. 162-169.
- MOWAFY, Y. M. and BAUER, G. E. (1985), "Prediction of Swelling Pressure and Factors Affecting the Swelling Behavior of Expansive Soils", Transportation Research Board, Washington, D.C., TRR No. 1032, pp. 23-28.
- MOWAFY, Y. M., BAUER, G. E. and SAKEB, F. H. (1985). "Treatment of Expansive Soils", Transportation Research Board, Washington, D.C., TRR No. 1032, pp. 34-40.
- SALEM, A. and KATKUDA, I. (1982). Laboratory Investigation of Geotechnical Properties of Clay: Location No. 1 and 2, Irbid-Jordan, Technical Report, Building Research Center, Royal Scientific Society, November, 1982.
- TUNCER, E. R., BASMA, A. A. and TAQUIDDIN, S. (1990). Geotechnical Properties of Selected Irbid Soils, Jordan Univ. of Sci. and Tech., Report No. 14/87, June 1990 (Unpublished).

# A PARAMETRIC STUDY OF THE BEARING CAPACITY EQUATION

N.S. Pandian<sup>1</sup>, A. Sridharan<sup>2</sup> and U. Sathidevi<sup>3</sup>

## ABSTRACT

The most important aspect of foundation design is that the pressure on the soil due to the foundation should not exceed the allowable value. Bearing capacity and settlement are the two criteria which determine the allowable pressure on the soil. This paper aims to study the effect of various parameters such as cohesion, angle of internal friction, unit weight, depth of foundation and length to width ratio on bearing capacity as reflected by the bearing capacity equation and identifies the significant parameters affecting the same. It is shown that the bearing capacity can decrease, or decrease and then increase marginally, with width of foundation depending on the value of the angle of internal friction.

## INTRODUCTION

Foundations need to be designed such that the soil is capable of carrying loads without undergoing shear failure. The evaluation of the limiting shear resistance or ultimate bearing capacity forms the main part of computation in bearing capacity analysis. Based on a trial and error procedure the dimensions of the footings for various loading and soil conditions can be evaluated such that the resulting pressure on the soil due to the foundation is equal to the safe bearing capacity of the soil. A parametric study has been carried out to clarify the effect of various parameters on safe bearing capacity as given by the bearing capacity equation, highlighting the significant parameters affecting the same. A computer programme developed for this study is given in appendix 2.

## LITERATURE SURVEY

Bearing capacity computation methods which have been formulated by various investigators assume the soil to behave like an ideally plastic material. The significant ones among them for rigid foundation are Terzaghi (1943), Meyerhof (1953), Hansen (1970) and Vesic (1973).

According to Terzaghi, for a strip footing and for a general shear failure, for  $c$ ,  $\phi$  and  $\gamma \neq 0$ ,

---

<sup>1</sup> Assistant Professor, Department of Civil Engineering, Indian Institute of Science, Bangalore 560 012, India.

<sup>2</sup> Professor and Chairman, Division of Mechanical Sciences, Indian Institute of Science, Bangalore 560 012, India.

<sup>3</sup> Technical Manager/Civil, Neyveli Lignite corp. Ltd., C.T.O. Buildings, Neyveli 607 801, India.

$$Q_u = CN_c + q(N_q - 1) + 0.5B\gamma N_\gamma \quad (1)$$

and for local shear failure,

$$Q'_u = \frac{2}{3} CN'_c + q(N'_q - 1) + 0.5B\gamma N_\gamma \quad (2)$$

where, the values of  $N_c$ ,  $N_q$  and  $N_\gamma$  can be calculated using the following equations (Vesic, 1973),

$$N_q = e^{9.8 \tan \phi} \tan^2(45 + \phi/2) \quad (3)$$

$$N_c = (N_q - 1) \cot \phi \quad (4)$$

$$N_\gamma = 2(N_q + 1) \tan \phi \quad (5)$$

and  $N'_c$ ,  $N'_q$  and  $N'_\gamma$  are the modified bearing capacity factors obtained by using reduced value for .

The ultimate bearing capacity obtained from the above equation is to be modified to take into account the shape of the footing, depth of footing, inclination of load and effect of water table. Hence in the case of general shear failure,

$$Q_u = CN_c S_c d_c i_c + q(N_q - 1) S_q d_q i_q + 0.5B\gamma N_\gamma S_\gamma d_\gamma i_\gamma w' \quad (6)$$

*Shape factors* (Indian Standards (6403 - 1981) adopted those given by Hansen (1970)).

	$S_c$	$S_q$	$S_\gamma$
i) Continuous strip	1.0	1.0	1.0
ii) Rectangle.	$1 + \frac{0.2B}{L}$	$1 + \frac{0.2B}{L}$	$1 - \frac{0.2B}{L}$
iii) Square	1.3	1.2	0.8
iv) Circle	1.3	1.2	0.6

*Depth factors* (Meyerhof, 1953)

$$d_c = 1 + \frac{0.2D_f}{B} \tan(45 + \phi/2) \quad (7)$$

For  $\phi < 10^\circ$ ,

$$d_q = d_\gamma = 1 \quad (8)$$

For  $\phi < 10^\circ$ ,

$$d_q = d_\gamma = 1 + \frac{0.1D_f}{B} \tan(45 + \phi/2) \quad (9)$$

## PARAMETRIC STUDY

For local shear failure the parameters  $c$  and  $\phi$  are reduced as suggested by Terzaghi (1943) to  $2/3c$  and  $2/3 \tan \phi$ .

*Inclination factors* (Meyerhof, 1953)

The inclination factors shall be,

$$i_c = i_q = (1 - \alpha/90)^2 \quad (10)$$

$$i_\gamma = (1 - \alpha/\phi)^2 \quad (11)$$

$$q_u = M + N \frac{B_{\text{found.}}}{B_{\text{plate}}}$$

where  $\alpha$  is the inclination of the load with vertical in degrees.

The above equations are used in the present study.

### Effect of water table

If the water table remains at/or below the depth of  $(D_f + B)$ ,  $w' = 1$ . If it is located at a depth of  $D_f$  or above,  $w' = 0.5$ . When the water table is in between the above two,  $w'$  can be obtained by interpolation.

In this study it is assumed that the load is acting vertically and depth of water table is far below the footing level. There are a few other factors which affect the bearing capacity of soil such as base roughness, base tilt, slope of ground, presence of footings nearby but these are not taken into account in this study.

### Safe Bearing Capacity

The ultimate bearing capacity obtained has to be divided by a suitable factor of safety to obtain the safe bearing capacity. Factor of safety varies from 2 to 5 for cohesionless materials and from 3 to 5 for cohesive materials (Tomlinson, 1986). In this investigation a factor of safety of 3.0 has been used.

### Pressure Distribution Beneath Foundation

The contact pressure depends on the rigidity of the footing and the type of soil (Faber 1933, Skopek 1961). If the footing is flexible, the distribution of contact pressure is uniform irrespective of the type of soil. If the footing is rigid, the contact pressure distribution depends on the type of soil. Since the footings are neither completely flexible nor rigid, the actual contact pressure distribution is intermediate between that due to rigid and flexible conditions. However for practical purposes, it is usually assumed that the contact pressure distribution is uniform. In the present analysis it is also assumed to be uniform.

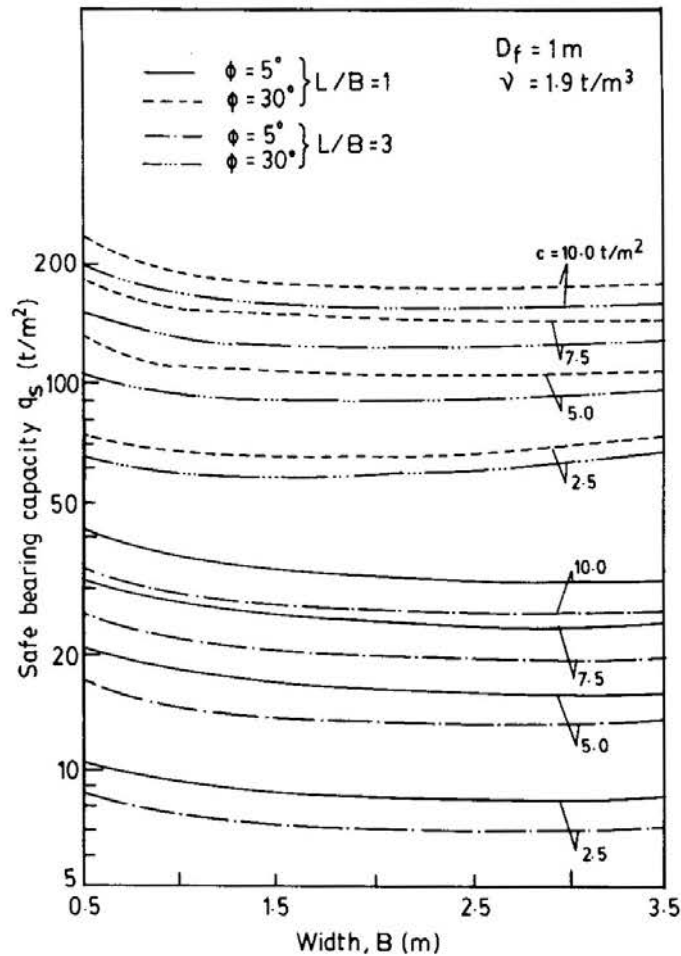
## PARAMETRIC STUDY

It is well known that the size ( $B$ ), shape ( $L/B$ ) and depth of foundations ( $D_f$ ) have great influence on the bearing capacity/allowable pressure of soil. In order to

study their influence on the economic design of foundations, a parametric study has been made of these factors.

**Effect of width of foundation (B) on safe bearing capacity**

Figure 1 shows the effect of B on the bearing capacity of soil according to Eq. 6. It can be seen that for cohesion, angle of internal friction, unit weight of soil, L/B and depth of foundation remaining unchanged, bearing capacity marginally decreases with increase in B up to a certain value of B, and then marginally increases with B. Table 1 reports the variation of each parameter involved in the computation of bearing capacity. It can be seen that though the value of B increases, values of  $S_c$ ,  $S_q$  and  $S$  remain constant for a given L/B ratio. But the value of  $d_c$  decreases with increase of B for a given depth of foundation. The values of  $d_q$  and  $d$  will be unity for values of  $\phi$  less than or equal to  $5^\circ$ . For higher values of  $\phi$ , the values of  $d_q$  and  $d$  also decrease with B. Hence when B increases, the net effect is either a decrease



**Fig. 1 Variation of  $q_s$  with B for Different Values of c.**



*PARAMETRIC STUDY*

**Table 1 Variation of  $q_s$  with B**

(a)  $\phi = 5^\circ$

For all the B values,  $d_q = 1$  and  $d_\gamma = 1$

B m	L/B = 1				L/B = 3	
	c = 2.5 t/m <sup>2</sup>		c = 10 t/m <sup>2</sup>		c = 2.5 t/m <sup>2</sup>	
	$d_c$	$q_s$ t/m <sup>2</sup>	$d_c$	$q_s$ t/m <sup>2</sup>	$d_c$	$q_s$ t/m <sup>2</sup>
0.50	1.44	10.59	1.44	40.89	1.44	8.73
1.00	1.22	9.11	1.22	34.81	1.22	7.54
1.50	1.15	8.66	1.15	32.82	1.15	7.18
2.00	1.11	8.46	1.11	31.86	1.11	7.03
2.50	1.09	8.36	1.09	31.30	1.09	6.97
3.00	1.07	8.32	1.07	30.95	1.07	6.94
3.50	1.06	8.30	1.06	30.71	1.06	6.94

(b)  $\phi = 30^\circ$

B m	L/B = 1				L/B = 3			
	c = 2.5 t/m <sup>2</sup>				c = 2.5 t/m <sup>2</sup>			
	$d_c$	$d_q$	$d_\gamma$	$q_s$ t/m <sup>2</sup>	$d_c$	$d_q$	$d_\gamma$	$q_s$ t/m <sup>2</sup>
0.50	1.69	1.35	1.35	76.96	1.69	1.35	1.35	65.37
1.00	1.35	1.17	1.17	66.19	1.35	1.17	1.17	57.12
1.50	1.23	1.12	1.12	64.49	1.23	1.12	1.12	56.42
2.00	1.17	1.09	1.09	65.06	1.17	1.09	1.09	57.61
2.50	1.14	1.07	1.07	66.54	1.14	1.07	1.07	59.55
3.00	1.12	1.06	1.06	68.47	1.12	1.06	1.06	61.87
3.50	1.10	1.05	1.05	70.66	1.10	1.05	1.05	64.41

or a decrease followed by an increase in bearing capacity. For example, in table 1, when  $c = 2.5\text{t/m}^2$  and  $\phi = 5^\circ$ , safe bearing capacity decreases as B increases from 0.5 m to 3.5 m. For values of  $c = 2.5\text{t/m}^2$  and  $\phi = 30^\circ$ ,  $q_s$  decreases from  $76.96\text{t/m}^2$  to  $64.49\text{t/m}^2$  as B increases from 0.5 m to 1.5 m and then starts increasing with increase of B. It is noted that when depth of foundation, L/B ratio and unit weight of soil remain constant, B is the only factor that leads to the increase in  $q_s$ . This is because, among the other parameters, the shape factors remain constant for a constant L/B ratio and the depth factors either remain constant or decrease with increase of B.

It is generally believed that bearing capacity increases with B especially in cohesionless soil. According to Bowles (1988),  $Q_u$  is independent of footing size in clayey soil, whereas in cohesionless as well as  $c - \phi$  soils all three terms of bearing capacity equation are applicable and recommends,

$$q_u = M + N \frac{B_{\text{found.}}}{B_{\text{plate}}} \quad (12)$$

where, M includes  $N_c$  and  $N_q$  terms and N is the  $N_\gamma$  term. Further Bowles (1988) recommends for sands,

$$q_u = q_{\text{plate}} \frac{B_{\text{found.}}}{B_{\text{plate}}} \quad (13)$$

where,  $q_{\text{plate}}$  is the value of bearing capacity obtained from a plate load test using a plate of size  $B_{\text{plate}}$  and  $q_u$  is that for the foundation of size  $B_{\text{found.}}$

According to Sowers (Leonards, 1962), a wide footing on a soil with a high angle of internal friction, such as gravel or sand, will have a very high bearing capacity, while a narrow footing on the same soil will have a much lower bearing capacity.

The above results and discussions, suggest the need to review bearing capacity values, that are based on model tests, being proportionately increased to arrive at the safe bearing capacity of prototype foundations.

### Effect of L/B on safe bearing capacity

Figure 2 reports the effect of L/B on bearing capacity of soil. Keeping constant the values for B,  $D_f$ ,  $\gamma$  and factor of safety, the safe bearing capacity has been determined for values of  $\phi = 5^\circ$  and  $30^\circ$  for different L/B ratios. As L/B increases bearing capacity decreases. This reduction is considerable when L/B changes from 1 to 2 and is in the range of approximately 15%. As L/B value changes from 2 to 7 the reduction in bearing capacity is about 6% only.

It can be seen from Table 2 that as L/B increases, the values of  $S_c$  and  $S_q$  decrease and the value of S increases. Since the values of B and  $D_f$  are kept constant, there will not be any change in the values of  $d_c$ ,  $d_q$  and  $d_\gamma$ . Hence the net effect is a reduction in bearing capacity.

### Combined effect of B and L/B

The combined effect of B and L/B is presented in Figure 3. Keeping the area of footing constant, width of footing has been varied necessitating a change in L/B also. The variation of safe bearing capacity with B as well as L/B is plotted in this figure. The footing areas considered are  $4\text{m}^2$  and  $16\text{m}^2$ . The values of B are chosen in such a

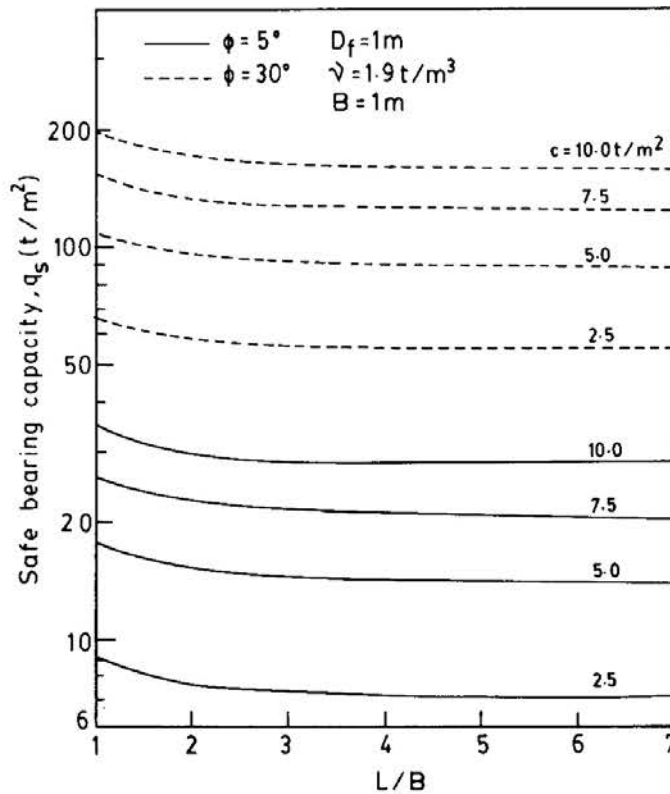
## PARAMETRIC STUDY

way that  $L/B$  lies between 1 and 16. For example when area is  $4\text{m}^2$ , the minimum value of  $B$  is taken as 0.5 m which corresponds to  $L/B$  of 16. The maximum value of  $B$  for area of  $4\text{m}^2$  is taken as 2m which corresponds to  $L/B$  value of 1.

From Table 3 it can be seen that as the value of  $B$  increases  $L/B$  decreases and hence the values of  $S_c$  and  $S_q$  increase. The value of  $S_\gamma$  decreases. It may be mentioned here that for square footings, the shape factor has been taken as 0.8. However, other investigators (Vesic, 1973) have recommended only 0.6. The shape factor  $S$  for rectangular foundation is given as  $1 - (0.4 B/L)$  which also reduces to 0.6 for a square footing. Since the depth of foundation is constant, as  $B$  increases,  $D_f/B$  decreases resulting in a decrease in the values of  $d_c$ ,  $d_q$  and  $d_\gamma$ . Hence the net effect is a decrease in bearing capacity with increase of  $B$  upto a certain value of  $B$  followed by an increase in bearing capacity. The decrease is about 10 to 15% for change of  $L/B$  value from 1 and 2.

### Effect of depth of foundation on safe bearing capacity

The variation of net bearing capacity with depth is shown in Figure 4. Bearing capacity increases with increase in depth. For increase of  $D_f$  from 1m to 4m, the increase in bearing capacity is about 55% when  $\phi = 5^\circ$  and is about 15 to 20% for increase of depth from 1m to 2m for all values of  $c$ . For higher values of friction angles, the increase in bearing capacity with depth is more significant.

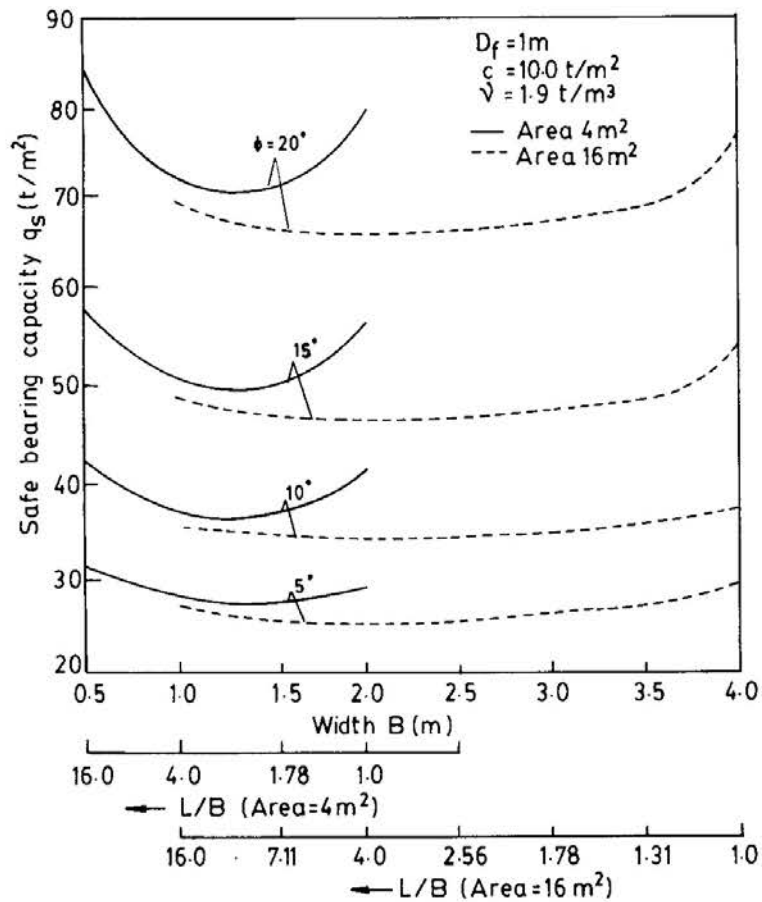


**Fig. 2** Variation of  $q_s$  with  $L/B$  for Different Values of  $c$ .

**Table 2 Variation of  $q_s$  with  $L/B$**

$L/B$	$S_c$	$S_q$	$S_\gamma$	$q_s$ ( $t/m^2$ )
(For $c = 2.5 t/m^2$ , $\phi = 5^\circ$ and $B = 1m$ ; $d_c = 1.22$ , $d_q = 1.0$ and $d_\gamma = 1.0$ )				
1.00	1.30	1.20	0.80	9.11
2.00	1.10	1.10	0.80	7.76
3.00	1.07	1.07	0.87	7.54
4.00	1.05	1.05	0.90	7.42
5.00	1.04	1.04	0.92	7.36
6.00	1.03	1.03	0.93	7.31
7.00	1.03	1.03	0.94	7.28
(For $c = 10 t/m^2$ , $\phi = 5^\circ$ and $B = 1m$ ; $d_c = 1.22$ , $d_q = 1.0$ and $d_\gamma = 1.0$ )				
1.00	1.30	1.20	0.80	34.81
2.00	1.10	1.10	0.80	29.50
3.00	1.07	1.07	0.87	28.62
4.00	1.05	1.05	0.90	28.18
5.00	1.04	1.04	0.92	27.92
6.00	1.03	1.03	0.93	27.74
7.00	1.03	1.03	0.94	27.62
(For $c = 2.5 t/m^2$ , $\phi = 30^\circ$ and $B = 1m$ ; $d_c = 1.35$ , $d_q = 1.17$ and $d_\gamma = 1.17$ )				
1.00	1.30	1.20	0.80	66.19
2.00	1.10	1.10	0.80	58.12
3.00	1.07	1.07	0.87	57.12
4.00	1.05	1.05	0.90	56.62
5.00	1.04	1.04	0.92	56.32
6.00	1.03	1.03	0.93	56.12
7.00	1.03	1.03	0.94	55.97
(For $c = 10.0 t/m^2$ , $\phi = 30^\circ$ and $B = 1m$ ; $d_c = 1.35$ , $d_q = 1.17$ and $d_\gamma = 1.17$ )				
1.00	1.30	1.20	0.80	198.17
2.00	1.10	1.10	0.80	169.81
3.00	1.07	1.07	0.87	165.42
4.00	1.05	1.05	0.90	163.22
5.00	1.04	1.04	0.92	161.91
6.00	1.03	1.03	0.93	161.03
7.00	1.03	1.03	0.94	160.40

## PARAMETRIC STUDY



**Fig. 3 Variation of  $q_s$  with  $B$  and  $L/B$  for Different Values of  $\phi$ .**

### Combined effect of $B$ and $D_f$ on safe bearing capacity

The combined effect of  $B$  and  $D_f$  or the effect of  $B/D_f$  presented in terms of modified bearing capacity factors is shown in Figure 5. According to Terzaghi, bearing capacity is proportional to  $B$ . As  $B$  increases bearing capacity increases irrespective of  $L/B$  and  $D_f$  (Eq.1.). The subsequent analyses take into account the effect of  $L/B$  and  $D_f$  on safe bearing capacity. Since Vesic's equations have been used in this investigation, the bearing capacity factors due to Vesic are modified using the depth factors and shape factors mentioned earlier. The modified bearing capacity factors are as follows.

$$N_{cc} = N_c S_c d_c \quad (14)$$

$$N_{qq} = N_q S_q d_q \quad (15)$$

$$N = N_\gamma S_\gamma d_\gamma \quad (16)$$

The modified bearing capacity factors for different values of  $B/D_f$  are plotted in fig. 5 for  $L/B$  values of 1 and 3. It can be seen that for a given value of  $L/B$ , the values of  $S_c$ ,  $S_q$  and  $S_\gamma$  remain same and hence the variations in the modified bearing capacity

Table 3 Variation of  $q_s$  with B for a Constant Area

B (m)	L/B	$S_c$	$S_q$	$S_\gamma$	$d_c$	$d_q$	$d_\gamma$	$q_s$ ( $t/m^2$ )
(Area = $4m^2$ , $c = 10 t/m^2$ , $\phi = 5^\circ$ )								
0.50	10.00	1.01	1.01	0.98	1.44	1.00	1.00	31.90
0.75	7.11	1.03	1.03	0.94	1.29	1.00	1.00	29.19
1.00	4.00	1.05	1.05	0.90	1.22	1.00	1.00	28.18
1.25	2.56	1.08	1.08	0.84	1.17	1.00	1.00	27.94
1.50	1.78	1.11	1.11	0.77	1.15	1.00	1.00	28.14
1.75	1.31	1.15	1.15	0.69	1.12	1.00	1.00	28.65
2.00	1.00	1.30	1.20	0.60	1.11	1.00	1.00	31.86
(Area = $4m^2$ , $c = 10 t/m^2$ , $\phi = 10^\circ$ )								
0.50	10.00	1.01	1.01	0.98	1.48	1.24	1.24	43.01
0.75	7.11	1.03	1.03	0.94	1.32	1.16	1.16	39.13
1.00	4.00	1.05	1.05	0.90	1.24	1.12	1.12	37.67
1.25	2.56	1.08	1.08	0.84	1.19	1.10	1.10	37.27
1.50	1.78	1.11	1.11	0.77	1.16	1.08	1.08	37.48
1.75	1.31	1.15	1.15	0.69	1.14	1.07	1.07	38.11
2.00	1.00	1.30	1.20	0.60	1.12	1.06	1.06	42.33
(Area = $4m^2$ , $c = 10 t/m^2$ , $\phi = 15^\circ$ )								
0.50	10.00	1.01	1.01	0.98	1.52	1.26	1.26	59.28
0.75	7.11	1.03	1.03	0.94	1.35	1.17	1.17	53.66
1.00	4.00	1.05	1.05	0.90	1.26	1.13	1.13	51.52
1.25	2.56	1.08	1.08	0.84	1.21	1.10	1.10	50.89
1.50	1.78	1.11	1.11	0.77	1.17	1.09	1.09	51.11
1.75	1.31	1.15	1.15	0.69	1.15	1.07	1.07	51.90
2.00	1.00	1.30	1.20	0.60	1.13	1.07	1.07	57.60
(Area = $16m^2$ , $c = 10 t/m^2$ , $\phi = 5^\circ$ )								
1.00	16.00	1.01	1.01	0.98	1.22	1.00	1.00	27.19
1.50	7.11	1.03	1.03	0.94	1.15	1.00	1.00	26.05
2.00	4.00	1.05	1.05	0.90	1.11	1.00	1.00	25.83
2.50	2.56	1.08	1.08	0.84	1.09	1.00	1.00	26.05
3.00	1.78	1.11	1.11	0.77	1.07	1.00	1.00	26.55
3.50	1.31	1.15	1.15	0.69	1.06	1.00	1.00	27.27
4.00	1.00	1.30	1.20	0.60	1.05	1.00	1.00	30.55
(Area = $16m^2$ , $c = 10 t/m^2$ , $\phi = 10^\circ$ )								
1.00	16.00	1.01	1.01	0.98	1.24	1.12	1.12	36.37
1.50	7.11	1.03	1.03	0.94	1.16	1.08	1.08	34.78

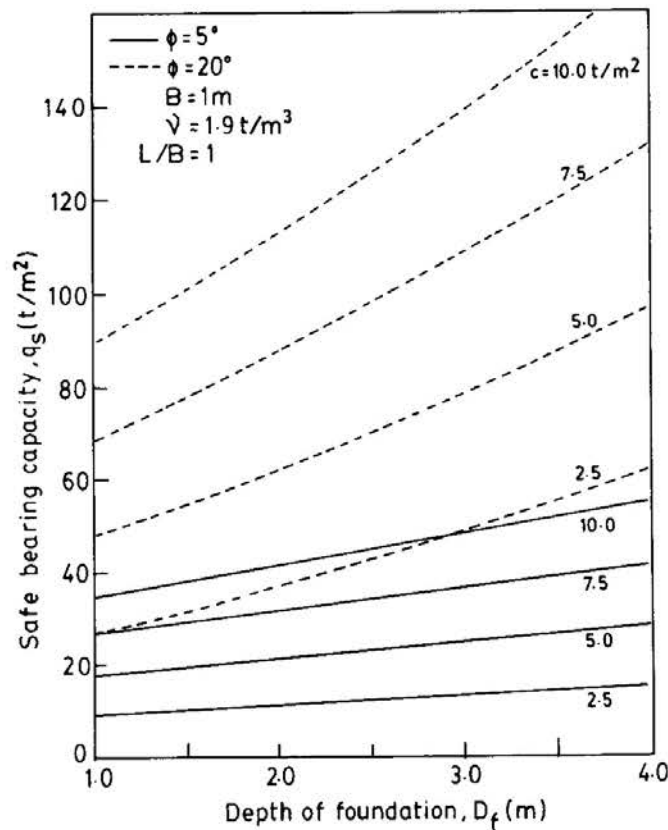
**PARAMETRIC STUDY**

**Table 3 Variation of  $q_s$  with B for a Constant Area (Cont.)**

B (m)	L/B	$S_c$	$S_q$	$S_\gamma$	$d_c$	$d_q$	$d_\gamma$	$q_s$ ( $t/m^2$ )
2.00	4.00	1.05	1.05	0.90	1.12	1.06	1.06	34.48
2.50	2.56	1.08	1.08	0.84	1.10	1.05	1.05	34.77
3.00	1.78	1.11	1.11	0.77	1.08	1.04	1.04	35.43
3.50	1.31	1.15	1.15	0.69	1.07	1.03	1.03	36.36
4.00	1.00	1.30	1.20	0.60	1.06	1.03	1.03	40.76

(Area =  $16m^2$ ,  $c = 10 t/m^2$ ,  $\phi = 15^\circ$ )

1.00	16.00	1.01	1.01	0.98	1.26	1.13	1.13	49.78
1.50	7.11	1.03	1.03	0.94	1.17	1.09	1.09	47.55
2.00	4.00	1.05	1.05	0.90	1.13	1.07	1.07	47.14
2.50	2.56	1.08	1.08	0.84	1.10	1.05	1.05	47.55
3.00	1.78	1.11	1.11	0.77	1.09	1.04	1.04	48.46
3.50	1.31	1.15	1.15	0.69	1.07	1.04	1.04	49.69
4.00	1.00	1.30	1.20	0.60	1.07	1.03	1.03	55.77



**Fig. 4 Variation of  $q_s$  with  $D_f$  for Different Values of  $c$ .**

factors depend on the values of only  $d_c$ ,  $d_q$  and  $d_\gamma$  which are dependent on the values of  $B/D_f$ . For values of  $\phi$  less than  $10^\circ$ , the values of  $d_q$  and  $d_\gamma$  are constant (eq. 8). For all other values of  $\phi$ , the values of  $d_c$ ,  $d_q$  and  $d_\gamma$  decrease with increase of  $B/D_f$ . The variation of modified bearing capacity factors for three values of  $\phi$ , namely,  $\phi = 0^\circ, 5^\circ$  and  $30^\circ$  are plotted in fig. 5 for  $L/B$  values of 1 and 3. It can be seen that the value of  $N_{cc}$  decreases with  $B/D_f$  for all values of  $\phi$  and  $L/B$ . The values of  $N_{qq}$  and  $N_{\gamma\gamma}$  are constant for  $\phi$  values of  $0^\circ$  and  $5^\circ$  and decrease with  $B/D_f$  when  $\phi = 30^\circ$ .

Table 4. shows the variation of modified bearing capacity factors as well as  $q_s$  with  $B/D_f$ . It can be seen that when  $c = 2.5 \text{ t/m}^2$ ,  $\phi = 5^\circ$  and  $L/B = 1$ , the value of  $N_{cc}$  decreases and  $N_{qq}$  and  $N_{\gamma\gamma}$  values remain constant with increase of  $B/D_f$ . As a result, the value of  $q_s$  decreases with increase in  $B/D_f$ . For higher values of  $\phi$ , say  $\phi = 30^\circ$  ( $c = 2.5 \text{ t/m}^2$  and  $L/B = 1$ ), even though the three modified bearing capacity factors decrease with  $B/D_f$ , the values of  $q_s$  decrease from  $116.09 \text{ t/m}^2$  (when  $B/D_f = 0.2$ ) to  $64.48 \text{ t/m}^2$  (when  $B/D_f = 1.6$ ) and then marginally increase. This

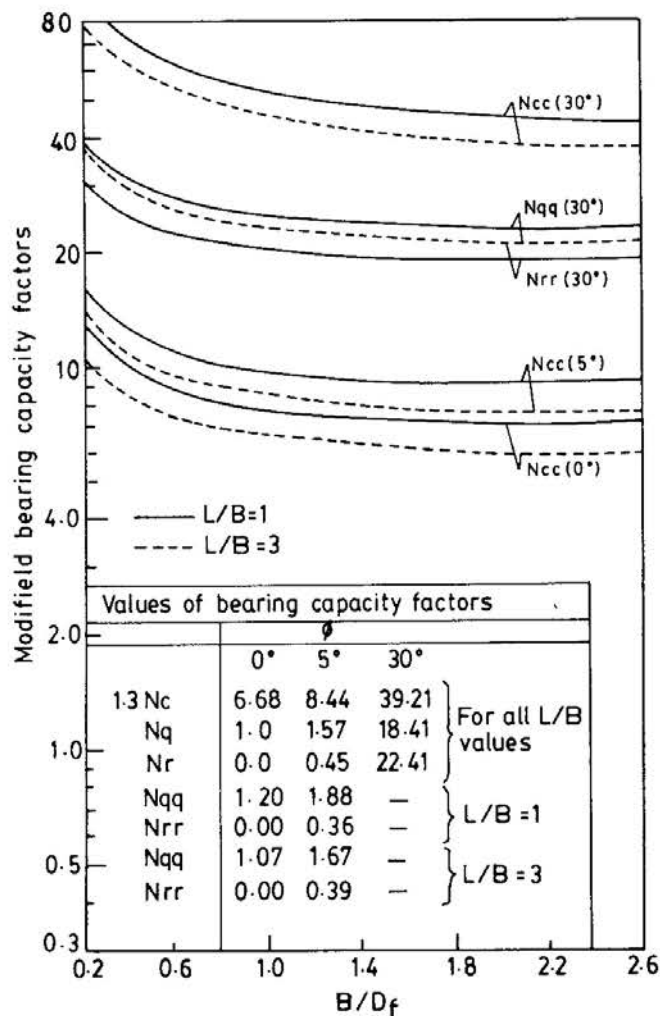


Fig. 5 Variation of Modified Bearing Capacity Factors with  $B/D_f$



## PARAMETRIC STUDY

marginal increase in  $q_s$  (even though all the modified bearing capacity factors decrease) is due to the higher values of  $N$  (compared to those at lower  $\phi$  values) contributing more by virtue of being multiplied by  $B$ .

### Effect of unit weight of soil on safe bearing capacity

The change in bearing capacity of soil with change in unit weight of soil is insignificant as shown in Table 5. For example, when  $c = 2.5 \text{ t/m}^2$ ,  $\phi = 5^\circ$ ,  $L/B = 1$ , the value of  $q_s$  is  $9.03 \text{ t/m}^2$  for a value of  $\gamma = 1.6 \text{ t/m}^3$ , it is  $9.08 \text{ t/m}^2$  for the value of  $\gamma = 1.80 \text{ t/m}^3$  and the value is  $9.14 \text{ t/m}^2$  when  $\gamma = 2.0 \text{ t/m}^3$ . Hence the effect of unit weight of soil can be taken as insignificant for the ranges normally met in practice.

## CONCLUDING REMARKS

The influence of various parameters like  $B$ ,  $L/B$ ,  $D_f$  and  $\phi$  on the safe bearing capacity of soil has been studied, and the following conclusions reacted.

1. For a given  $L/B$ ,  $B$  does not affect the safe bearing capacity ( $q_s$ ) significantly even in cohesionless soils. The decrease of safe bearing capacity is in the range of 10 to 20% for a change of  $B$  from 0.5 to 1.5 m. Beyond this there will not be much variation.

**Table 4 Variation of Modified Bearing Capacity Factors with B/D**

$B/D_f$	$N_{cc}$	$N_{qq}$	$N_{\gamma\gamma}$	$q_s \text{ (t/m}^2\text{)}$
$(c = 2.5 \text{ t/m}^2, \phi = 5^\circ, L/B = 1, N_c = 6.49, N_q = 1.57, N_\gamma = 0.45 \text{ and } D_f = 1\text{m})$				
0.20	17.65	1.88	0.36	15.16
0.40	13.04	1.88	0.36	11.35
0.60	11.51	1.88	0.36	10.09
0.80	10.74	1.88	0.36	9.47
1.00	10.28	1.88	0.36	9.11
1.20	9.97	1.88	0.36	8.88
1.40	9.75	1.88	0.36	8.72
1.60	9.59	1.88	0.36	8.60
1.80	9.46	1.88	0.36	8.52
2.00	9.36	1.88	0.36	8.46
2.20	9.28	1.88	0.36	8.41
2.40	9.21	1.88	0.36	8.38
2.60	9.15	1.88	0.36	8.35
$(c = 2.5 \text{ t/m}^2, \phi = 30^\circ, L/B = 1, N_c = 30.16, N_q = 18.41, N_\gamma = 22.40 \text{ and } D_f = 1\text{m})$				
0.20	107.13	41.23	33.44	116.09
0.40	73.17	31.67	25.68	83.19
0.60	61.85	28.48	23.09	72.99

**Table 4 Variation of Modified Bearing Capacity Factors with B/D (Cont.)**

B/D <sub>f</sub>	N <sub>cc</sub>	N <sub>qq</sub>	N <sub>γγ</sub>	q <sub>s</sub> (t/m <sup>2</sup> )
0.80	56.19	26.88	21.80	68.45
1.00	52.80	25.92	21.02	66.18
1.20	50.13	25.29	20.51	65.05
1.40	48.91	24.83	20.14	64.56
1.60	47.70	24.49	19.86	64.48
1.80	46.76	24.22	19.64	64.67
2.00	46.00	24.01	19.47	65.05
2.20	45.39	23.84	17.33	65.57
2.40	44.87	23.69	19.21	66.19
2.60	44.44	23.57	19.11	66.88
(c = 2.5 t/m <sup>2</sup> , φ = 5°, L/B = 3, N <sub>c</sub> = 6.49, N <sub>q</sub> = 1.57, N <sub>γ</sub> = 0.45 and D <sub>f</sub> = 1m)				
0.20	14.48	1.67	0.39	12.47
0.40	10.70	1.67	0.39	9.35
0.60	9.44	1.67	0.39	8.33
0.80	8.81	1.67	0.39	7.83
1.00	8.43	1.67	0.39	7.54
1.20	8.18	1.67	0.39	7.35
1.40	8.00	1.67	0.39	7.23
1.60	7.87	1.67	0.39	7.14
1.80	7.76	1.67	0.39	7.08
2.00	7.68	1.67	0.39	7.03
2.20	7.61	1.67	0.39	7.00
2.40	7.55	1.67	0.39	6.97
2.60	7.50	1.67	0.39	
(c = 2.5 t/m <sup>2</sup> , φ = 30°, L/B = 3, N <sub>c</sub> = 30.16, N <sub>q</sub> = 18.41, N <sub>γ</sub> = 22.40 and D <sub>f</sub> = 1m)				
0.20	87.90	36.65	36.23	97.50
0.40	60.04	28.15	27.82	70.41
0.60	50.75	25.31	25.02	62.21
0.80	46.11	23.89	23.62	58.72
1.00	43.32	23.04	22.78	57.11
1.20	41.46	22.48	22.22	56.46
1.40	40.13	22.07	21.82	56.34
1.60	39.14	21.77	21.51	56.56
1.80	38.37	21.53	21.28	57.00
2.00	37.75	21.34	21.09	57.60
2.20	37.24	21.19	20.94	58.31
2.40	36.82	21.06	20.81	59.11
2.60	36.46	20.95	20.71	59.98

*PARAMETRIC STUDY*

**Table 5 Variation of  $q_s$  with Unit Weight of Soil**

$t/m^2$	0	L/B	B m	$t/m^3$	$q_s$ $t/m^2$
2.5	5.0	1.0	1.00	1.60	9.03
2.5	5.0	1.0	1.00	1.70	9.05
2.5	5.0	1.0	1.00	1.80	9.08
2.5	5.0	1.0	1.00	1.90	9.11
2.5	5.0	1.0	1.00	2.00	9.14
2.5	5.0	1.0	2.00	1.60	8.35
2.5	5.0	1.0	2.00	1.70	8.39
2.5	5.0	1.0	2.00	1.80	8.42
2.5	5.0	1.0	2.00	1.90	8.46
2.5	5.0	1.0	2.00	2.00	8.49
2.5	5.0	1.0	3.00	1.60	8.19
2.5	5.0	1.0	3.00	1.70	8.24
2.5	5.0	1.0	3.00	1.80	8.28
2.5	5.0	1.0	3.00	1.90	8.32
2.5	5.0	1.0	3.00	2.00	8.36
10.0	5.0	1.0	1.00	1.60	34.73
10.0	5.0	1.0	1.00	1.70	34.75
10.0	5.0	1.0	1.00	1.80	34.78
10.0	5.0	1.0	1.00	1.90	34.81
10.0	5.0	1.0	1.00	2.00	34.84
10.0	5.0	1.0	2.00	1.60	31.75
10.0	5.0	1.0	2.00	1.70	31.79
10.0	5.0	1.0	2.00	1.80	31.82
10.0	5.0	1.0	2.00	1.90	31.86
10.0	5.0	1.0	2.00	2.00	31.89
10.0	5.0	1.0	3.00	1.60	30.82
10.0	5.0	1.0	3.00	1.70	30.87
10.0	5.0	1.0	3.00	1.80	30.91
10.0	5.0	1.0	3.00	1.90	30.95
10.0	5.0	1.0	3.00	2.00	30.99
10.0	30.0	1.0	1.00	1.60	194.67
10.0	30.0	1.0	1.00	1.70	195.83
10.0	30.0	1.0	1.00	1.80	197.00
10.0	30.0	1.0	1.00	1.90	198.17
10.0	30.0	1.0	1.00	2.00	199.34
10.0	30.0	1.0	2.00	1.60	175.84
10.0	30.0	1.0	2.00	1.70	177.25
10.0	30.0	1.0	2.00	1.80	178.65
10.0	30.0	1.0	2.00	1.90	180.06

**Table 5 Variation of  $q_s$  with Unit Weight of Soil (Cont.)**

$t/m^2$	0	L/B	B m	$t/m^3$	$q_s$ $t/m^2$
10.0	30.0	1.0	2.00	2.00	181.46
10.0	30.0	1.0	3.00	1.60	172.75
10.0	30.0	1.0	3.00	1.70	174.44
10.0	30.0	1.0	3.00	1.80	176.12
10.0	30.0	1.0	3.00	1.90	177.80
10.0	30.0	1.0	3.00	2.00	179.49

2. For a given B, the influence of L/B on  $q_s$  is marginal between L/B values of 1 and 2 and the reduction is in the range of 10 to 15%. Beyond this the bearing capacity is more or less same.

3. The depth of foundation,  $D_f$  has significant influence on  $q_s$ . For increase of  $D_f$  from 1m to 4m, the increase in bearing capacity is about 55% when  $\phi = 5^\circ$  and is about 15 to 20% for increase of depth from 1m to 2m for all values of c. For higher values of friction angles, the increase in bearing capacity with depth is more significant.

4. The unit weight of soil has negligible influence on  $q_s$ .

5. It is considered to be unsafe to assume that the safe bearing capacity increases with B. This highlights the need to review the interpretation of plate load test results for design purposes.

#### REFERENCES

- BOWLES, J.E. (1988). Foundation analysis and design, 4th edition, McGraw-Hill, Kogakusha Ltd., Tokyo.
- FABER, O. (1933). Pressure distribution under bases and stability of foundations, The Structural Engineer, Vol. 11, No. 3, p. 113.
- HANSEN, J.B. (1970). A revised and extended formula for bearing capacity, Danish Geotechnical Institute Bulletin No. 28, Copenhagen, pp. 21.
- INDIAN STANDARDS 6403-1981. Indian Standard Code of Practice for determination of bearing capacity of shallow foundations, ISI, New Delhi.
- LEONARDS, G.A. (1962). Foundation Engineering, McGraw-Hill Book Company Inc., New York.
- MEYERHOF, G.G. (1953). The bearing Capacity of Foundations under eccentric and inclined loads, 3rd ICSMFE, Vol - 1, pp. 440-445.

## PARAMETRIC STUDY

- SKOPEK, J. (1961). The influence of foundation depth on stress distribution, 5th ICSMFE., Vol. 1, p. 815.
- TERZAGHI, K. (1943). Theoretical soil mechanics, John Wiley and Sons, New York.
- TOMLINSON, M.J. (1986). Foundation design and construction, English Language Book Society, Longman.
- VESIC, A.S. (1973). Analysis of ultimate loads of shallow foundations, JSMFD, ASCE, Vol. 99, SM 1, pp. 45-73.

### APPENDIX 1

#### NOMENCLATURE USED

- B - Width of footing.
- $B_{\text{found}}$  - Width of foundation.
- $B_{\text{plate}}$  - Width of plate.
- c - Cohesion of soil.
- $c' = \frac{2}{3} c$  - Modified cohesion in case of local shear failure.
- D - Thickness of footing.
- $D_f$  - Depth of foundation.
- $d_c, d_q, d_\gamma$  - Depth factors.
- FS - Factor of safety.
- $i_c, i_q, i_\gamma$  - Inclination factors.
- L - Length of footing.
- M - Constant depending on the value of  $N_c$  and  $N_q$ .
- N - Constant depending on the value of  $N_\gamma$ .
- $N_c, N_q, N_\gamma$  - Bearing capacity factors.
- $N'_c, N'_q, N'_\gamma$  - Modified bearing capacity factors for local shear failure.
- q - Overburden due to soil.
- $q_s$  - Safe bearing capacity/allowable pressure based on both criteria.
- $q_u$  - Bearing capacity of foundation based on plate load test results.
- $Q_u$  - Ultimate bearing capacity of soil.
- $q_{\text{plate}}$  - Bearing capacity of plate as obtained from plate load test.
- $S_c, S_q, S_\gamma$  - Shape factors.
- $w'$  - Correction factor for water table.
- X - L/B ratio.
- Z - Depth at which the vertical stress due to foundation load is to be determined.
- $\gamma$  - Unit weight of soil.
- $\phi$  - Angle of internal friction of soil.
- $\phi'$  - Modified value of angle of internal friction given by  $\tan \phi' = \frac{2}{3} \tan \phi$ .
- $\alpha$  - Inclination of load with vertical.

APPENDIX 2 (PROGRAMME FOR PARAMETRIC STUDY)

```
C      DES36
      IMPLICIT REAL (M,N,L)
      OPEN (2, FILE = 'DS4.OUT')
      U = 1.9
C      DO 100 SF = 1, 3, 1
      DO 101 X = 1, 3, 2
      DO 101 A = 5, 30, 5
      DO 101 C = 2.5, 10, 7.5
        SF = 3
      DO 101 b1 = 0.5, 3.5, 0.5
c      DO 98 D = 1, 4, 1
      D = 1
      L1 = B1 *X
33      IF (X.EQ.1.0) GO TO 610
      T = 1.0
      GO TO 620
610     T = 2.0
620     B = A *3.1415927/180.0
      N1 = (45.0 + A/2.0) *3.1415927/180.0
      N2 = TAN (N1)
      N3 = TAN (B)
      N4 = 22.0 *N3/7.0
      NQ = N2**2* (EXP (N4))
      NC = (NQ - 1.0)/TAN (B)
      NR = 2.0* (NQ + 1.0) *TAN (B)
      IF (T.EQ.1) GO TO 80
      SC = 1.30
      SQ = 1.2
      SR = 0.80
      GO TO 110
80      SC = 1.0 + 0.2 *B1/L1
      SQ = SC
      SR = 1.0 - 0.4 *B1/L1
110     DC = 1.0 + (0.2 *D/B1) *TAN (N1)
      IF (A.LT.10.0) GO TO 40
      DQ = 1.0 + (0.1 *D/B1) *TAN (N1)
      GO TO 50
40      DQ = 1.0
50      DR = DQ
111     QU = C*NC*SC*DC + D*U* (NQ - 1.0) *SQ*DQ + B1
      *U*NR*SR*DR*0.5
      QS = QU/SF
      WRITE (2,257) C, A, X, nc, nq, nr, sc, sq, sr, dc, dq, dr, B1, qs
257     FORMAT (3f5.1, 3f6.2, 6f6.2, 2f6.2)
101     CONTINUE
100     CONTINUE
      STOP
      END
```

# PERFORMANCE OF POLYPROPYLENE-STRIP-REINFORCED SOIL RETAINING STRUCTURE

Y.H. Wang<sup>1</sup> and M.C. Wang<sup>2</sup>

## SYNOPSIS

The performance of polypropylene-strip-reinforced soil retaining structures was investigated through model testing. The model had 1.8 m width by 3.1 m length by 2.0 m height and contained five levels of reinforcing strips. Each strip was 15 mm wide by 1 mm thick by 2.5 m long and was spaced 40 cm vertically and 10 cm horizontally center-to-center. Two backfill materials -- a fine sand and a silty clay, each with two density levels, were investigated. The backfill surface carried either a uniform surcharge pressure or a strip pressure. Both weight-induced and surcharge-induced vertical pressure, lateral pressure, tensile strip force, and lateral facing deformation were measured and analyzed.

The results of the study show that there is little difference in performance between the polypropylene-strip-reinforced and the metal-strip-reinforced soil retaining structures. Under a uniform surcharge pressure over the entire backfill surface, the commonly adopted approach of replacing the surcharge pressure by an equivalent backfill height cannot provide correct vertical pressure, since the surcharge-induced vertical pressure decreases with depth as a rate faster in the looser state than in the denser state. To determine the vertical pressure induced by a finite-sized surcharge loading using the approximate method of spreading the loading out uniformly at a slope, e.g. 2(V): 1(H), it is reasonable to use the internal friction angle as the slope angle in order to take into consideration the effect of soil density. The surcharge-induced lateral earth pressure, tensile strip force, and lateral facing deformation decrease with depth. Also, they are greater when the backfill is looser, and are larger for the fine sand than for the silty clay backfill.

## INTRODUCTION

The various types of reinforcement which have been used in construction of reinforced soil retaining structures can be categorized into strip, rod, grid, and sheet reinforcements. The materials used in strip reinforcement are either metallic or synthetic. Of the two materials, metal strips have been used more widely and therefore considerable information on the performance of metal strip-reinforced soil structure is currently available (Jones, 1985 & 1991; Mitchell & Villet, 1987; Yamanouchi et. al. 1988). Although synthetic strip reinforcement has been adopted quite frequently in

---

<sup>1</sup> Associate Professor, Department of Civil Engineering, Changsha Railway Institute, Hunan, China; presently Visiting Scholar at Department of Civil and Environmental Engineering, The Pennsylvania State University, University Park, PA, U.S.A.

<sup>2</sup> Professor, Department of Civil and Environmental Engineering, The Pennsylvania State University, University Park, PA 16802, U.S.A.

other countries such as China, published information on the performance of such structures is very scarce.

In order to provide adequate bonding between the reinforcing strip and surrounding soil, cohesionless soils are generally required as the backfill material. As a result, a great majority of the available information on the performance of reinforced soil structures are for cohesionless backfills. For reasons of economy and material availability, cohesive soils have been used as backfills. Some performance data for reinforced cohesive backfills are available (Temporal et. al. 1989; Zornberg & Mitchell, 1992; Wang & Wang, 1993).

Reinforced soil retaining structures often support engineering structures such as highways (Wu, 1990; Wang et. al. 1990), bridge abutments (Juran et. al. 1978; McCaul & Snowdon, 1990), railroads (Kobayashi, 1980), and railroad station and warehouse (Hua et. al. 1991). Since surcharge loading may greatly influence the structure performance, information on surcharge loading effect are essential data base for sound structural design. The data base should involve surcharge effect on vertical pressure, lateral pressure, tensile strip force, and facing deformation. Available information on these matters are limited and scattered.

In an effort to provide some of the needed information, a study was undertaken using large scale model tests. The test models were constructed of polypropylene strips with cohesionless and cohesive backfills separately. The performance of the test models was monitored for both with and without a surcharge loading conditions. This paper presents the construction, instrumentation, measurements, analysis of test data, and engineering significance of the test results.

## TEST MODELS

Seven large scale models were constructed one at a time at the Changsha Railway Institute, China. Each model had dimensions of 2.0 m (height), 1.8 m (width), and 3.1 m (length). Of the seven models, a fine sand was used as the backfill material in five and a silty clay was used in two models. The silty clay had a liquid limit, plasticity index and classification of 30.6%, 10.4, and CL, respectively. The fine sand was somewhat well graded with a median size of about 0.2 mm and a classification of SW. Under the Standard Proctor compaction, the optimum water contents and maximum dry unit weights, respectively, are 16.5% and 17.9 KN/m<sup>3</sup> for the silty clay, and 9.5% and 18.7 KN/m<sup>3</sup> for the fine sand. Each backfill material was tested in two density levels -- 80% and 85% compaction for the silty clay, and 35.3% and 47.0% relative densities for the fine sand. The compaction water contents with dry unit weights for the low and high density levels are, respectively, 14.9% with 14.4 KN/m<sup>3</sup>, and 14.4% with 15.2 KN/m<sup>3</sup> for the silty clay; and 0.5% with 16.6 KN/m<sup>3</sup>, and 0.4% with 17.2 KN/m<sup>3</sup> for the fine sand. The moist unit weights are 16.5 and 17.4 KN/m<sup>3</sup> for the silty clay, and 16.7 and 17.3 KN/m<sup>3</sup> for the fine sand. The corresponding undrained internal friction angles are, respectively, 25.5° and 26.1° for the silty



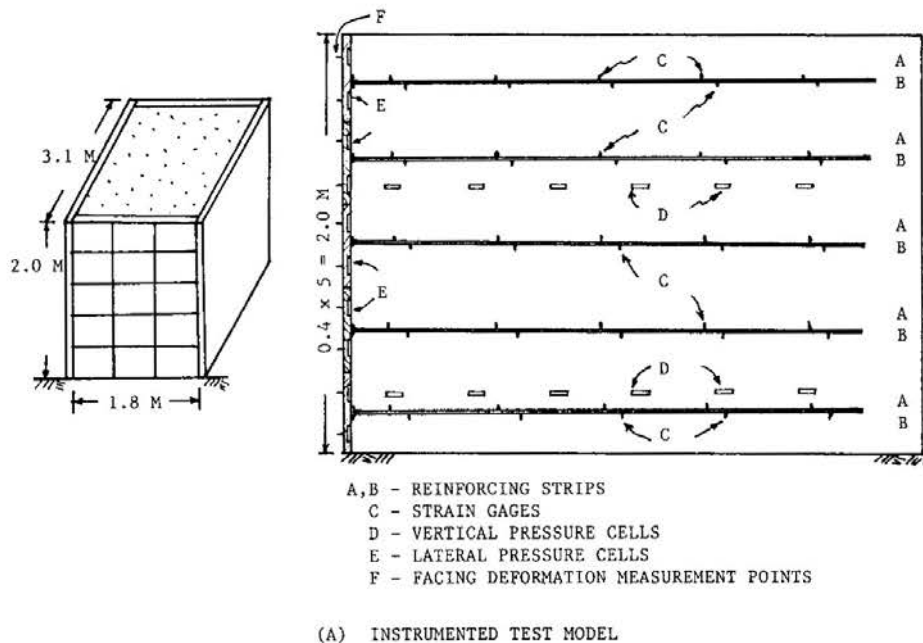
## POLYPROPYLENE-STRIP-REINFORCED SOIL

clay, and  $35.0^\circ$  and  $36.3^\circ$  for the fine sand. Meanwhile, the undrained cohesions of the silty clay are 15.6 and 16.0 kPa for the low and high density conditions, respectively.

The polypropylene reinforcing strip was 15.0 mm wide, 1.0 mm thick and 2.5 m long. The tensile strength, rupture strain, and tensile modulus were 2.39 KN/strip, 8.0% and 2000 MPa, respectively. The facing was constructed of plain concrete blocks with smooth mosaic back surface to minimize friction; each block was 60 cm long by 40 cm high by 5 cm thick. On the hind side of the concrete block were equipped with two U-shaped metal hooks, each about 5 cm wide, for tying the reinforcing strips. Each hook was located in the center of one-half of the block. There were three reinforcing strips tied onto each hook.

The entire test model was built on a concrete floor; there was no footer to support the facing. The backfill soil was deposited in lifts; each lift was approximately 10 cm thick after compaction. The backfill was compacted using an electrically operated vibratory compactor of about 140 N in weight which was either pushed or towed by hand in the direction parallel with the facing. The compaction started from the midsection, gradually moving away first then toward the facing; the process repeated until the desired density was achieved. Along the facing, the compaction was done by using a smaller hand-operated vibratory compactor. After compaction, the reinforcing strips were placed on top then followed by deposition of the subsequent lift. The center-to-center strip spacings were 10 cm horizontally and 40 cm vertically.

The model contained five levels of reinforcing elements as shown in Figure 1 (A), which presents the elevation and overall views of the test model. Also shown in



**Fig. 1 Laboratory Test Model and Instrumentation**

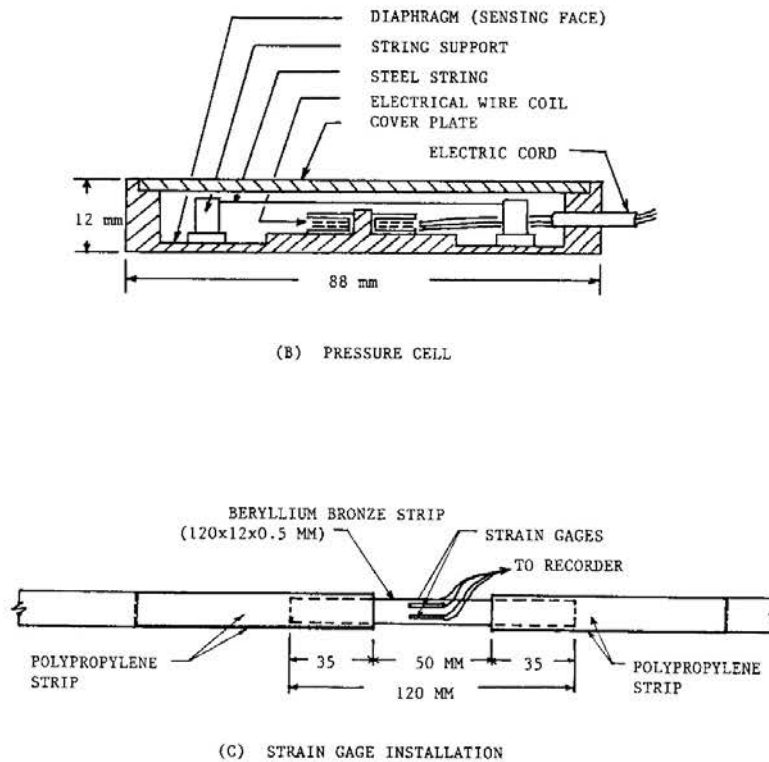


Fig. 1 (continued)

the figure are the locations of instrumentations. It should be noted below that to minimize possible boundary effects, all instruments were installed along the longitudinal center line of the test model. The instrumentations included pressure cells for measuring vertical and lateral pressures, and strain gages for measuring tensile strip force. Figure 1 (B) shows the cross-section of a pressure cell which had a diameter of 88 mm and a height of 12 mm. As shown, main components of the cell included a thin diaphragm, a fine steel string, and an electrical coil surrounding a steel core for generating magnetism to excite the string. Under pressure, the diaphragm deflected inward increasing the tensile stress in the string. Upon stressing, the natural frequency of the steel string varied. A readout unit was used to monitor the natural frequency which, in turn, was used to determine the pressure acting on the diaphragm. For vertical pressure measurements, the pressure cells were placed along the longitudinal center line of the model on two horizontal planes at depths of 0.9 and 1.9 m in the silty clay backfill, and at a depth of 1.7 m in the fine sand backfill. There were six pressure cells on each plane. For measurements of lateral pressures, the pressure cells were installed on the back side of the center line of the facing such that the sensing face of the cell was flush with the surface of the facing. There were a total of ten cells, two on each facing block.

The strain gages for tensile strip force measurements were installed on the reinforcing strip at the locations shown in Figure 1 (A). At each depth, there were two instrumented strips (labeled as A and B); all of the instrumented strips were located at the longitudinal center of the model. Details on the attachment of the strain gage

## *POLYPROPYLENE-STRIP-REINFORCED SOIL*

onto the reinforcing strip are given in Figure 1 (C). As seen, the strain gages were glued on a strip of beryllium bronze. Over the strain gage surface was sealed with a thin layer of wax and soft bond master. The beryllium bronze strip, 12.0 mm wide by 0.5 mm thick by 120.0 mm long, was an alloy containing 2.0% to 2.5% of beryllium and 97.5% to 98.0% of bronze. The 35 mm long segment at each end of the beryllium bronze strip was bonded on the polypropylene strip. On top of the 35 mm long segment was covered and bonded by another polypropylene strip to secure the beryllium bronze strip, leaving 50 mm long beryllium bronze strip exposed between two ends of the polypropylene strips. In the middle of this 50 mm long beryllium bronze strip were the strain gages.

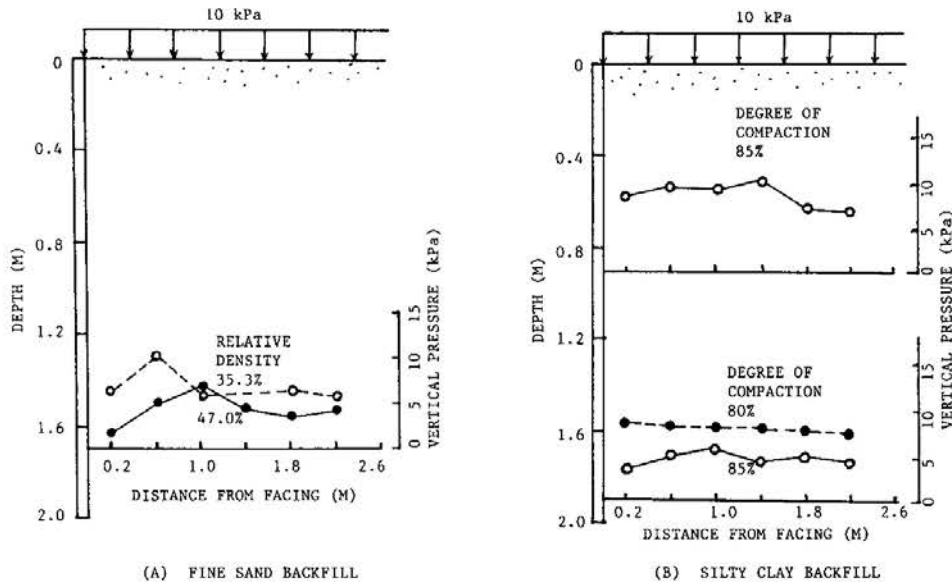
On the front face of the facing are shown the locations for measuring the lateral deformation of the facing. A total of ten measurement points along the center line of the facing, two on each facing block, are seen in Figure 1 (A). The measurements were made using an indium ruler and a transit. In measurement, the indium ruler having a 0.5 mm division was placed horizontally at the measuring points. The transit was located at a front corner, and a reference point was placed at the opposite corner of the test model. Both transit location and reference point were fixed on a line parallel with and at 10 cm in front of the facing. Based on the reference point position, the transit was used to take readings on the indium ruler.

The surcharge loading was applied by means of cast iron ingots of two different weights -- 50 N and 100 N. For uniform surcharge, these ingots were placed side by side covering the entire backfill surface. For strip loading, the ingots were placed within a desired width continuous in the facing direction.

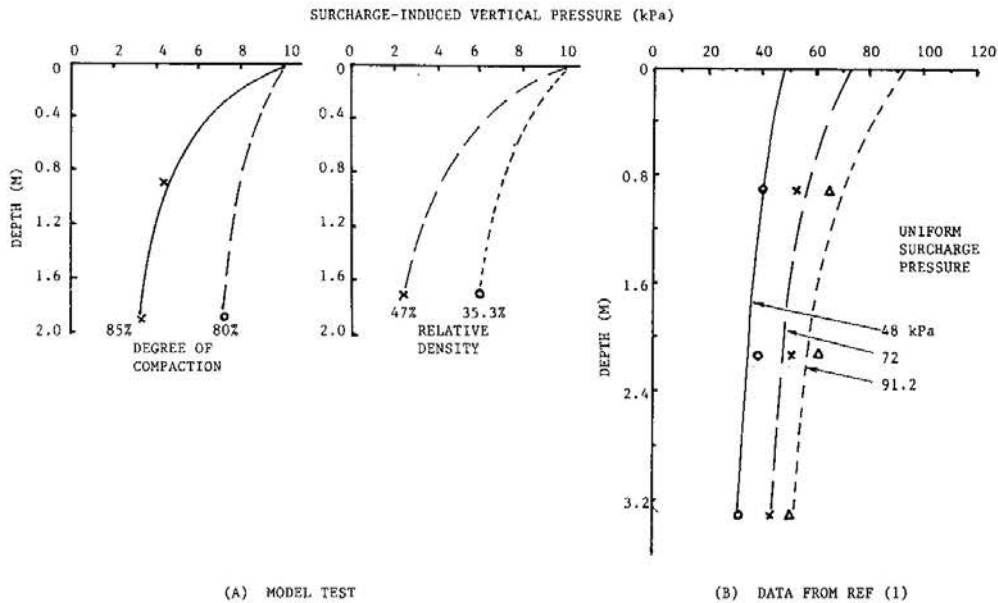
### **VERTICAL EARTH PRESSURE**

The surcharge-loading-induced vertical earth pressure inside the reinforced retaining structure was investigated for two loading conditions -- uniformly distributed over the entire backfill surface and strip loading. For a uniform surcharge pressure of 10 kPa, the surcharge-induced vertical pressures measured at two depths (0.9 m and 1.9 m) in the silty clay backfill and at 1.7 m depth in the fine sand backfill are shown in Figure 2. The figure presents the surcharge-induced vertical pressure distributions on horizontal planes for the two density levels stated earlier. As would be expected, the data points fluctuate. The trend of fluctuation reveals that the vertical pressure can be considered as uniform along the horizontal plane.

On each horizontal plane, the average vertical pressure is computed and plotted against the depth in Figure 3. A total of four conditions -- a silty clay and a fine sand with two levels of density for each backfill -- are included in the figure. Also included for comparison are the results of analysis of the test data presented by Al-Hussaini and Perry (1978); they are interpreted from the data in Figure 10 of the reference paper. Note that Al-Hussaini and Perry's test results are for a metal-strip-reinforced sand supported by a silty soil known as Vicksburg loess. A similar trend of vertical



**Fig. 2 Surcharge-Induced Vertical Pressure Distribution**



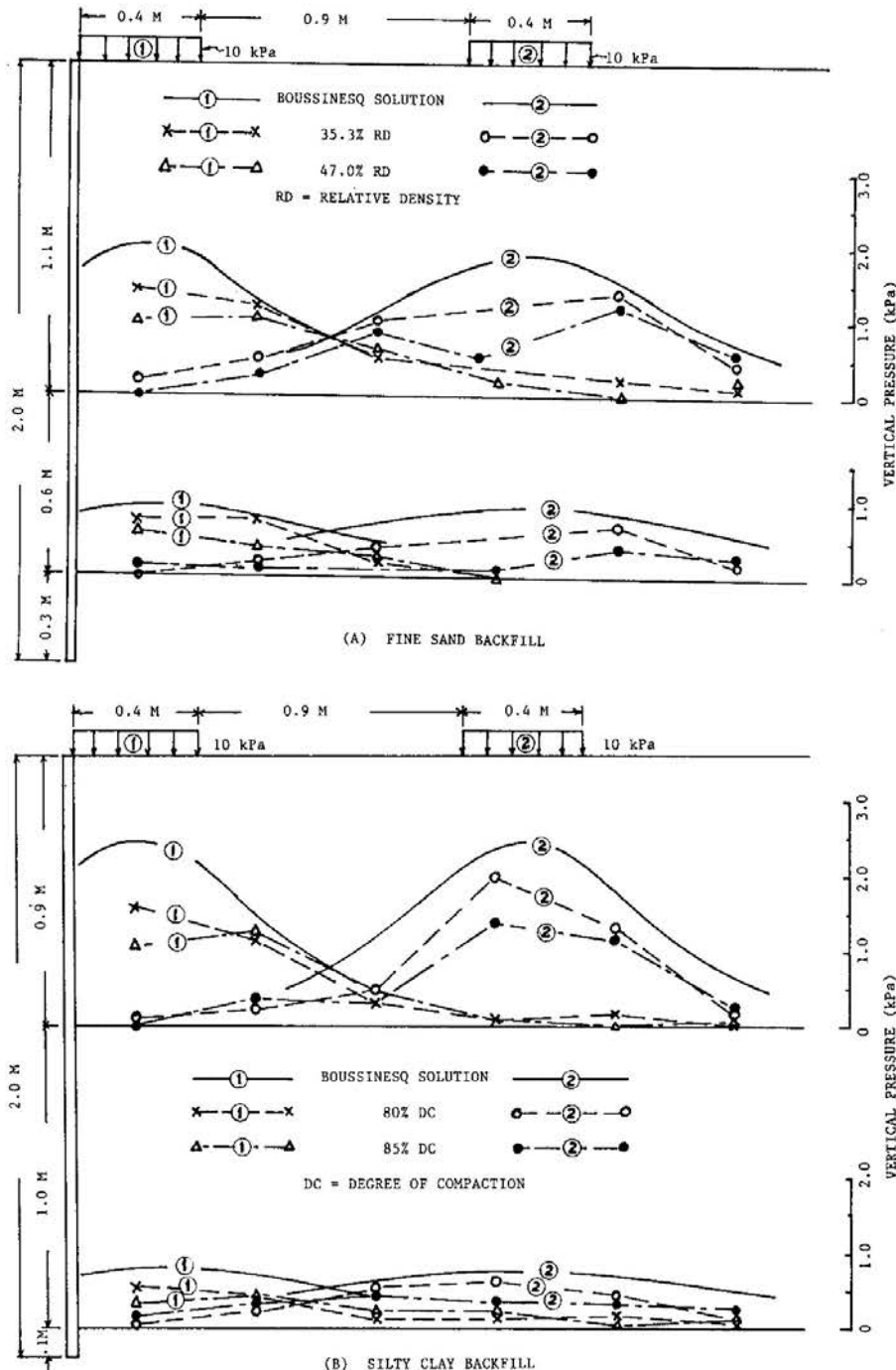
**Fig. 3 Variation of Surcharge-Induced Vertical Pressure with Depth**

pressure variation with depth is seen, suggesting that the effect of concrete support on the vertical pressure distribution in the test model, if any, is small, at least for the conditions investigated.

Contrary to what is often assumed that the surcharge-induced vertical pressure is constant independent of depth and equals the uniform surcharge pressure, all three data sets in Figure 3 indicate that the vertical pressure decreases with increasing depth regardless of soil type and reinforcing strip material. This suggests that the often used approach of approximating the uniform surcharge loading by an equivalent

## POLYPROPYLENE-STRIP-REINFORCED SOIL

height of backfill is invalid. Figure 3 also demonstrates that for both soil types the vertical pressure decreases with increasing depth more in dense state than in loose state of the backfill. The smaller vertical pressure than the surcharge loading can be attributed to the effect of load transfer in which part of the surcharge loading is transferred through the reinforcing strips to either the facing or the rear portion of the reinforced soil mass or both. Since denser soils are more effective in transferring load, a smaller vertical pressure observed in the denser state than in the looser state



**Fig. 4 Strip Surcharge-Induced Vertical Pressure Distribution**

can be expected.

Under a 40-cm wide strip surcharge pressure of 10 kPa, the horizontal distributions of the surcharge-induced vertical pressure are presented in Figure 4. Shown in the figure are the distribution curves at two depths of the vertical pressure due to each strip loading for four different backfill conditions plus the curves obtained from the Boussinesq solution. As shown, the shape of pressure distribution curves follows that of the theoretical curve, although the theoretical value is higher than the measured data. Also, as before, the vertical pressure is lower for the denser state than for the looser state irrespective of soil type. Since the theoretical solution is independent of material property, the use of the Boussinesq solution to determine the surcharge-induced vertical pressure is at best only a crude approximation.

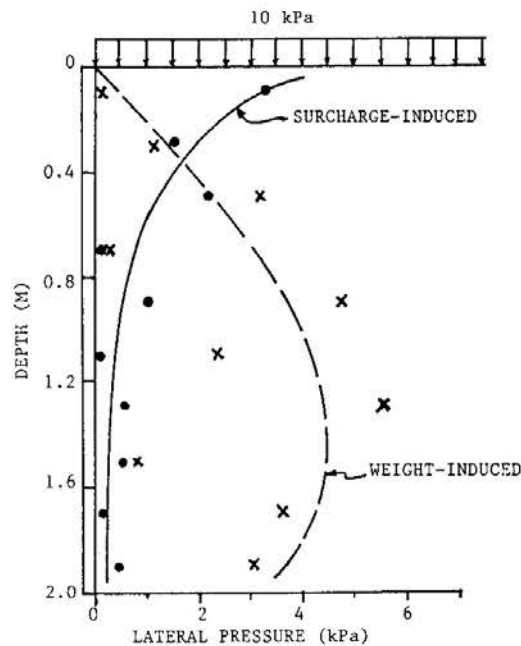
Based on the Boussinesq solution, a commonly adopted approximate method for computing the surcharge-induced vertical pressure at a depth assumes that the surcharge loading spreads out uniformly at a slope varying between 2V : 1H (26.6°) and 1V : 1H (45.0°). For applications to reinforced soil structures, Juran et al (1978) showed that 1V : 1H slope works more satisfactorily than 2V : 1H slope, while Laba and Kennety (1986) selected 2V : 1H slope in their analysis. The previously presented test results of a smaller vertical pressure associated with a greater density suggest a flatter slope for a denser state than a looser state. Thus, taking the internal friction angle as the load spread angle could be a reasonable approximation.

### LATERAL EARTH PRESSURE

Under a uniform surcharge pressure of 10 kPa, the lateral earth pressures against the facing for the fine sand backfill are presented in Figure 5. Though the data points are scattered, the trend reveals that the weight-induced lateral pressure first increases, then slightly decreases with depth; whereas the surcharge-induced lateral pressure decreases with depth quite abruptly at top then becomes almost constant in the lower portion. Such a trend of variation of lateral earth pressure with depth agrees well with Al-Hussaini and Perry's test results for a metal strip reinforced sand supported on a silty soil subgrade (Al-Hussaini & Perry, 1978). Thus, the concrete floor support of the test model appears to have little effect, if any, on the lateral earth pressure distribution.

The surcharge-induced lateral pressures are divided by the surcharge-induced vertical pressures to obtain the lateral earth pressure coefficient. From the model test results with the sand backfill, the computed earth pressure coefficients are 0.21 and 0.32 for the dense and loose states, respectively. These two values are close to the active earth pressure coefficients which equal 0.25 and 0.27 for the dense and loose states, respectively. From Al-Hussaini and Perry's results (1978) on a metal-strip-reinforced sand, the computed earth pressure coefficient is approximately 0.29 which is also close to the active earth pressure coefficient of 0.27 of their test sand. Based on

## POLYPROPYLENE-STRIP-REINFORCED SOIL



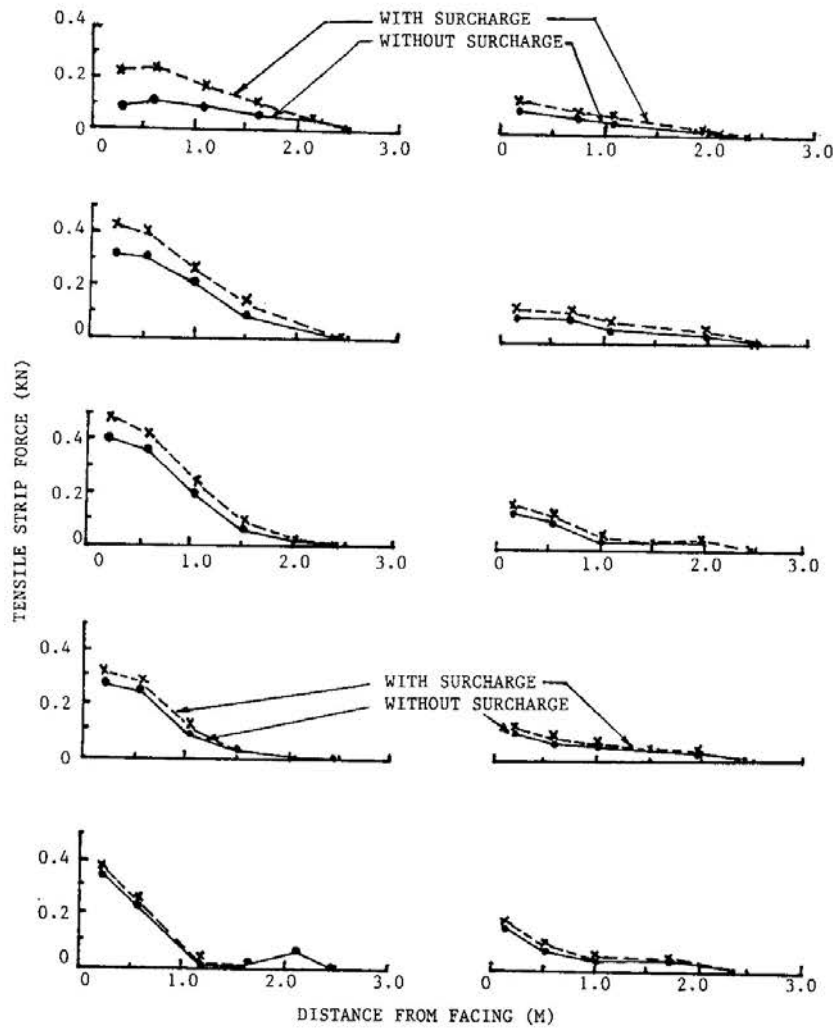
**Fig. 5 Lateral Earth Pressure on Facing**

these two sets of data, it is reasonable to use the active earth pressure coefficient to determine the lateral earth pressure from the vertical pressure both induced by the surcharge loading.

For the silty clay backfill, the measured lateral earth pressure on the facing is not presented graphically since it is negligibly small throughout the entire height for both with and without surcharge loading conditions. The very small lateral earth pressure could be attributed to the effect of tension. Note that the silty clay backfill has a cohesion of 15.6 to 16.0 kPa, an internal friction angle of 25.5° to 26.1° and a moist unit weight of 16.5 to 17.4 KN/m<sup>3</sup>. According to the Rankine theory, the depth of tension zone equals approximately 3.0 m which exceeds the height of facing (2.0 m), suggesting that the entire backfill is under the influence of tension. However, such an estimate is only a crude approximation since the effect of reinforcement is not considered. With reinforcement, the shear strength parameters of the backfill will vary, and therefore the depth of tension zone must be different.

### TENSILE STRIP FORCE

The tensile strip force data at five depths are presented in Figures 6 (A) and (B). Figure 6 (A) is for the fine sand backfill at 47.0% relative density and Figure 6 (B) is for the silty clay backfill at 85.0% compaction. For each data set, the tensile strip forces for both with and without a uniform surcharge pressure of 10 kPa are shown. The figure demonstrates, as would be expected, that both the weight-induced and the surcharge-induced tensile strip forces decrease with increasing distance from the facing, this is in agreement with the results for metal strip reinforcement (Al-



**Fig. 6 Tensile Strip Forces with and Without Uniform Surcharge Pressure**

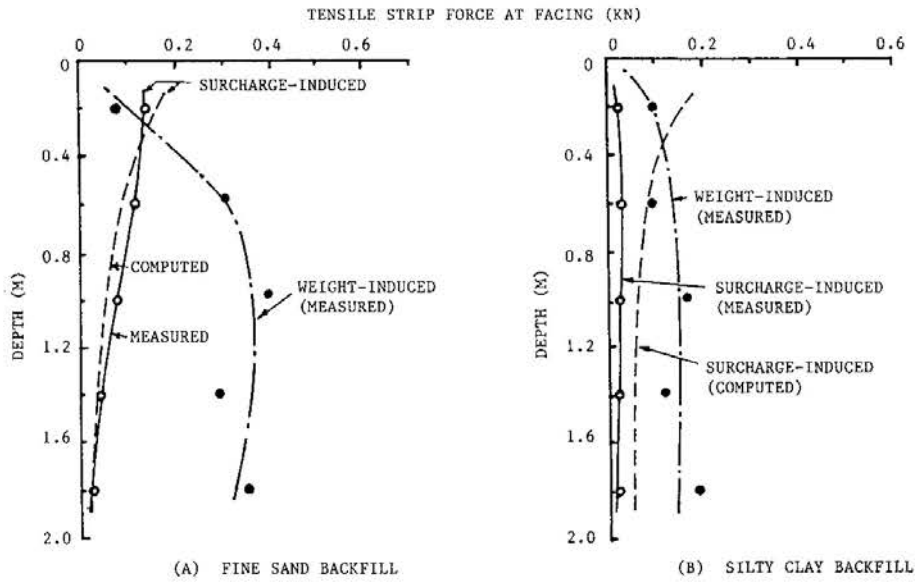
Hussaini & Perry, 1978). The figure also shows that the tensile strip forces both with and without surcharge loading are considerably smaller in the silty clay than in the fine sand backfill.

Both the weight-induced and surcharge-induced tensile strip forces near the facing are plotted versus the depth in Figures 7 (A) and (B), which are for the fine sand at 47.0% relative density and for the silty clay at 85% compaction, respectively. The shape of the curves for the fine sand backfill resembles that of the lateral earth pressure curves shown in Figure 5. Such a trend of variation is in good agreement with that of Al-Hussaini and Parry (1978).

For the surcharge-induced tensile strip force, the measured data are accompanied by the computed results. The strip force is computed from the surcharge-induced vertical pressure times the active earth pressure coefficient and the vertical and horizontal strip spacings. The agreement between the measured and the computed data is fairly good for the fine sand but is less than satisfactory for the silty clay. For the silty clay backfill, cohesion may induce potential tension crack effect which, in



## POLYPROPYLENE-STRIP-REINFORCED SOIL



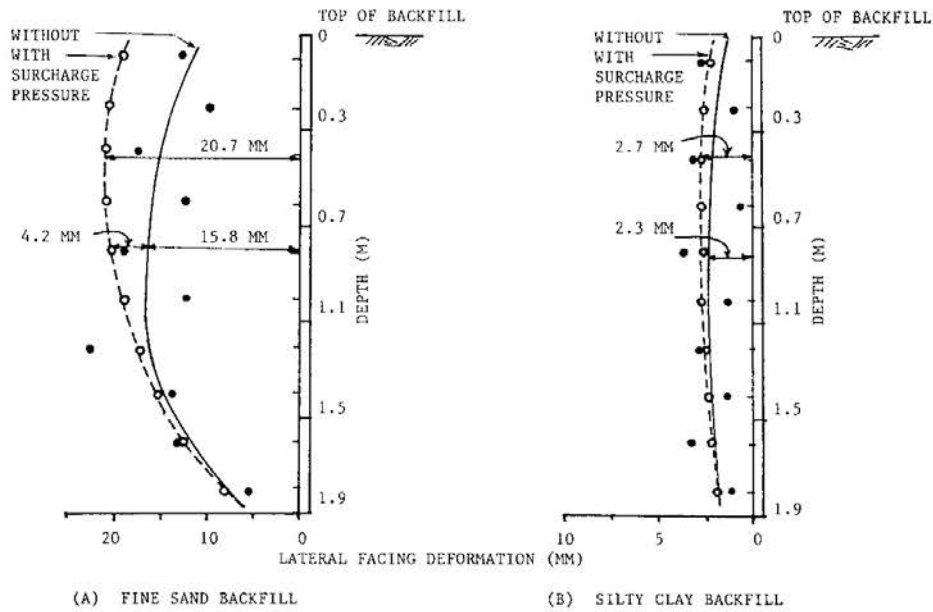
**Fig. 7 Tensile Strip Force at Facing Vs. Depth**

turn, may result in negligibly small lateral earth pressures, as mentioned earlier, and hence very small tensile strip forces. The significantly large tensile strip force data shown in Figure 7 (B) may be attributable to the compaction-induced lateral earth pressure. Such a lateral earth pressure is primarily caused by the lateral displacement of soil during compaction. According to the data, the compaction effect on tensile strip force appears to be less for the sand than for the silty clay backfill.

### LATERAL FACING DEFORMATION

The measured lateral deformations of the facing both with and without a uniform surcharge pressure of 10 kPa are presented in Figure 8 (A) for the fine sand backfill at 47.0% relative density and in Figure 8 (B) for the silty clay backfill at 85% compaction. Although the data points are scattered, the trend of variation is clear that for both backfill materials, the surcharge-induced facing deformation decreases with increasing depth from a maximum at top, that the maximum weight-induced facing deformation takes place around the midheight, and that the maximum facing deformation due to weight plus surcharge loading is located closer to the top of the facing. Meanwhile, the facing deformation is many times greater for the fine sand than for the silty clay backfill.

At the lower density level of 35.5% relative density for the fine sand and 80% compaction for the silty clay backfill, the facing deformation data show the same trend of variation as that of the higher density level. Numerically, for the higher and lower density levels, the maximum values of the weight-induced facing deformations are, respectively, 15.8 mm and 33.5 mm for the fine sand, and 2.3 mm and 4.6 mm for the silty clay backfill. Meanwhile, the maximum values of the surcharge-induced



**Fig. 8 Variation of Lateral Facing Deformation with Depth**

facing deformations are, respectively, 7.0 mm and 7.7 mm for the fine sand, and 0.85 mm and 1.7 mm for the silty clay backfill.

These data indicate that the weight-induced maximum facing deformation is about twice greater in the looser state than in the denser state for both backfill soils. When comparing the surcharge-induced maximum facing deformation, the difference between the two density levels is also double for the silty clay but is only about 10% for the fine sand backfill. Since the difference in the lateral earth pressure on the facing between the two density levels is only about 7%, there must be more factors, in addition to lateral earth pressure, controlling the facing deformation.

### SUMMARY AND CONCLUSIONS

A model study was undertaken to investigate the performance of polypropylene-strip-reinforced soil retaining structures. The model was 1.8 m wide by 3.1 m long by 2.0 m high, and contained five levels of reinforcing strips. The reinforcing strip had 15 mm width by 1 mm thickness by 2.5 m length and was spaced center-to-center 40 cm vertically and 10 cm horizontally. Two different backfill materials -- a fine sand and a silty clay, each with two levels of density, were investigated. Two types of surcharge loading -- a uniformly distributed and a strip pressure each 10 kPa in magnitude were applied, one at a time, on top of the backfill. The vertical pressure, lateral pressure, tensile strip force, and lateral facing deformation due to weight and surcharge loading were measured and analyzed. All of the measurements were made along the longitudinal center line of the model in order to minimize possible side effects.

## *POLYPROPYLENE-STRIP-REINFORCED SOIL*

The test results indicate that the vertical pressure induced by the 10 kPa uniform surcharge pressure is not constant independent of depth, instead it decreases from 10 kPa at top with increasing depth. Also, the rate of decrease is greater in the looser state than in the denser state. Thus, the often used approximation of replacing the uniform surcharge pressure by an equivalent height of backfill material is invalid. Under a strip surcharge pressure, the surcharge-induced vertical pressure also decreases with increasing depth faster in the denser state than in the looser state. The shape of pressure distribution on a horizontal plane resembles that obtained from the Boussinesq solution; however, the theoretical solution overpredicts significantly for all of the four cases. Based on these data, use of the Boussinesq solution to determine the surcharge-induced vertical pressure is at best only a crude approximation. Additionally, for the commonly used approximation of spreading the surcharge pressure out at a certain slope angle, it is reasonable to use the internal friction as the slope angle in order to consider the effect of backfill density.

For the fine sand backfill, the weight-induced lateral pressure on the facing first increases, then decreases with depth, and the surcharge-induced lateral pressure decreases with depth at a decreasing rate. The lateral earth pressure coefficient computed from the surcharge-induced lateral and vertical pressures is approximately equal to the active earth pressure coefficient. For the silty clay backfill, the lateral earth pressure on the facing is very small due primarily to the effect of tension.

The weight-induced tensile strip force near the facing is much smaller in the upper portion of the facing, but the surcharge-induced tensile strip force decreases with depth from a maximum at top. For the surcharge-induced tensile strip force, the measured data agree fairly well with the data computed from the surcharge-induced lateral earth pressure. However, less than desirable agreement is found for the silty clay backfill.

The surcharge-induced lateral facing deformation is maximum at top of the facing, but the maximum weight-induced facing deformation takes place around the mid height. The lateral facing deformation is much greater for the fine sand backfill than for the silty clay backfill. Furthermore, for a backfill soil, the lateral facing deformation is greater when the backfill is looser.

Based on the results of the study, it may be concluded that there is little difference in performance between the polypropylene-strip-reinforced and the metal-strip-reinforced soil retaining structures. It is not valid to replace the uniform surcharge pressure by an equivalent backfill height to determine the surcharge-induced vertical pressure. The surcharge-induced vertical pressure decreases with depth faster when the backfill is denser. The surcharge-induced lateral earth pressure, tensile strip force, and lateral facing deformation also decrease with depth; they are greater in the looser state than in the denser state, and are larger for the fine sand backfill than for the silty clay backfill.

ACKNOWLEDGEMENT

The authors are grateful to Karen M. Detwiler for her typing the manuscript.

REFERENCES

- AL-HUSSAINI, M. and PERRY, E.B. (1978). "*Field Experiment of Reinforced Earth Wall.*" Proceedings, Symposium on earth Reinforcement, ASCE, Pittsburgh, PA, April, pp. 127-156.
- HUA, Z.K., WANG, Y.H., and LIU, Q.F. (1991). "*Testing and studies of the Reinforced Earth Retaining Wall on Heng-Guang Double-Railline.*" Proceedings of the 6th Chinese Conference of Soil Mechanics and Foundation Engineering, Shanghai, June, pp. 487-490, (in Chinese).
- JONES, C.J.F.P., (1985). "*Earth Reinforcement and Soil Structures,*" Butterworth, London, England.
- JONES, C.J.G.P., (1991). "*Construction Influences on the Performance of Reinforced Soil Structures*" in *Performance of Reinforced Soil Structures*. Edited by A McGown, K. Yeo, & K.Z. Andrawes. Thomas Telford, London, pp. 98-116. Proceedings of the International Reinforced Soil Conference organized by the British Geotechnical Society and held in Glasgow, September 1990.
- JURAN, I., SCHLOSSER, F., LONG, N.T., and LEGEAY, G., (1978). "*Full Scale Experiment on a Reinforced Earth Bridge Abutment in Lille.*" Proceedings, Symposium on Earth Reinforcement, ASCE, Pittsburgh, PA, April, pp. 556-584.
- KOBAYASHI, K., (1980). "*New Railroad on Reinforced Earth Embankment with Strip Reinforcements in Both Slopes,*" Construction Technology, Special Issue, Vol. 10, No. 10, (in Japanese).
- LABA, J.T. and KENNEDY, J.B., (1986). "*Reinforced Earth Retaining Wall Analysis and Design,*" Canadian Geotechnical Journal, Vol. 23, pp. 317-326.
- McCAUL, C., and SNOWDON, R.A., (1990). "*Early Performance of a Reinforced Earth Bridge Abutment.*" Proceedings of the International Reinforced Soil Conference, Glasgow, September, pp. 78-88.
- MITCHELL, J.K. and VILLET, W.C.B., (1987). "*Reinforcement of Earth Slopes and Embankments,*" NCHRP Report 290, TRB, Washington, D.C., June.
- TEMPORAL, J., CRAIG, A.H., HARRIS, D.H., BRADY, K.C., (1989). "*The Use of Locally Available Fills for Reinforced and Anchored Earth.*" Proceedings, 12th International Conference on Soil Mechanics and Foundation Engineering, Rio de Janeiro, August, Vol. 2, pp. 1315-1320.
- WANG, Y.H. and WANG, M.C., (1993). "*Internal Stability of Reinforced Soil Retaining Structures with Cohesive Backfills,*" Transportation Research Record, No. 1414. Transportation Research Board, Washington, D.C. pp. 38-48.

*POLYPROPYLENE-STRIP-REINFORCED SOIL*

- WANG, X.X., LI, C.C., YEN, Y., and YAO, D.L., (1990). "*Prototype Scale Design and Test of Reinforced Earth Retaining Wall with Cohesive Backfill.*" Proceedings, Third National Symposium on Reinforced Earth Engineering, October, pp. 38-59 (in Chinese).
- WU, W.L., (1990). "*In-Situ Test and Analysis of the Reinforced Earth Retaining Wall on Cheng-Yu Highway at Yinshanzhen.*" Proceedings, Third National Symposium on Reinforced Earth Engineering, October, pp. 67-108 (in Chinese).
- YAMANOÛCHI, T., MIURA, N., and OCHIAI, H., (1988). "*Theory and Practice of Earth Reinforcement,*" Balkema, Rotterdam, The Netherlands.
- ZORNBERG, J.G. and MITCHELL, J.K., (1992). "*Poorly Draining Backfills for Reinforced Soil Structures - A State of the Art Review.*" Geotechnical Engineering Report No. UCB/GT/92-10, University of California at Berkeley, October.

# PRELIMINARY GROUNDWATER MODELLING OF MAE MOH LIGNITE MINE IN THAILAND WITH REFERENCE TO FLOOR HEAVE

Y. Honjo<sup>1</sup>, P.H. Giao<sup>2</sup>

## SYNOPSIS

The Mae Moh basin is an intermontane basin of about 135 km<sup>2</sup> located 28 km east of Lampang City in Northern Thailand (Fig. 1), where a large scale lignite open pit mine has been developed by EGAT (The Electricity Generating Authority of Thailand). In 1988, an aquifer with very high artesian pressure was found under the open pit excavation area which needs to be treated to ensure the stability of the excavation when the mine depth increases in the future.

This study is a first attempt to model the complicated aquifer system which occurs in the basin. A steady state analysis using a quasi three dimensional model was carried out. The model is capable of simulating the three dimensional nature of this multiaquifer system in a very efficient way. By fitting the calculated head distribution with the currently observed ones, the main features of the aquifer system are found to be (1) strong North to South flow (2) together with flow from East and West to the central part of the basin, and (3) strong upward vertical flow. A safety factor distribution against floor heave in the proposed excavation area for future lignite production development was also estimated, suggesting a possible need for depressurizing.

## INTRODUCTION

The Mae Moh Mine is the largest lignite mine in Thailand. Its operation started in 1955 and since then the production capacity has increased gradually. At present, the daily maximum lignite production is 30,000 tonnes which is planned to be increased to more than 80,000 tonnes daily (EGAT, 1991). One of the critical problems related to this expansion is the influence of groundwater on excavation and slope stability when deepening the excavation from the actual depth of 150 m to a greater depth of about 500 m below the ground surface.

The immediate aim of this study is to help understand the important features of the very complicated aquifer system of Mae Moh basin by using the quasi-three dimensional finite element method (FEM). Consequently, the next goal of this modelling work is to enable people to carry out the feasibility study of dewatering or

---

<sup>1</sup> Associate Professor and Chairman, Division of Geotechnical and Transportation Engineering, Asian Institute of Technology, P.O. Box 2754, Bangkok 10501, Thailand.

<sup>2</sup> Research Associate, Division of Geotechnical and Transportation Engineering, Asian Institute of Technology, P.O. Box 2754, Bangkok 10500, Thailand.

depressurizing systems to reduce adverse groundwater pressures for safe excavation.

The quasi-3D model has been proposed and modified by many authors (e.g., Neumann & Witherspoon, 1969; Herrera & Rodate, 1973; Fujinawa, 1977; Neumann, Preller & Narasimhan (1982); Nuyakorn & Pinder, 1983 etc.). It is an efficient tool to handle a leaky multiaquifer system. For this study on groundwater modelling of Mae Moh Basin, a computer code named QUASI has been developed based on Smith and Griffiths's FE Subroutines Library (Smith & Griffiths, 1988; Hossain, 1990).

### MAE MOH LIGNITE BASIN

#### General

The Mae Moh Mine is located on undulated terrain of a graben. The elevation of the valley is about 200 to 300 meters above the mean sea level. It is a big open pit mine, which is divided into several mining pits (Fig. 1). The Mae Moh area has a tropical climate dominated by two seasonal monsoon winds. There are three distinct seasons (Tandicul, 1991); the hot and dry season from mid February to mid May; the rainy season from mid May to mid October; and the cool and dry season from mid

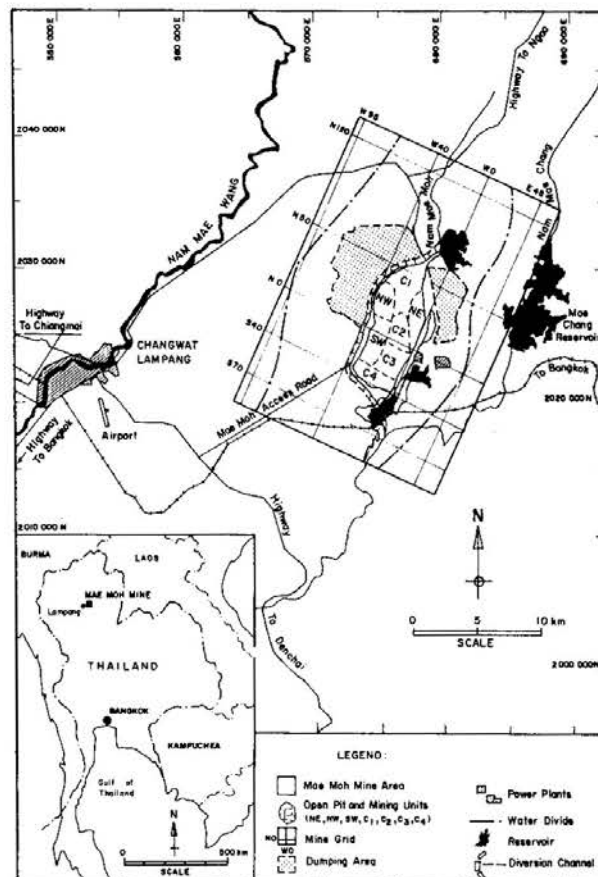


Fig. 1 Mae Moh Lignite Basin : Location and Extent.

## GROUNDWATER MODELLING

October to mid February. Monthly rainfall is shown in Fig. 2. A yearly average precipitation is 1,150 mm, while the average number of rainy days is 111 per year. The runoff in the mine area is mainly induced by rainfall. The surface runoff, especially from the eastern mountain range is dammed up by ash and waste dump, creating high heads upstream of the low wall (Fig. 3). The coefficient of runoff for the Mae Moh area has been estimated to be 0.75 (Tandicul, 1991). The main stream draining the Mae Moh basin area is the Nam Mae Moh River. The Nam Mae Moh flows from the Northern part of the basin to the Southern part where it meets Nam Mae Chang River (Fig. 1). The natural water table fluctuates from about 10 m below ground surface during the dry season to close to the surface in the wet season (Voigt, 1991). The ground water divides on the eastern and western sides are shown in Fig. 1.

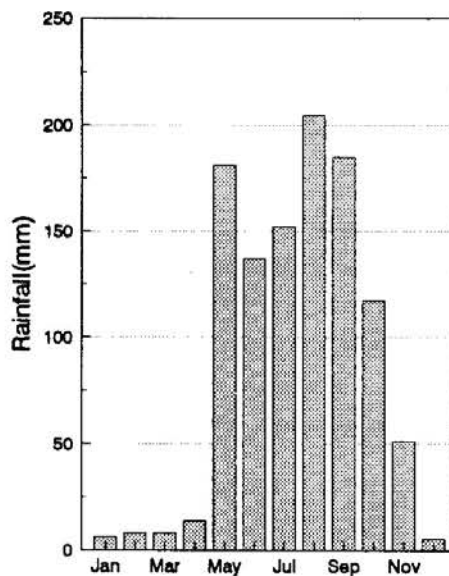


Fig. 2 Average Monthly Rainfall

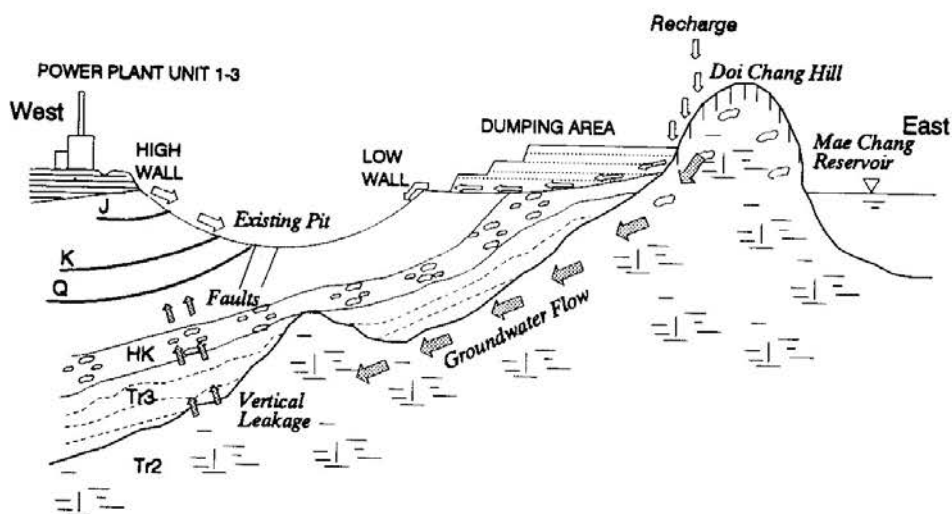


Fig. 3 Conceptual Hydrogeological Model of Mae Moh Basin (McMahon & Forth, 1988)



The northern water divide is outside the study area and the southern one is considered absent in the analysis because of the presumption that the basin is open in the south.

In the Mae Moh Mine, a local coordinate system introduced by EGAT and called Mine Grid is commonly used (Fig. 1). This is a network of regularly spaced lines, oriented N23°E. Most graphic representations in this study are drawn according to this coordinate system.

### Geology of the Mae Moh Basin

The Mae Moh Basin is one of the several structural tertiary basins in the mountainous region of Northern Thailand. It is mainly bounded by marine Triassic (Lampang Group), it consists of limestone, shale, siltstone and sandstone. These rocks are folded and faulted trending from N15°W to N40°E. The most recent geological interpretation of the Mae Moh basin is given in Fig. 4a. There are three major geological units as follows:

(1) **Post-tertiary** : In the southern part of the Mae Moh Basin, a sheet of basalt of at least 100 m thick overlies Tertiary sediments, Pleistocene gravel beds, and marine Triassic rocks. Unconsolidated sediments of fluvial origin cover parts of the basin. They consist of gravel deposits at the bottom and alluvium deposits at the top. The thickness varies from less than 1 meter to 10 meters. The Quaternary deposits overlay the Tertiary sediments unconformably.

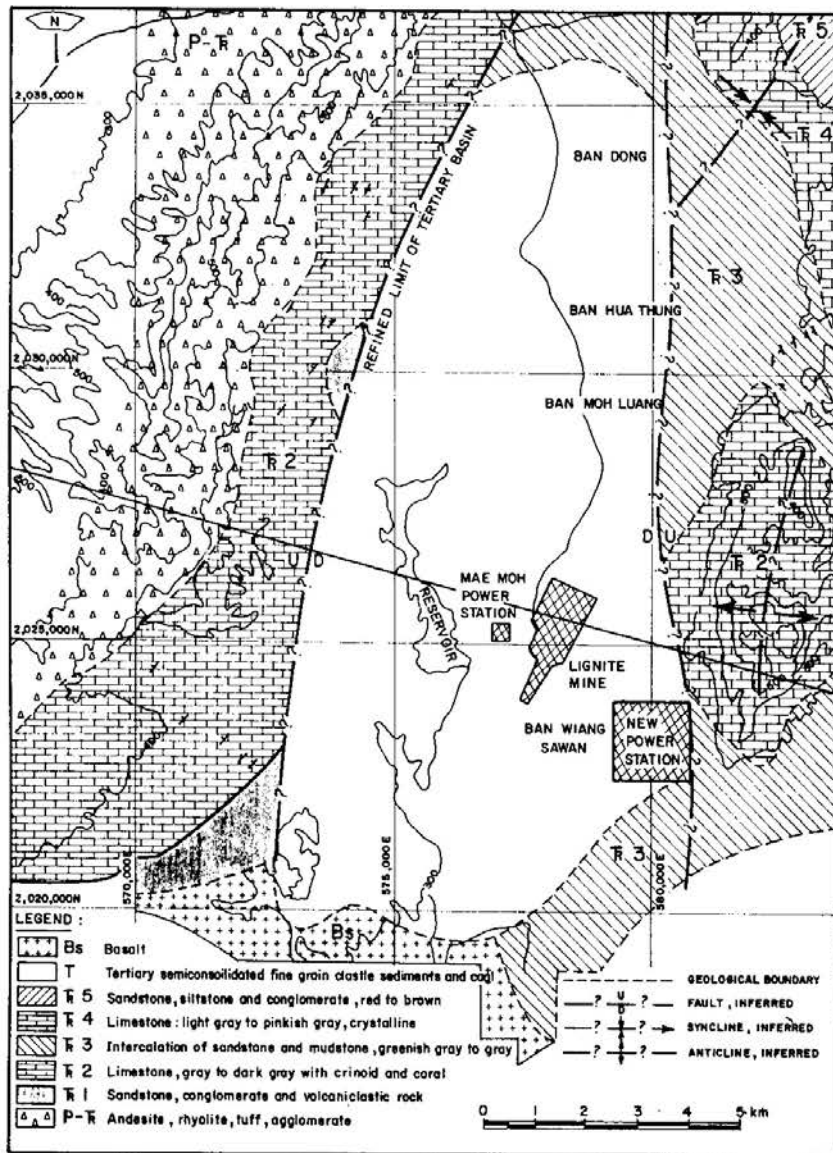
(2) **Tertiary** : Tertiary formations overlay the basement of Triassic rocks. Tertiary succession of Mae Moh Basin can be separated into three formations (Fig. 4b) as follows:

*Huai Luang Formation (HL)* : This upper formation consists of red to brownish red sediments with some grey layers interbedded in some parts. Almost all are claystone, siltstone and mudstone with some lenses of sandstone and conglomerate in the central part of the basin. The thickness of this formation varies from less than 5 meters to 250 meters. It is thickest in the central part of the Main Basin, thinning rapidly towards the eastern and western margins, where it is entirely absent or only a few meters thick.

*Na Khaem Formation (NK)* : This middle sequence of strata consists of grey to greenish grey, highly calcareous rocks and zones of coal. The thickness varies from 250 meters to 400 meters. The Na Khaem formation consists of five zones of coal which can be separated according to lithological and economic criteria. The two major economic zones of coal are named K and Q (Fig. 4b).

*Huai King Formation (HK)* : This is at the bottom of Tertiary succession, in contact with Triassic basement rocks. It consists of mudstone, siltstone, sandstone, conglomeratic sandstone, conglomerate and some claystone. It is variegated in color : red, grey, green, yellow, blue and purple, and commonly is cemented with a slightly calcareous cement. The typical character is a fining upward sequence grading from

## GROUNDWATER MODELLING




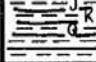

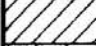



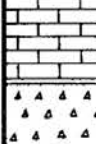


**Fig. 4a Geological Map of Mae Moh Basin (EGAT, 1985)**

conglomerate to mudstone or claystone at the top. The thickness of the Huai King formation varies from less than 15 meters on the eastern border to 150 meters on the western border of the Main Basin

(3) **Triassic** : Below the Tertiary succession the basement consists of marine Triassic rocks, which are exposed on the western and eastern margins of the basin. The basement consists mainly of limestone, shale, and sandstone. From the youngest to the oldest, there are:

*The Doi Long Formation (TR4)* has a limited exposure at the northeast of mine and consists of finely crystalline limestone.

SIMBOL	DESCRIPTION	FORMATION	GROUP	AGE
	River gravel, sand, clay			Recent
	Colluvium, gravel, semi-consolidated sandy clay	Quaternary Terrace	Mae Taeng (Post-Tertiary)	Pleistocene
	Red clay and semiconsolidated clay	Huai Luang (HL)	Mae Moh (Tertiary)	Pliocene Miocene
	Grey claystone and lignite	Na Khaem (NK)		
	Yellow and red clay, clayed sand and grey claystone	Huai King (HK)		
	Limestone, light grey to pinkish white, crystalline	Doi Long (TR4)	Lam Pang (Triassic)	Middle Triassic
	Sandstone, medium grain interbedded with shale and siltstone, greenish and grey, conglomerate limestone, recrystalline, well bedded, grey to dark grey	Hong Hoi (TR3)		
	Limestone, pure and crystalline, massive bedded, grey to dark grey	Doi Chang (TR2)		
	Limestone, banded, dark grey. Basal conglomerate, red sandstone and grey shale.	Phra That (TR1)		
	Volcanic rocks, andesite, rhyolite agglomerate and tuff.	Volcanic (P-TR)	Volcanic	Permo-Triassic

**Fig. 4b Stratigraphic Sequence of Mae Moh Basin (Based on EGAT Geological Report, 1985)**

The Hong Hoi Formation (TR3) is the most widespread formation of shales, sandstones and bedded limestones.

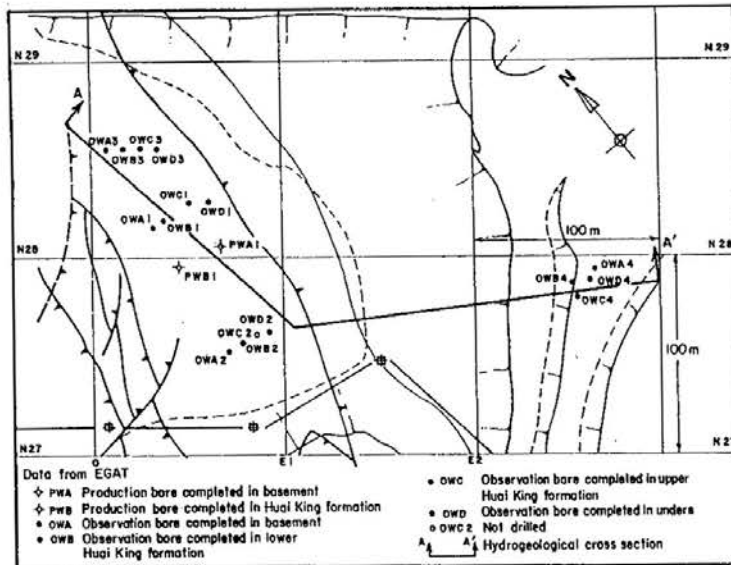
The Doi Chang Formation (TR2) is exposed to the northwest, southwest, and south of Mae Moh, as well as at Doi Chang. This formation consists of massive and recrystallized limestones.

The Phra That Formation (TR1) overlies the volcanics of the Permo-Triassic age. It consists of basal conglomerates and associated limestone.

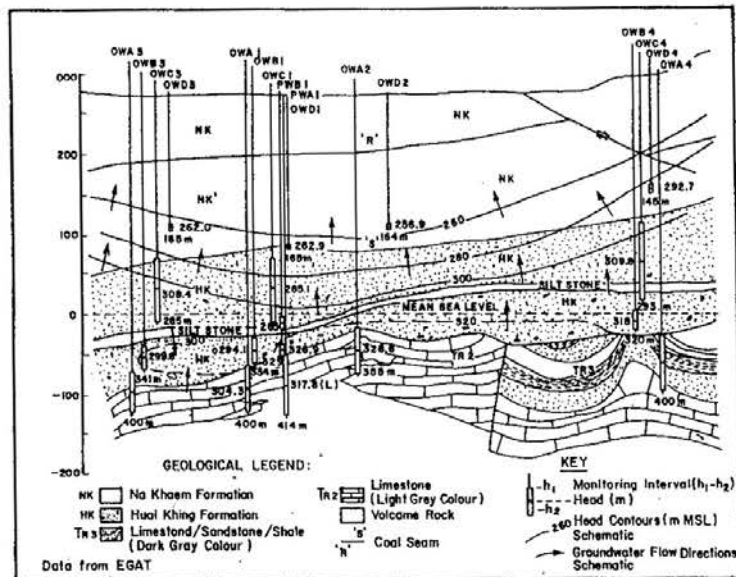
**Hydrogeology**

In the latter half of 1988, a piezometer was drilled in the basement (Doi Chang Formation) and confirmed the presence of an artesian aquifer with a potentiometric head of 333 m above Mean Sea Level or 13 m above ground surface. Since then a Groundwater Drilling and Testing Project has been initiated by EGAT in order to investigate the hydrogeology of the Mine area and the whole basin. The Phase 1 was completed at the end of 1991. Two production wells and 18 observation piezometers at Site 1 or Groundwater Site 1 (GTS 1) have been completed (Fig. 5a). Based on the results of Phase 1, an approximate hydrogeological section and groundwater head distribution has been proposed (Fig. 5b) by Vogwill (1990). The essential data

## GROUNDWATER MODELLING



**Fig. 5a Hydrogeological Details of Piezometer P128 (Vogwill, 1990)**



**Fig. 5b Head Distribution along Section A-A' (Vogwill, 1990)**

obtained in Phase 1, concerning head measurements and estimated hydraulic parameters, are presented in Table 1. At present, nearly 50 additional drill holes of phase 2 have been completed. The updated results are, however, still not processed and synthesized.

Based on the current level of understanding of the hydrogeology of the Mae Moh Basin, there appear to be two main aquifer systems below the mine area:

**(1) Basal Tertiary Aquifer System :** The Huai King formation represents a potential aquifer system although it becomes quite thin under the western portion of

**Table 1 Results of Phase 1 Obtained at GTS-1 (VOGWILL, 1990)**

Bore	Formation	Static Head (MSL)	Head when Flowing (MSL)	Drawdown (m)	Flow (m <sup>3</sup> /d)	Q/s (m <sup>3</sup> /d/m)	Estimated T (m <sup>2</sup> /d)	Estimated K (m/d)
OWA1	BMT	288.6	273.8	14.8	2.6	0.18	< 1.0	< 0.01
OWB1	LHK	285.2	272.7	12.5	0.4	0.03	< 1.0	< 0.01
OWC1	UHK	286.3	272.8	13.5	1.5	0.11	< 1.0	< 0.01
OWA2	BMT	328.6	274.5	54.1	203.9	3.77	4 - 6	0.07 - 0.1
OAW3	BMT	327.8	273.7	54.1	55.3	1.02	1.1 - 1.3	0.03
OWB3	LHK	295.1	273.8	21.3	0.2	0.009	< 1.0	< 0.2
OWC3	UHK	310.8	273.5	37.3	0.1	0.003	< 1.0	< 0.08
OWB4	LHK	324.1	298.4	25.7	0.7	0.03	< 1.0	< 0.2
OWC4	UHK	313.3	298.5	14.8	2.6	0.18	< 1.0	< 0.07
PWA1	BMT	317.8	272.8	45.0	28.0	0.62	< 1.0	< 0.01
PWB1	HK	326.9	272.7	54.2	13.0	0.24	< 1.0	< 0.03
PI28	BMT	333.5	320.0	13.5	27.6	2.0	2 - 4	0.06 - 0.1

Note :

- (1) The locations and denotations of the bores are shown and explained in Fig. 5a.
- (2) BMT : Top of Basement; HK : Huai King; UHK : Upper Huai King; LHK : Lower Huai King.

the mining area. The results obtained in Phase 1 reveal the existence of a siltstone layer, the Huai King (HK) can be separated into the Upper Huai King (UHK) and the Lower Huai King (LHK) in some locations (Vogwill, 1990). However, Phase 2 data do not to confirm this separation.

**(1) Triassic Bedrock Aquifer System** : Most of the Triassic rocks have little or no primary intergranular permeability. The occurrence of Triassic bedrock aquifers, therefore, is a result of secondary structures in the bedrock such as weathering, karst development, joints, fractures, and faults. Up to now the Doi Chang Formation (TR2) has been targeted as the main potential aquifer. It is the authors' opinion that the permeable zones are related firstly to faulted zones, and they are developed not only in Doi Chang Formation (TR2) but also in Hong Hoi Formation (TR3) and other Triassic Formations. The fractured or faulted zones are most sensitive to weathering where triassic rocks are exposed. Thus, locally brecciated zones could be formed in the uppermost part of the basement.

## GROUNDWATER MODEL ANALYSIS

The objective of groundwater modelling of the Mae Moh Basin is to investigate groundwater conditions in Tertiary sediments and Top of Basement, which can affect the excavation stability of the mine pit. At the present stage, the hydrogeological data are still very limited and not finally synthesized. Therefore, groundwater modelling can only be of a preliminary character.

**Quasi-3D model**

Geology and hydrogeology of Mae Moh Basin show that groundwater flow is possibly carried in a leaky and fractured multiaquifer system. Thus, a quasi-3D model may be most applicable, taking into account the actual available hydrogeological data. The most fundamental assumption of a quasi-3D model is that it considers only the horizontal flow in aquifers and the vertical flow in the interconnecting aquitards. If the permeability of the aquifers is at least two orders of magnitude larger than that of the aquitards, it is known that the calculated results based on this assumption produce an error less than 5% (Neumann & Witherspoon, 1969; 1982). Since this situation holds in most practical cases, the fundamental assumption mentioned above is satisfactory to obtain practical solutions. The flow equations used in Quasi-3D are as follows:

The 2-D unsteady horizontal flow equation in the  $i^{th}$  aquifers is:

$$\frac{\partial}{\partial x} \left( T_{xx} \frac{\partial h}{\partial x} \right) + \frac{\partial}{\partial y} \left( T_{yy} \frac{\partial h}{\partial y} \right) + Q + q_i - q_{i+1} = S_i \frac{\partial h}{\partial t} \quad (1)$$

where :

- $T_{xx}, T_{yy}$  : the aquifer transmissivities along X and Y-directions
- $S_i$  : the aquifer storage
- $Q$  : discharge (-) or recharge (+) rate
- $q_i$  : flow rate from the top aquitard to the current aquifer
- $q_{i+1}$  : flow rate from the bottom aquitard to the current aquifer

The 1-D vertical flow the the  $i^{th}$  and  $i+1^{th}$  aquitard are :

$$\frac{\partial}{\partial z} \left( K'_i \frac{\partial h'_i}{\partial z} \right) = S'_{s,i} \frac{\partial h'_i}{\partial t} (2\alpha) ; \quad \frac{\partial}{\partial z} \left( K'_{i+1} \frac{\partial h'_{i+1}}{\partial z} \right) = S'_{s,i+1} \frac{\partial h'_{i+1}}{\partial t} \quad (2b)$$

The leakage flux terms or inflow at boundaries between the aquitards and the current aquifer are as follows:

$$q_i = \left( K'_i \frac{\partial h'_i}{\partial z} \right)_{z_i = 0} \quad (3a)$$

$$q_{i+1} = \left( K'_{i+1} \frac{\partial h'_{i+1}}{\partial z} \right)_{z_{i+1} = b'_{i+1}} \quad (3b)$$

where

- $h'_i$  &  $h'_{i+1}$  : heads in the  $i^{th}$  and  $i+1^{th}$  aquitard
- $K'_i$  &  $K'_{i+1}$  permeability of the  $i^{th}$  and  $i+1^{th}$  aquitard
- $S'_{s,i}$  &  $S'_{s,i+1}$  specific storage of the  $i^{th}$  and  $i+1^{th}$  aquitard
- $b'_{i+1}$  : thickness of the  $i+1^{th}$  aquitard

The key issue in treating the solution of a quasi-3D model is the technique of coupling of those governing equations of flow in aquifers and in aquitards (Eqs. 1 & 2). In this study, a combined approach of Finite Element and Convolution Integral

techniques has been applied (Nuyakorn & Pinder, 1983). A complete Quasi-3D solution has been found and coded in Fortran 77. However, due to very limited hydrological data as mentioned above, all analyses have been done only for steady state.

The main advantage of the quasi-3D model with respect to a fully 3D one is computation time saved, hence the processing cost without sacrificing the 3D character of the groundwater flow. A fully 3D model may require 100-1000 times more computation time than the quasi-3D one (Nerrera et al, 1980). Another advantage of the Quasi-3D model might be avoiding (Mercer and Faust, 1980) the use of an unnecessarily sophisticated model (for example, a fully 3D model) for a simpler situation or a situation with insufficient data, especially those data related to three dimensional boundary conditions.

### Some Important Observations

Some of the important observations taken into account in setting the assumptions for the numerical simulation can be summarized as follows:

(1) Hydrogeologically, Huai Luang (HL) and Na Khaem (NK) formations form a very effective top aquitard. Huai King (HK) was considered before a continuous confined aquifer, but some geological data indicated that HK can be divided into Upper and Lower Huai King (UHK and LHK) separated by a thin siltstone layer of up to 15 meters thick in some locations. LHK is speculated to be a major aquifer. Another major aquifer is the Triassic Bedrock Aquifer System, whose permeability depends on the secondary porosity due to weathering, stratification, joints, fractures; this aquifer, in the present study, is represented by its uppermost part of Basement called Top of Basement (BMT).

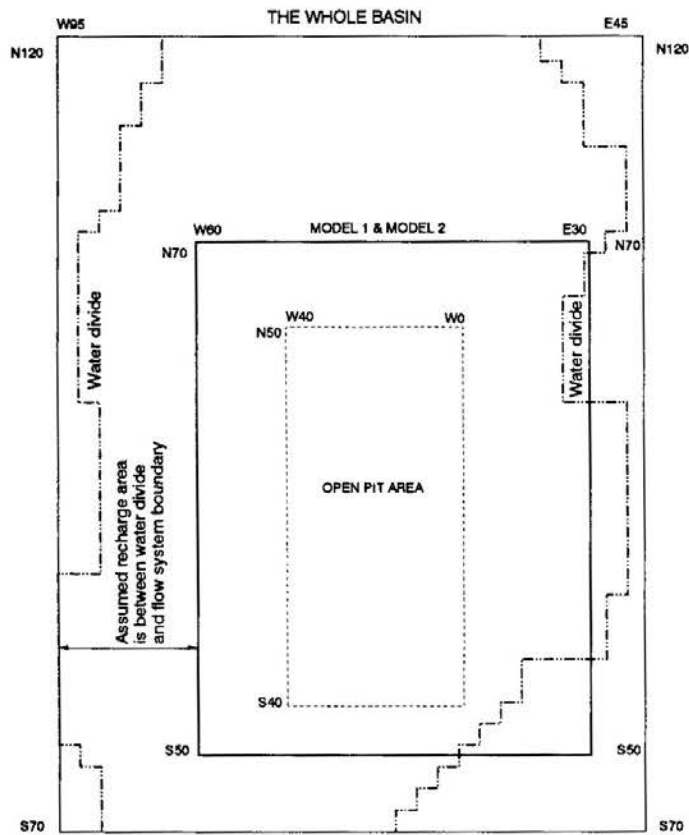
(2) The regional flow pattern comprises of 3 distinct zones, e.g. recharge zone under and adjacent to the hills on the flanks on the basin; zone of lateral flow under the dumping area and discharge zone with upward flow of steep hydraulic gradients (Fig. 3). By analyzing the head measurements in the boreholes in GTS1, it can be roughly realized a difference of about 10 meters in head value between LHK and UHK as well as between BMT and LHK (Table 1 and Fig. 5b).

(3) Based mainly on the head observations that there are three possible groundwater flow directions in the basin : one is from East and Westward to the central part, moving across geological structures and Triassic rocks; the second is from North to South and the third one is an upward vertical flow.

### Model Parameters

*Geometry of aquifer systems* : The extent of the basin related to lignite development is delimited by the EGAT geologists from N54 to S30 mine grid line. The modelling area in this study, namely Model 1 and Model 2 is more extended, i.e. from N60 to S50 and from W60 to E30 mine grid line, to cover the testing boreholes of EGAT Geohydrology Project. A general view of different flow and FEM analysis domains is illustrated in Fig. 6.

## GROUNDWATER MODELLING



**Fig. 6 Schematic FEM Analysis Domains Used in Groundwater Modelling of Mae Moh Basin**

*Hydraulic Property* : The input parameters employed in the current models are shown in Fig. 7. Some of the input hydraulic parameters, for example the vertical permeability and specific storage of aquitards, are assumed based on the typical values of soil and rock permeabilities published (Canmet, 1977).

*Boundary conditions* : boundary conditions are specified in Figs. 8 and 10a, for Model 1 and 2, respectively. Most boundaries of quasi-3D models analyzed in this study are of fixed head type based on the groundwater static levels observed (Fig. 10a) in the Geohydrology Project and made available to the authors.

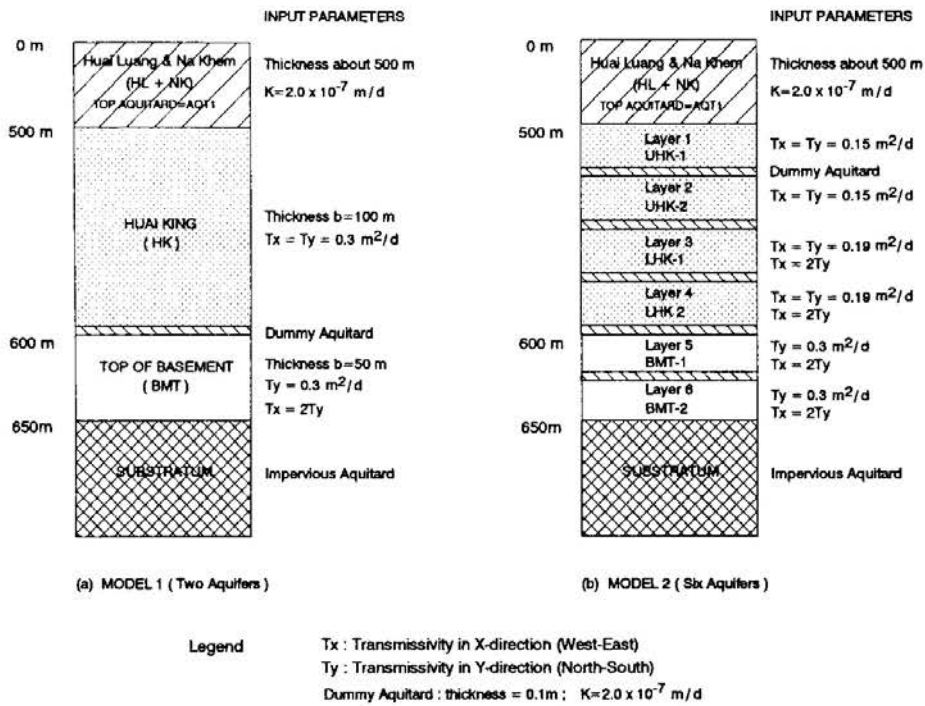
### Model Settings and Results

Two quasi-3D models were employed in this study. Model 1 investigated the 2-D flow in major aquifers, i.e HK and BMT, the boundary conditions, the horizontal flow directions etc. MODEL 2 attempts to investigate the vertical flow aspect of the aquifer system

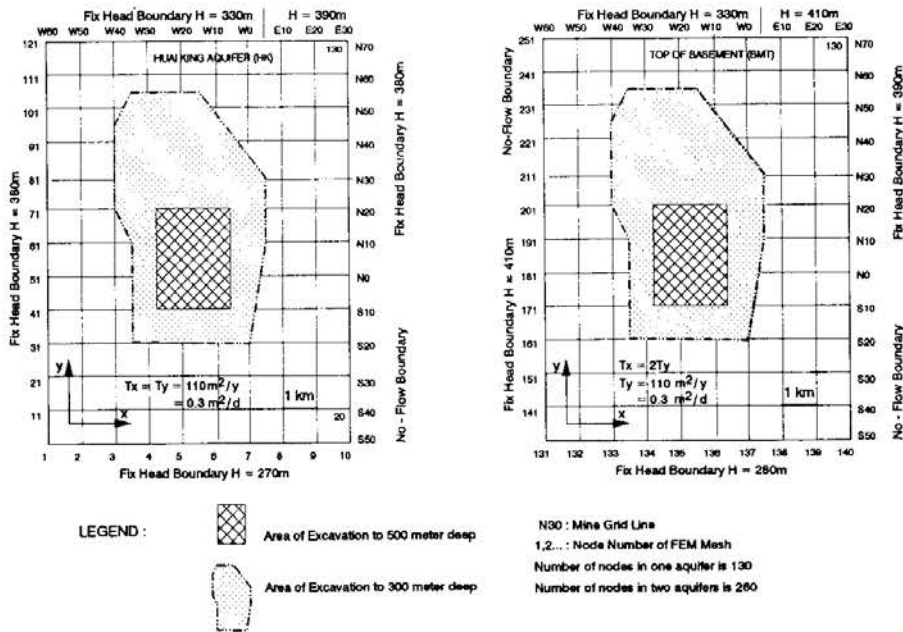
(1) MODEL 1 - This model simulates a 2-aquifer system consisting of the whole Huai King aquifer (HK) and Top of Basement aquifer (BMT). On top is a very thick aquitard consisting of Huai Luang (HL) and Na Khaem (NK), Triassic



## HONJO and GIAO



**Fig. 7 Hydrogeological Models used in Groundwater Flow Analysis**



**Fig. 8 Hydraulic Parameters and FEM Mesh Used for MODEL 1**

crystalline limestone constitutes the substratum. From seismic data (Vogwill, 1991), a lot of faults were identified both in Huai King and Top of Basement. The Top of Basement aquifer is assumed to be anisotropic with  $T_x = 2T_y$ , where  $T_x$  is transmissivity in E-W direction, while  $T_y$  is the transmissivity along N-S direction. The reasoning of anisotropy is due to limestone stratification and the fault presence.

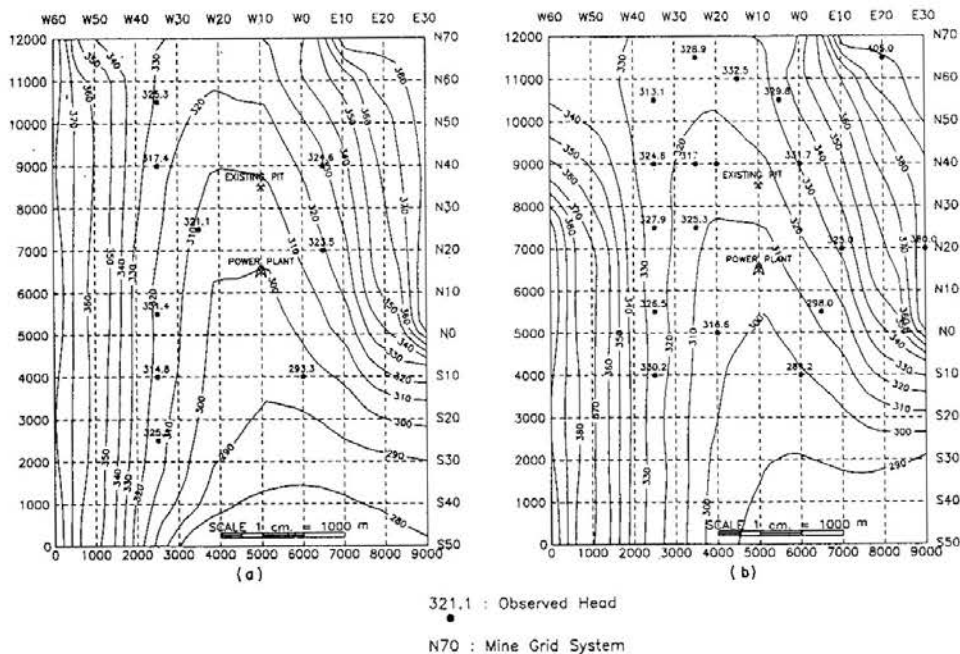
## GROUNDWATER MODELLING

The anisotropy coefficient, which is 2, was chosen by trial and error during the model calibration.

The finite element mesh is shown in Fig. 8. A mesh of rectangular elements  $1.0 \times 1.0$  km has been used to cover the central area of the basin, whose area is  $9 \times 12$  km<sup>2</sup> corresponding to a set of 130 nodes ( $10 \times 13$ ) for each aquifer and a total of 260 nodes for two aquifers.

The boundary conditions are shown in Fig. 8. For the Top of Basement aquifer, the northwestern boundary is of no-flow type because of the presence of the assumed low permeability permo-triassic volcanics. The southeastern boundaries for both aquifers are set up to be no-flow boundaries due to the presence of Hong Hoi formation (TR3) of crystalline limestone. The northern and southern boundaries are assumed to be fixed head boundaries to check one of the geological interpretations of the EGAT geologists, which state that main groundwater flow into the mine area in the central part of the basin is from north to south (Vogwill, 1991).

The model results are shown in Fig. 9 a & b. The head distributions fit to head observations in both aquifers rather well. A notable feature of head distribution is steepened hydraulic gradient on the eastern and western sides, while in the central and southern parts the head gradient is gentle. From the head distributions of Huai King and Top of Basement aquifers, one realizes the existence of three flow components, namely, from North to South, from East and West to the central part and



**Fig. 9a** Head Distribution Obtained by FEM Analysis for MODEL 1 - Huai King Aquifer (HK)

**Fig. 9b** Head Distribution Obtained by FEM Analysis for MODEL 1 - Top of Basement Aquifer (BMT)

upward flow from the lower equifer to the upper one. This was investigated in more detail by MODEL 2.

(2) **MODEL 2** The whole aquifer system of Mae Moh Basin is divided into 6 smaller components as shown in Fig. 7.

The finite element mesh is shown in Fig. 10a. A mesh of  $1.0 \times 1.0$  km has been used to cover an area of  $9 \times 12$  km<sup>2</sup> from N70 to S50 and from W60 to E30, which is the same as Model 1. The number of nodes in each component aquifer is 130 and the total number of nodes for 6 aquifers is 780 nodes.

The boundary conditions and hydraulic parameters for this 6-layer model is presented in Fig. 10a. The anisotropy coefficient of 2, i.e.  $T_x = 2T_y$ , was used for the lower aquifers as shown in Fig. 10a. The setting of boundary conditions follows model 1, i.e. most boundaries are of fixed head type, only the southeastern part, where crystalline limestone of Hong Hoi formation (TR3) occurs, is assumed to be a no-flow boundary. The whole western boundary was, however, set up to be a fixed head boundary for all six aquifers.

The results obtained are plotted in Fig. 10b. The major features of head distribution in each component aquifer are similar to the ones obtained in Model 1. Vertical flow is clearly illustrated by using flow vector picture as follows:

*Quasi-3D Flow Picture* : it has been attempted to calculate the flow vector distribution for two vertical sections, one along N30 mine grid line (E-W or X-direction) and another one along W0 grid line (N-S or Y-direction). The flow vector has been calculated with  $k_x = k_y = 2.0$  m/y ( $5.48 \times 10^{-3}$  m/d),  $k_z = 2.0 \times 10^{-4}$  m/y

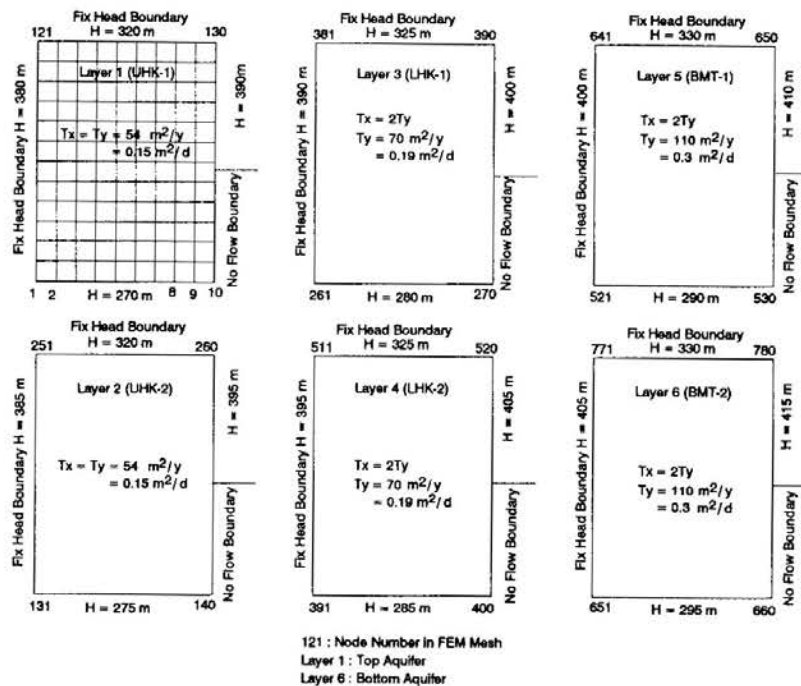
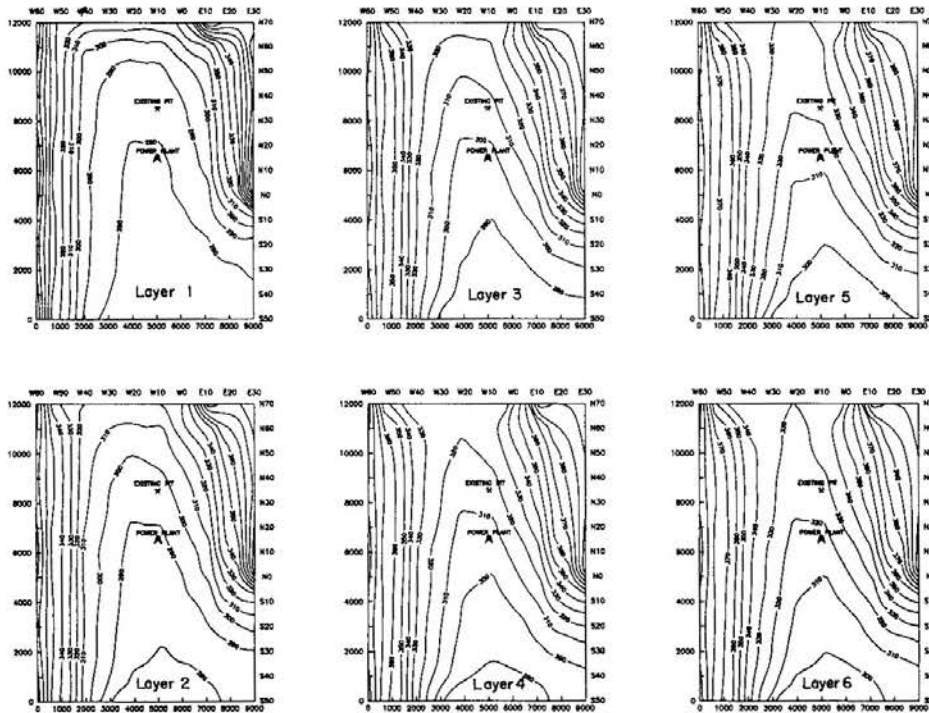


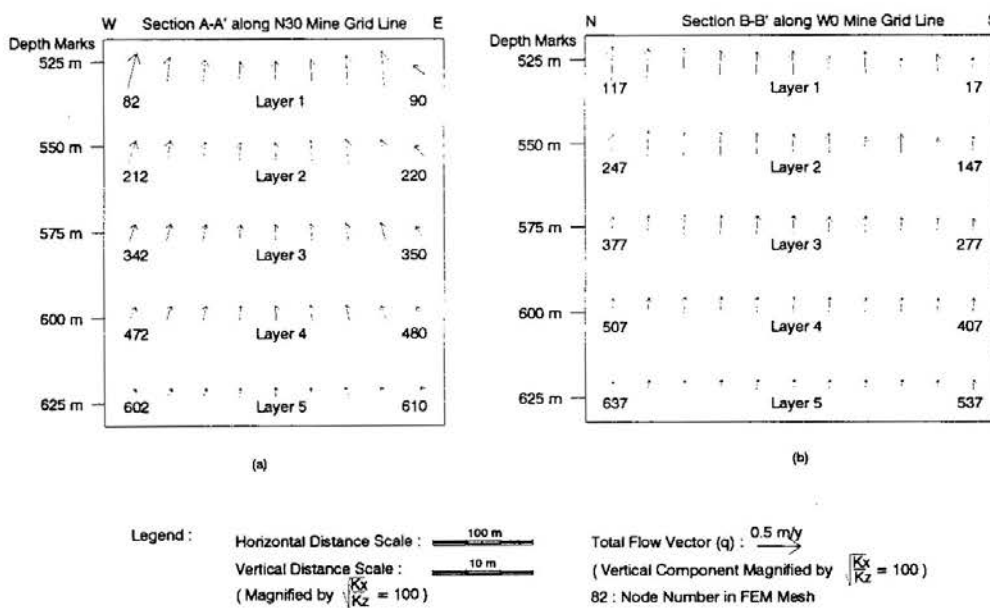
Fig. 10a Hydraulic Parameters and FEM Mesh Used for MODEL 2

## GROUNDWATER MODELLING



**Fig. 10b Head Distribution Obtained by FEM Analysis for MODEL 2**

( $5.48 \times 10^{-7}$  m/d). The resultant flow vectors are shown in Fig. 11a & b. They reveal the existence of a pronounced upward vertical flow zone in the central part of the basin as McMahon & Forth (1988) and Vogwill (1990) expected.



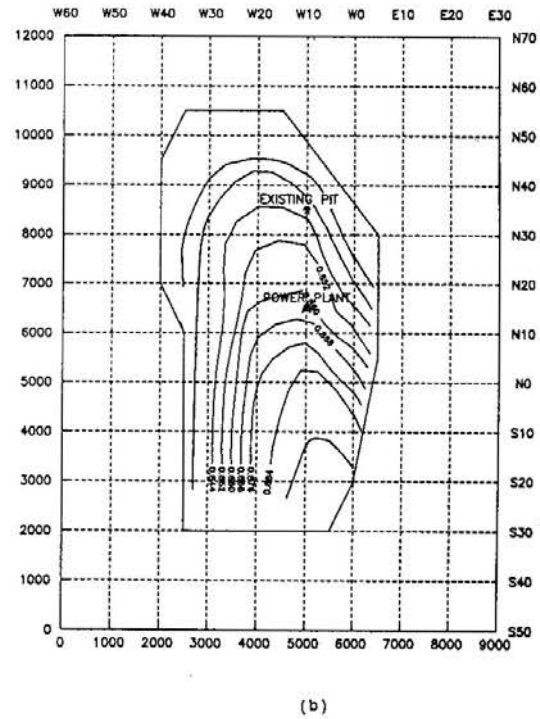
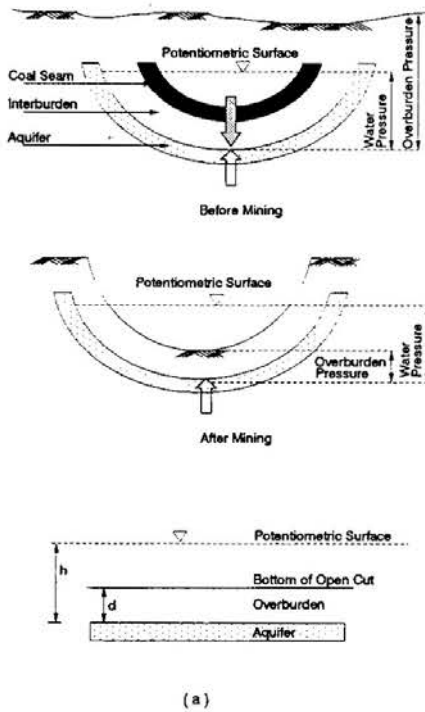
**Fig. 11 Quasi-3D Flow Picture in Vertical Sections of Mae Moh Mine**

**Calculation of Factor of Safety**

*Excavation and Factor of Safety* : Related to high water pressure, the floor heave is one of main concerns for excavation stability (Fig. 12a). The factor of safety against floor heave is defined as the ratio between the weight of material overlaying the equifer and the force exerted by the aquifer water pressure (Fraser Pitt, 1979) Fraser and Pitt, 1979) and expressed as follows:

$$FS = \frac{\gamma \cdot d}{\gamma_w \cdot h} \tag{4}$$

where



**Fig. 12 Floor Heave and Factor of Safety.**

- FS : Factor of safety against floor heave
- h : Aquifer water pressure, m
- d : Thickness of overlaying material layer (Overburden), m
- $\gamma$  : Total density of overburden, g/cm<sup>3</sup>
- $\gamma_w$  : Density of water, g/cm<sup>3</sup>

In this case, the distribution of the factor of safety has been calculated for an area, which is planned to be excavated to the depth of 300 m and 500 m below the original ground surface (Fig. 8). The overburden thickness d, i.e. the thickness from the open cut bottom to the aquifer roof (Fig. 12a) is assumed to be constant and equal to 120 m based on phase 1 results. The excavated overburden total unit weight

## GROUNDWATER MODELLING

averages  $2.20 \text{ g/cm}^3$ . The calculations take into account the head values of the Top of Basement Aquifer (BMT) from MODEL 1 (Fig. 9b). It can be seen that the factor of safety varies from 0.84 to 0.88 (Fig. 12b), which suggests the necessity of depressurizing in future stages of mine excavation.

### CONCLUSIONS

The following conclusions are drawn from the preliminary groundwater modelling of Mae Moh Lignite Basin:

(1) The groundwater flow system in Mae Moh Basin Area is characterized by the general features of small basins (Sullivan & Burman, 1985) in such aspects as : existence of strong upward hydraulic gradients; existence of limestone with karstic development; existence of a weathered rock layers at the base of the tertiary rock; the faults occur in the basement and along the basin margins, which can be locations of extensive groundwater flow.

(2) The basic components of the hydrological model of Mae Moh basin are two major aquifers, i.e Huai King (HK) and Top of Basement (BMT) together with an effective aquitard formed by Huai Luang (HL) and Nakhaem (NK) on top and a fine crystalline Triassic Limestone rock sub-stratum. These two major aquifers are not simple confined ones; they can be separated into smaller component aquifers constituting a leaky multiaquifer system due to high heterogeneity and discontinuity of many permeable and impermeable layers. Any groundwater modelling carried out here should take into account this characteristic.

(3) There are three dominant flow directions, e.g. North to South, east and West to the central part and upward vertical flow. The basin is, therefore, open in the South. The authors' opinion is that the flow from East and West to the central area is more important than the flow from North to South, because only by calibrating the eastern and western boundary conditions could a reasonable head distribution be obtained. The anisotropy of Top of Basement in E-W direction, due to limestone stratification and probably faults, seems to have a strong influence on the head distribution.

(4) For such an aquifer system, a quasi-3D model can be successfully used in characterizing the seepage flow of a small basin like Mae Moh Basin in an effective way

(5) The observed head values in the Basement do not expose a smooth spatial variation, one often sees a low value next to a high value. This might suggest the necessity of introducing a model of flow in fractured media, e.g. double porosity model (Stretsova-Adams, 1974; Huyakorn et al, 1983).

(6) The deepening of open pit mine to the depth of 300 m or 500 m in the central part of basin might require depressurization. However, to draw an accurate conclusion on this aspect as well as to design an adequate depressurization scheme more hydrogeological data are needed.

### ACKNOWLEDGEMENTS

The authors would like to express their sincere appreciation to The Electricity Generation Authority of Thailand, to the Mae Moh Mine Operation Department in general and Groundwater Project in particular for providing data concerning Mae Moh Lignite Basin. The authors deeply acknowledge Dr. Noppadol Phien-wej, Associate Professor, Geotechnical and Transportation Engineering Division, AIT and Mr. Somchai Plangpongpun, Chief of Geotechnical Division, Mine Engineering Department, EGAT for their valuable discussion and correction, which helped to bring the study results to this final form.

### REFERENCES

- CANMET (1977). *Pit Slope Manual. Chapter 4, Groundwater*. Ministry of Supply and Services Canada.
- EGAT (1985). *Mae Moh Coal Deposit, Geological Report*, Thailand-Australia Lignite Mines Development Projects. Chapter 4.
- EGAT (1991). *Mae Moh Lignite Mine*. Introduction Document.
- EVANS P.R. and S. JITAPUNKUL (1989). *Geology of The Mae Moh Basin, Northern Thailand*. EGAT Technical Report, 1989.
- EVANS P.R. (1990). *Notes on the Geology of The Mae Moh Basin*. EGAT Technical Report, Feb., 1990.
- FRASER C.I. and H.A. PITT (1979). Artesian Dewatering Operations at Morwell Open Cut. Proc. 1st Intern. Mine Drainage Symp. Denver Colorado, May 1979.
- FUJINAWA K. (1977). Finite Element Analysis of Groundwater Flow in Multiaquifer Systems, II. A Quasi Three-Dimensional Flow Model. J. Of Hydrology, 33 (1977) 349-362.
- HERRERA I.J.P. HENNART and R. YATES (1980). A Critical Discussion of Numerical Models for Multiaquifer Systems. Advanced Water Resources, Vol. 13, pp. 159-163.
- HOSSAIN Z. (1990). *Quasi-3D Modelling of Multi-Aquifer with reference to Ground Subsidence*. AIT Thesis no GT-89-14, Bangkok, Thailand.
- HUYAKORN P.S. and G.F. PINDER (1983). *Computational Methods in Subsurface Flow*. Academic Press, Inc., New York.
- HUYAKORN P.S., H.L. BARRY and R.F. CHARLES (1983). Finite Element Techniques for Modelling Groundwater Flow in Fractured Aquifers. Water Resources Research, Vol. 19. No. 4, pp. 1019-1035.
- McMAHON B.K. and J. FORTH (1989). *Review of Geotechnical Evaluation*. EGAT Technical Report. Jan 1989.

- MERCER J.W. and C.R. FAUST (1980). Ground-Water Modeling : An Overview. Ground Water, Vol. 18, No. 2, pp. 108-115.
- NEUMANN S.P. and P.A. WITHERSPOON (1969). Applicability of current theories of flow of leaky aquifers. Water Resources Research, Vol. 5, No. 4, pp. 817-829.
- NEUMANN S.P., C. PRELLER and I.N. NARASIMHAN (1982). Adaptive Explicit-Implicit Quasi Three-Dimensional Finite Element Model of Flow and Subsidence in Multiaquifer System. Water Resources Research, Vol. 18, No. 5, pp. 1551-1561.
- STRETSOVA-ADAMS, T.D. (1978). Well Hydraulics in heterogeneous aquifer formations. Adv Hydrosci., 11, 357-423.
- SMITH I.M. and D.V. GRIFFITHS (1988). *Programming the Finite Element Method*. John Wiley & Sons.
- SULLIVAN T.D. and B.C. BURMAN (1985). Geological and Geotechnical Aspects of Small Basins and Their Effects on Mining. IMM Conference, Asian Mining 85, Manila.
- TANDICUL W. (1991). *Criteria for the Design of Mae Moh Drainage System*. EGAT Technical Report.
- TOTH J. (1963). A Theoretical Analysis of Groundwater Flow in Small Drainage Basins. Journal of Geophysical Research 68 (10) : 4795-4812.
- VOGWILL R. (1989). *Mining Geology and Open Pit Depressurization*. EGAT Technical Report, Aug. 1989.
- VOGWILL R. (1990). *Hydrogeological Review*. EGAT Technical Report, Oct. 1990.
- VOGWILL R. (1991). *Hydrogeological Review*. EGAT Technical Report, Jun. 1991.
- VOIGT R. (1991). *Hydrogeological Review*. EGAT Technical Report, July 1991.



# HYPERBOLIC METHOD FOR EVALUATION OF SETTLEMENT OF GROUND PRETREATED BY DRAINS AND SURCHARGE

S.A. Tan<sup>1</sup>

## SYNOPSIS

The common method of determining degree of soil improvement in clay deposits treated with vertical drains and surcharge is by means of the settlement record, where the degree of settlement is a reliable measure of the degree of consolidation achieved. Thus, reliable estimation of the ultimate settlement is critical to the estimate of degree of soil improvement before surcharge removal is permissible. The rectangular hyperbola fitting method ( $T_v/U$  vs  $T_v$ ) is extended to the case of drains and surcharge by considering the hyperbolic plots for combined vertical and radial flow consolidation in a soil cylinder with varying thickness of clays and drain spacing ratio for typical soil properties of marine clays with  $c_v$  of 1 to 5 m<sup>2</sup>/yr, and  $c_h/c_v$  ratio of 3. The results showed that the hyperbolic plots have an initial linear portion between  $U_{50\%}$  and  $U_{90\%}$  and linear regression gives the values of these slopes with regression coefficients of at least 0.99. For the lines radiating from the origin to  $U_{50\%}$  point the slope is ( $1/0.5 = 2.0$ ), and to the  $U_{90\%}$  point the slope is ( $1/0.9 = 1.11$ ). Thus the ratio of the slopes of these radiating lines to the slope of the initial linear portion of the hyperbolic plots enable the identification of the  $U_{50\%}$  and  $U_{90\%}$  for any settlement record using drains and surcharge. With these points, the ultimate settlement can be estimated as twice the settlement of the 50% point, or 1.11 the settlement of the 90% point. The method is examined through a case history, involving sand drains at Ska-Edeby, Sweden, where long term settlements and pore pressures data of 14 years are available. For the long term loading tests at Ska-Edeby, the prediction of ultimate settlement by the proposed method agrees very well with actual records. Thus, the method can serve as an additional simple means, apart from compressibility calculations, of monitoring the progress of consolidation for ground treatment with drains and surcharge.

## INTRODUCTION

The use of vertical drains and surcharge to accelerate the consolidation of thick deposits of clay for soil improvement is well established. Several methods are available to evaluate the degree of soil improvement achieved. These include the monitoring of the amount of pore pressure dissipation, the gain in undrained shear strength, the average degree of consolidation from settlement records and the gain in preconsolidation pressures in the treated clays before and after surcharge application. Of these methods, the two most reliable indicators of the degree of improvement were settlement records to determine the average degree of consolidation achieved and care-

---

<sup>1</sup>Senior Lecturer, National University of Singapore, Singapore 0511.

fully determined preconsolidation pressures before and after soil treatment (Hansbo 1981). To determine the average degree of consolidation, taken as the average degree of settlement, reliable estimate of the ultimate settlement is necessary.

Apart from calculating the ultimate settlement from one-dimensional compression properties of the sublayers, which is the standard practice, the ultimate settlement can also be estimated from a rectangular hyperbolic plot of time/settlement vs time of the settlement records, where at large time, the inverse of the slope of the hyperbolic plot is an estimate of the ultimate settlement. Sridharan and Sreepada, 1981 has shown how the rectangular hyperbola method can be used to obtain the coefficient of consolidation,  $c_v$  from oedometer tests. Yoshikuni et al 1981 reported the Japanese experience in using the hyperbolic method for field monitoring of the consolidation process, but the work is only available in Japanese. Tan et al 1991 extended the work to cover the case of finite strain consolidation with nonhomogeneous initial conditions and nonlinear compression properties and permeabilities in clay-sand mixes. In the latter work, it is reported that the hyperbolic method is particularly useful in the field because the field data also incorporate the effects on secondary compression which often cannot be separated from the primary compression settlements.

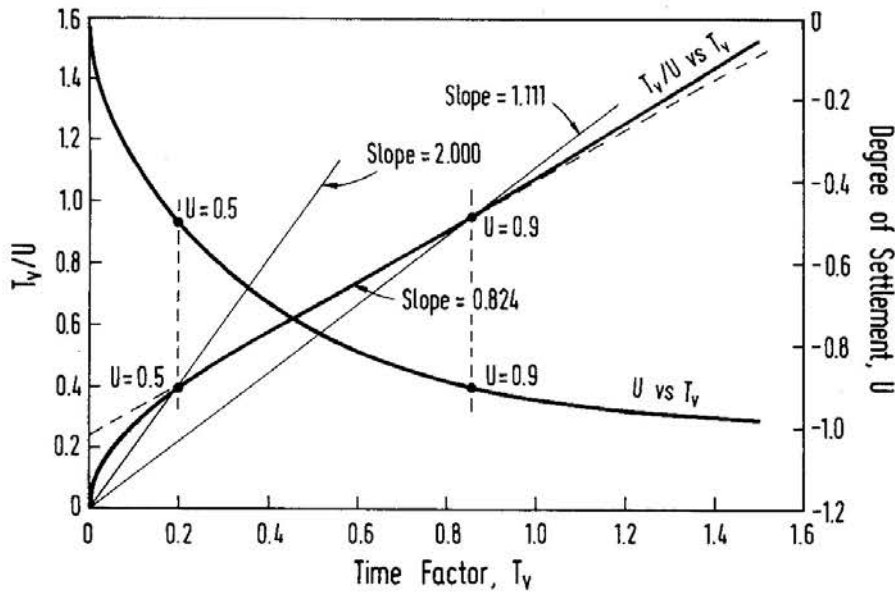
In this paper, a careful study of the hyperbolic method is made to see at what range do the consolidation settlement record for infinitesimal strain theory actually converge to the linear hyperbolic plot. This is done for both the vertical flow (Terzaghi) type and the combined problem of the vertical and radial flow (Barron) type consolidation which describes fairly well the field behavior of clays with vertical drains and surcharge. This method was proposed by Tan (1993), with a preliminary examination of one of the settlement record of the Ska-Edeby test field. The results are now applied to all available settlement records of the well documented case history involving vertical sand drains at Ska-Edeby, Sweden to validate its applicability in a situation where measured field primary and ultimate settlements are both available. It can be seen that judicious use of the method can predict both the primary and the ultimate settlements once field data within the 50% and 90% consolidation stage becomes available.

## HYPERBOLIC METHOD

### *Application to Terzaghi Theory*

The hyperbolic method is well known in other areas of mechanics. In soil mechanics, the settlement of vertical piles has been shown to follow the hyperbolic rule (Chin 1971). Terzaghi theory gives a unique settlement-time plot in terms of  $U$ , the average degree of consolidation versus  $T_v$ , the time factor as shown in Fig. 1. Following Sridharan and Sreepada 1981, a plot of  $T_v/U$  versus  $T_v$  obtained from Terzaghi consolidation theory is also shown in Fig. 1. This plot starting from the

## HYPERBOLIC METHOD



**Fig. 1 Hyperbolic Plot of  $T_v/U$  vs  $T_v$  for Terzaghi Theory**

origin, is a concave curve for some portion initially, but approaches an initial straight line over a range of values of  $T_v$  between 0.25 to 0.9, corresponding to percent  $U$  values between 60% to 95%. For practical applications, without a significant drop in accuracy, the initial straight portion can be assumed to be between  $U$  of 50% to 90%, which are points of interests in soil mechanics (corresponding to  $T_v$  of 0.196 to 0.848). The average slope of this line is 0.824, and analysis of  $U$  versus  $\Delta(T_v/U)/\Delta T_v$  shows a variation of  $\pm 0.04$ , which is 5% of the average value of 0.824. If the straight line portion of the curve is represented by the equation.

$$\frac{T_v}{U} = \alpha T_v + \beta \quad (1)$$

From Eq.(1), it is obvious that as  $T_v \rightarrow \infty$ ,  $1/U \rightarrow \alpha$ . Thus, for large values of  $T_v$ , the degree of consolidation is given by  $1/\alpha$ , which is the inverse of the slope of Eq.(1). The settlement at any time  $T_v$  can now be easily calculated from Eq.(1) once sufficient data are available to show that the behavior approaches the linear hyperbolic line and that  $\alpha$  and  $\beta$  (the slope and intercept of straight line portion) can be estimated.

A few points should be noted. First, the hyperbolic settlement prediction is only valid for  $U$  between 50% to 90%, if  $\alpha$  is taken to be the slope between these points. For  $U$  less than 50%, the settlement estimated by the hyperbolic line will be an under-estimate, whereas for  $U$  more than 90% the hyperbolic method will over estimate the theoretical settlement. The slope of the straight line portion ( $U = 60\%$  to  $95\%$ ) of the theoretical curve is  $\alpha = 0.824$ . This corresponds to an ultimate settlement of  $1/0.824$  which is 1.21, an overestimate of ultimate primary settlement of 21%, which is unacceptable. Thus for the inverse slope method to work as a means of

predicting ultimate settlement, two approaches are possible. The first approach is to use the inverse of the slope of the initial linear segment of the hyperbolic fitted field data ( $1/S_i$ ), and multiply it by the theoretical slope  $\alpha$ . This should give an estimate of the ultimate primary compression. The second approach is the inverse of the slope of the final linear segment involving data beyond the 90% point. This would be an estimate of ultimate settlement including the effects of secondary compression. As data beyond 90% consolidation is needed, this approach is less useful for field monitoring applications.

However, if radiating lines from the origin is drawn to the  $U = 50\%$  and  $U = 90\%$  points on the hyperbolic line, the corresponding slopes are  $1/0.5$  and  $1/0.9$ , which are 2.00 and 1.11 respectively. This represent slopes of 2.43 and 1.35 times of the linear portion. Using this knowledge, the settlement points at 50% and 90% degree of consolidation can be determined from the field data. Firstly, the field data are replotted as  $t/\delta$  vs  $t$  plot, from which the initial straight line portion can be discerned, and the slope  $S_i$  determined. This portion should actually be somewhere between 50% and 90% degree of consolidation. Next, two straight lines, having slopes 2.43 and 1.35 times of the slope  $S_i$ , are drawn from the origin, which will intersect the  $t/\delta$  vs  $t$  plot at the points representing the 50% and 90% degree of consolidation points, respectively. Hence the ultimate settlement can be estimated as  $1/0.5 \delta_{50}$  or  $1/0.9 \delta_{90}$ , which theoretically should give the values of the ultimate primary compression, ignoring the secondary compression effects. To make the method useful in field consolidation applications, it has to be extended to the case of clay deposits pretreated with vertical drains (either sand drains or prefabricated flexible drains) and surcharge which is the common situation in soil improvement for soft clays.

#### ***Application to Vertical Drains and Surcharge***

The consolidation process in soils of low permeability accelerated by vertical drains can be described by Barron's (1948) solution. According to Hansbo (1981), the ideal drain without the effects of smear and well resistance on the average degree of consolidation  $U_h$  at a certain depth  $z$  and at any time  $t$  can be described by the following relationships:

$$U_h(t) = 1 - \exp\left[\frac{-8T_h}{\mu}\right] \quad (2a)$$

Time factor  $T_h = c_h t / D^2 \quad (2b)$

$$\mu = n^2 / (n^2 - 1) \log_e(n) - (3n^2 - 1) / 4n^2 \quad (2c)$$

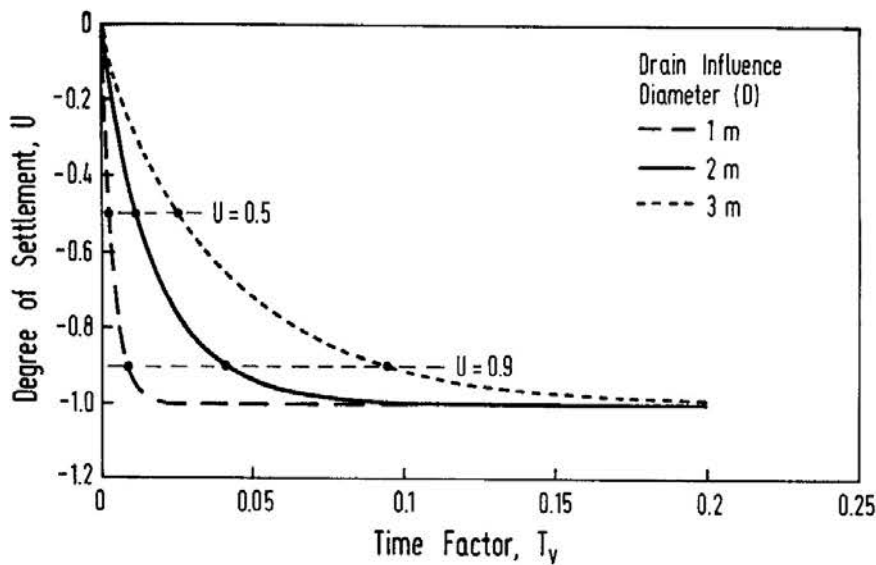
where  $n$  = drain spacing ratio,  $D/d$ ;  $D$  = diameter of equivalent cylinder of soil influenced by each drain, which is equal to 1.13s for a square pattern and 1.05 s for a triangular pattern;  $s$  = drain spacing;  $d$  = diameter of sand drain or equivalent diameter of prefabricated flexible drain, for which Hansbo (1981), recommended that  $d = 2(a + b)/\pi$ . The average degree of consolidation (which is also the degree of primary settlement) of a soil cylinder due to combined vertical drainage in

## HYPERBOLIC METHOD

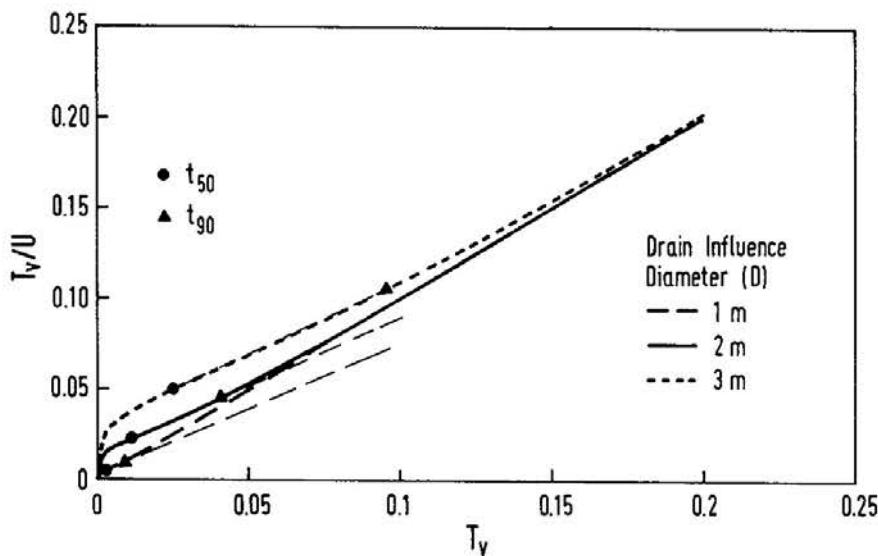
the clay and radial drainage into a vertical drain is obtained from Carillo (1942) as

$$U = 1 - (1 - U_v)(1 - U_h) \quad (3)$$

Using the Terzaghi solution for  $U_v$  and Eqs. 2 and 3, the theoretical settlement time curves for a variety of practical vertical drain problems for the range of soil parameters ( $c_v$  and  $c_h$  of 1 to 5  $\text{m}^2/\text{yr}$  for  $c_h/c_v$  of 3, clay drainage depth of 2.5 to 12.5 m) and drain installation parameters (drain spacing ratio,  $n$  of 5 to 70) in typical marine clays were produced. A typical settlement plot and the corresponding hyperbolic plots for the specific case of a clay layer with drainage depth of 10 m, and  $c_v = 1$  and  $c_h = 3 \text{ m}^2/\text{yr}$ , with equivalent drain diameter  $d = 50 \text{ mm}$  for drain influence diameter,  $D$  of 1 to 3 m are shown in Figs. 2a-b. The unique characteristics



**Fig. 2a Typical Plots of  $U$  vs  $T_v$  for Drains and Surcharge**



**Fig. 2b Typical Hyperbolic Plots of Data from Fig. 2**

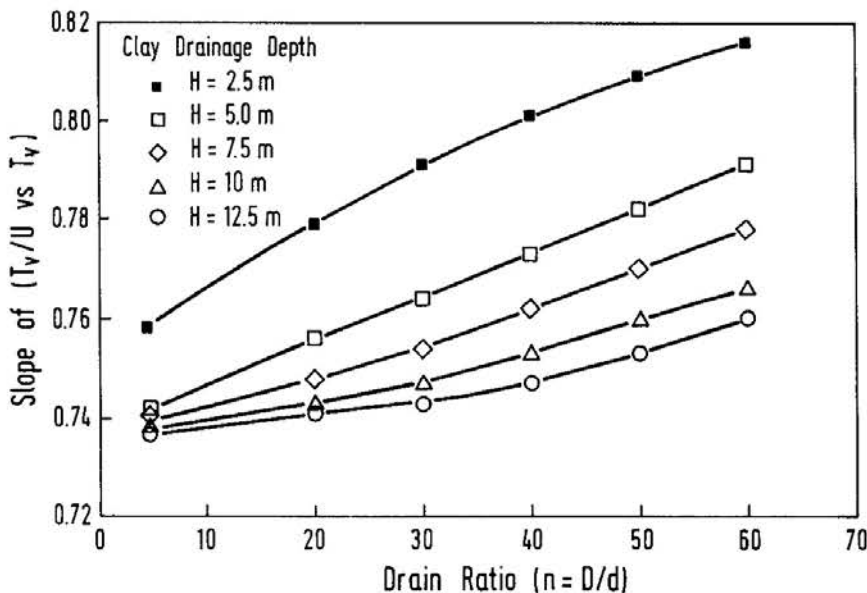
of all the hyperbolic plots are the initially concave curved portion, followed immediately by the initial straight-line linear portion from the  $U = 50\%$  to  $U = 90\%$  points on the settlement curves. After the  $U = 90\%$  point, the curve tends toward a second straight-line portion which is much steeper than the first. The slopes of the radiating lines from the origin through the  $U = 50\%$  point is 2.00, and through the 90% points is  $1/0.9 = 1.11$ . Thus if  $S_i$ , the slopes of the initial linear portion of the hyperbolic plots between the  $U = 50\%$  and  $U = 90\%$  are known during field monitoring of settlements, the slopes of the  $U = 50\%$  and  $U = 90\%$  radiating lines can be determined as follows:

$$S_{50} = (1/0.5)(S_i / \alpha) \tag{4}$$

$$S_{90} = (1/0.9)(S_i / \alpha) \tag{5}$$

When these lines are plotted, the intercept of these lines with the field  $t/\delta$  vs  $t$  line will locate the 50% and 90% settlement points on the field settlement curve, once sufficient settlement data is available to identify the first linear portion on the field settlement hyperbolic plot. This, in essence, is the power of the hyperbolic method for monitoring settlement behavior of clay deposits with drains and surcharge.

The slopes  $\alpha$  of the first linear portion of these hyperbolic settlement plots between the 50% and 90% settlement points for a comprehensive range of practical drain installations as defined above were determined and plotted in Fig. 3. From the parametric studies, it is found that the values of this slope is not very sensitive to the values of  $c_v$  and  $c_h$  used (1 to 5  $m^2/yr$ ), but is strongly dependent on the clay drainage depth and the drain spacing ratio as depicted in Fig. 3. It is observed that the slope  $\alpha$  vary from as low as 0.73 to as high as 0.824, which is the case without vertical



**Fig. 3 Relationship of Slopes of Linear Portion of Hyperbolic Plots with Drain Spacing Ratio,  $n$ , and Clay Drainage Depth,  $H$ , for Drains and Surcharge for  $c_h/c_v$  of 3**

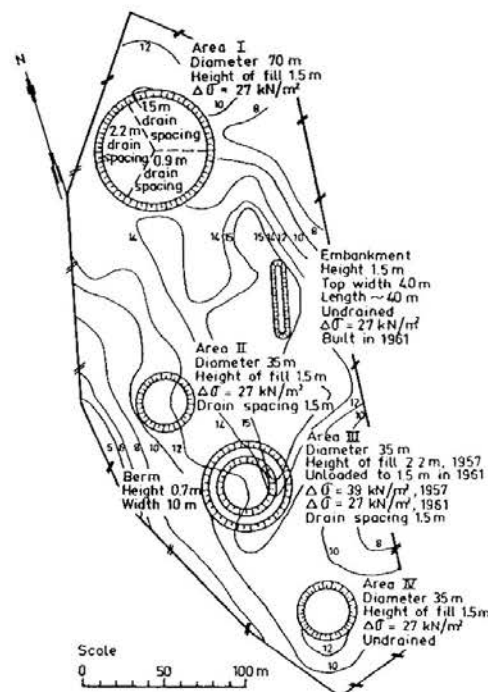
## HYPERBOLIC METHOD

drains. It is obvious that as the clay thickness is reduced and drain spacing is increased, the situation converge to that of Terzaghi consolidation without vertical drains. These results will now be used to re-examine settlement data from the well documented long-term case history of Ska-Edeby, Sweden.

### LONG-TERM LOADING TESTS WITH SAND DRAINS AT SKA-EDEBY, SWEDEN

This well documented case history was created by the Swedish Geotechnical Institute in 1957, in connection with the use of vertical sand drains for a new airport in Stockholm, Sweden. The test site 25 km west of Stockholm, as shown in Fig. 4, consists of four extensively instrumented circular test fills up to 70 m in diameter, three of which are provided with sand drains of 18 cm diameter with varying spacing, which details were reported by Hansbo (1960). The soils are soft, normally consolidated, medium sensitive post-glacial and glacial varved clays, 9 to 15 m thick. The summaries of 14 years of settlement and pore pressures observations were presented and analyzed by Holtz and Broms (1972).

For the scope of this paper, all the detailed settlement records of test fills Area I, II and IV are considered. These are settlements V03, V08 and V13 of Area I, which are test fills in clays of about 10 m depth with drained boundaries at both ends, with 18 cm diameter vertical sand drains at triangular spacings of 2.2, 0.9 and 1.5 m

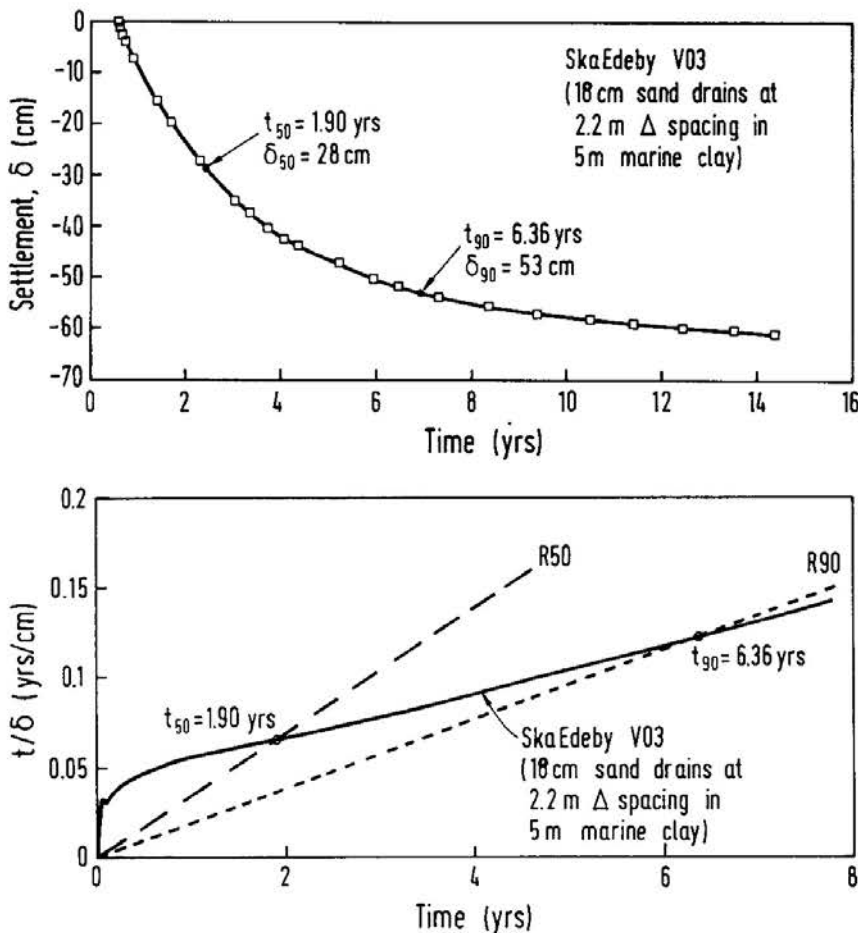


PLAN OF THE SKA-EDEBY TEST FIELD. CONTOUR LINES INDICATE DEPTH TO FIRM BOTTOM, IN m.

**Fig. 4 Plan of the Ska-Edeby Test Field**

respectively. Area II is a smaller test fill of 35 m diameter pretreated with 0.18 m vertical sand drains at 1.5 m triangular spacings, and Area IV is a test fill of 35 m diameter of an untreated area. The indicated settlements correspond to compression of the 5 m thick clay layer located between 2.5 m and 7.5 m below the ground surface, measured by screw-type deep settlement gages. The behavior of this layer was analyzed by Hansbo (1960) and Holtz and Broms (1972) because the clays above 2.5 m are undoubtedly overconsolidated due to dessication. The surcharge load of 1,5 m fill was an initial load of 27 kPa, but the net applied load decreased with time due to the settlement of the fill into the high water table, reducing the load to a constant value of 18 kPa after 1.5 years of loading.

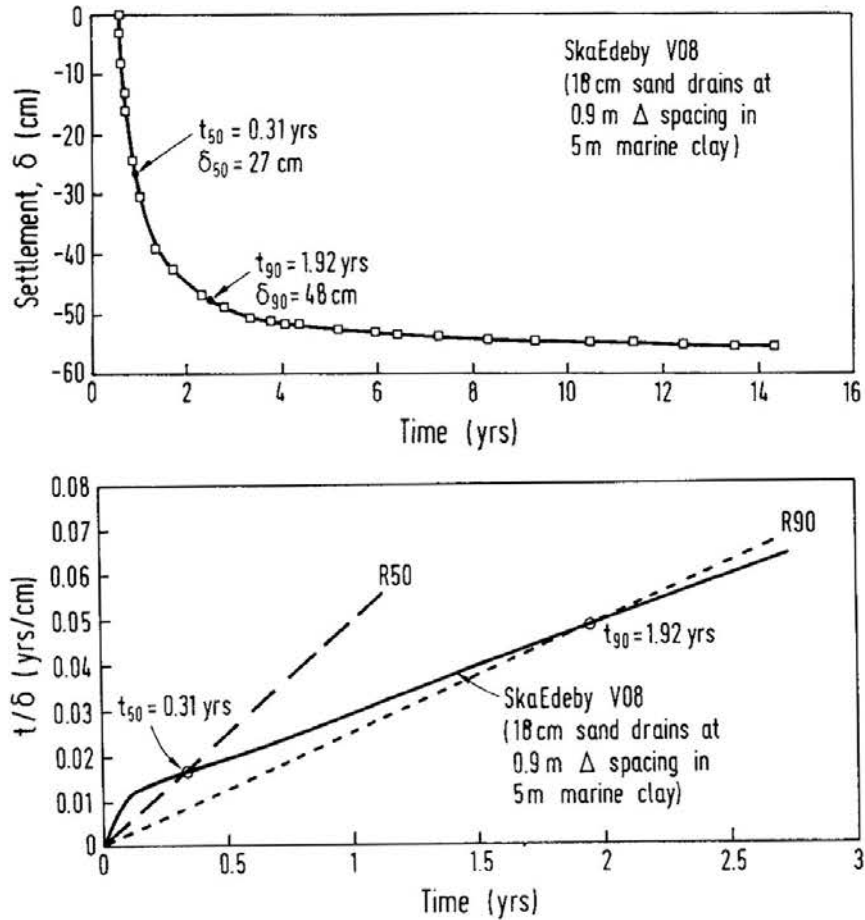
Figs. 5 to 9 present the settlement records of Area 1 (V03, V08, V13), Area II and Area IV, from 1957 to 1971, together with their corresponding hyperbolic plots. The relevant drain and soil parameters ( $n$ ,  $H$  and  $c_h/c_v$ ) for each case are tabulated in Table 1, from which the theoretical slope  $\alpha$  of the initial linear segment are determined by using Fig. 3. With the measured values of the initial linear segments of the field hyperbolic plots from Figs. 5b to 9b ( $S_1$ ), the slopes ( $S_{50}$  and  $S_{90}$ ) of the radial lines from the origin to the  $U_{50}$  and  $U_{90}$  are calculated from Eqs, 4 and 5, as shown in



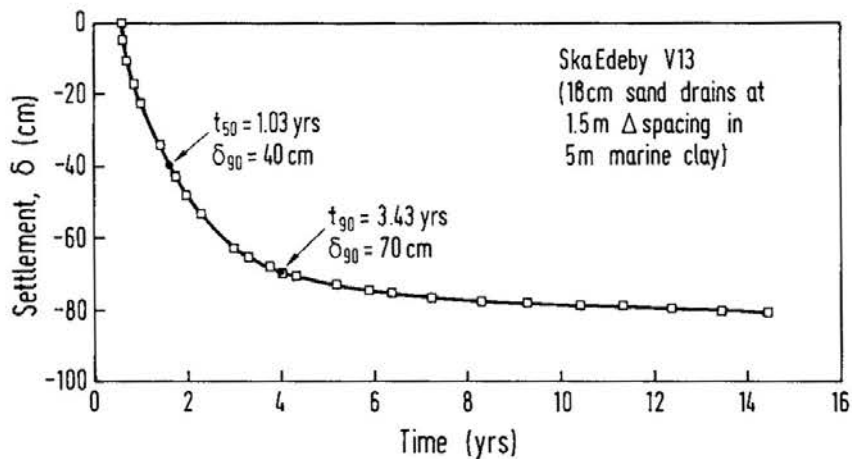
**Fig. 5a,b Settlement Record and Hyperbolic Plot of V03 (18 cm Sand Drain at 2.2 m Triangle Spacing) at Ska-Edeby**



### HYPERBOLIC METHOD



**Fig. 6a,b Settlement Record and Hyperbolic Plot of V08 (18 cm Sand Drain at 0.9 m Triangle Spacing) at Ska-Edeby**



**Fig. 7a Settlement Record and Hyperbolic Plot of V13 (18 cm Sand Drain at 1.5m Triangle Spacing) at Ska-Edeby**

Table 1. From the intercept of these lines to the hyperbolic line,  $U_{50}$  and  $U_{90}$  are identified on the field hyperbolic plot, as shown in Figs. 5b to 9b.

Table 2 summarized the comparisons of estimates of ultimate settlements with the observed primary ultimate settlement, as indicated by the complete dissipation of

TAN

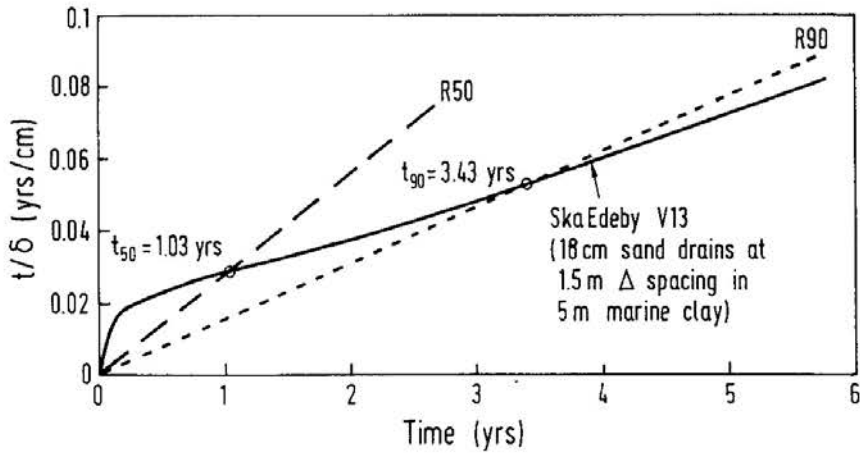


Fig. 7 b Settlement Record and Hyperbolic Plot of V13 (18 cm Sand Drain at 1.5 m Triangle Spacing) at Ska-Edeby

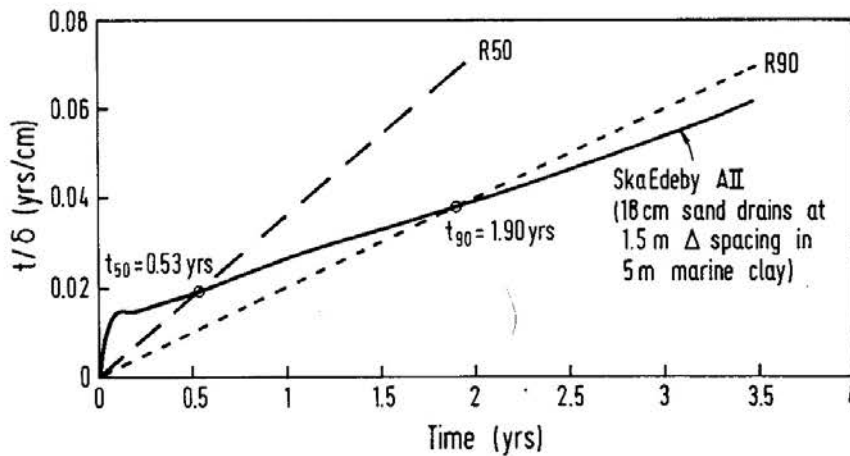
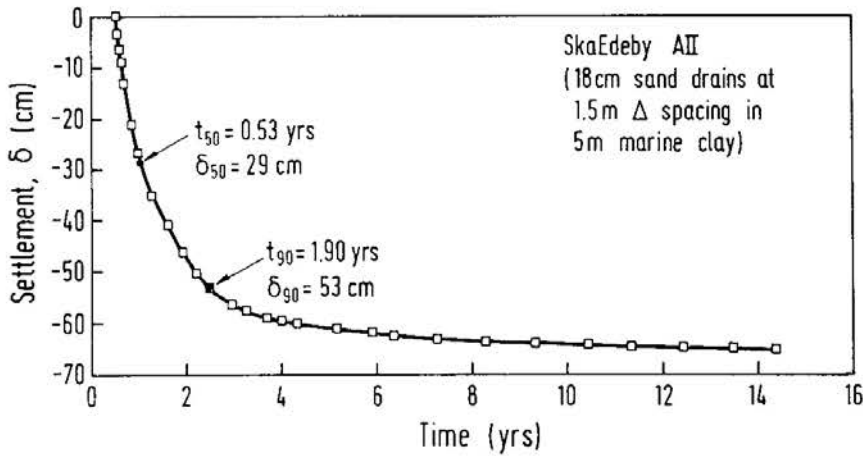
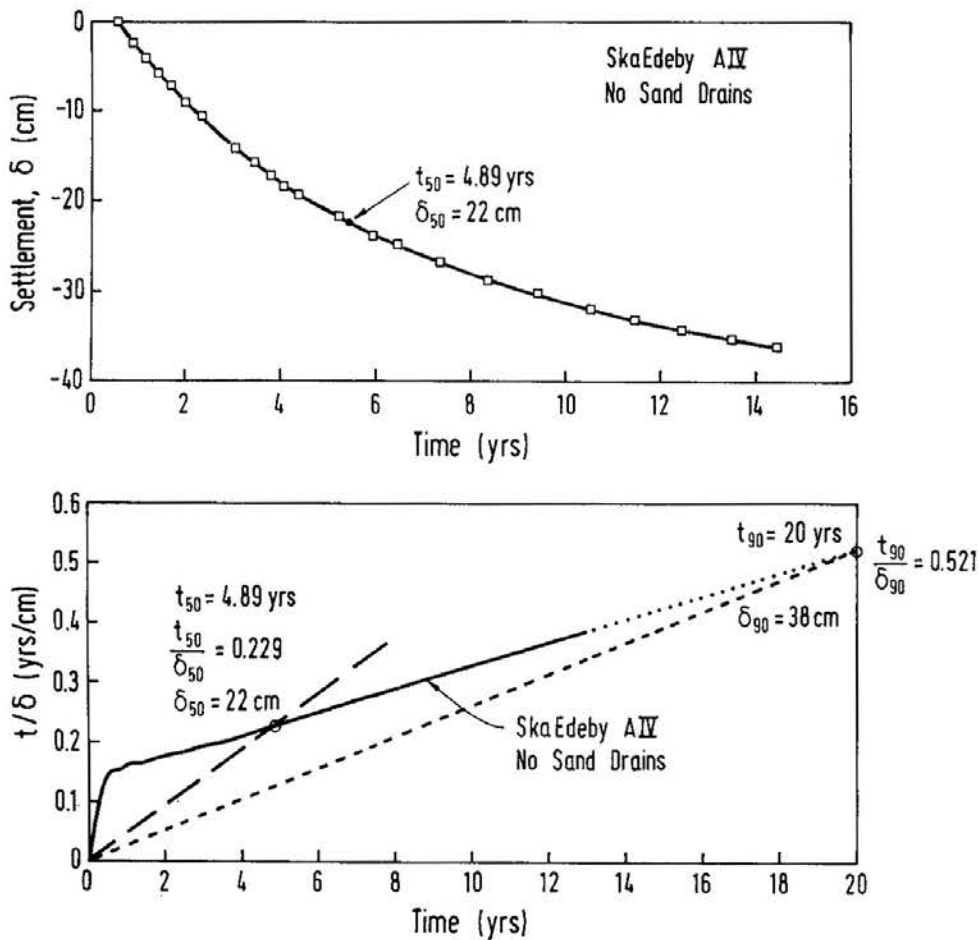


Fig. 8a,b Settlement Record and Hyperbolic Plot of AII (18 cm Sand Drain at 1.5 m Triangle Spacing) at Ska-Edeby

## HYPERBOLIC METHOD



**Fig. 9,b Settlement Record and Hyperbolic Plot of AIV (no drains test area)**

mid-plane excess pore pressures as measured by installed piezometers. The prediction of ultimate settlements can be made from the inverse of the slope of the initial linear segment multiplied by  $\alpha$  as  $(\alpha / S_i)$ , or the inverse of the slope of points beyond 90% consolidation  $(1/S_f)$ . The ultimate settlements can also be estimated from the settlements of the 50% and 90% consolidation points as  $2 \delta_{50}$  or  $1.11 \delta_{90}$ . It is observed that  $\alpha / S_i$  gave excellent agreement with the measured primary ultimate settlement, whereas  $1/S_f$  consistently over-estimate this value by 5 to 17%. The use of  $2 \delta_{50}$  and  $1.11 \delta_{90}$  estimate primary ultimate settlement to within 10%. Holtz (1972) reported that the original predictions by Hansbo (1960), using compressibility calculations are within 5% to 25% of the measured values for the Ska-edeby data.

Table 3 show the comparison of the observed ultimate settlement with the hyperbolic method estimates for the Ska-Edeby cases, after 14 years of constant surcharge loading. This correspond to settlements with about 9 to 11 years of secondary compression after complete primary consolidation in the areas pretreated with vertical drains. In this instance, it is evident that the inverse of the sloped beyond the 90% consolidation points  $(1/S_f)$  gave the best agreement with measured data. The use of all the other hyperbolic estimates would consistently under-estimate the total ultimate settlements because of the neglect of secondary compression.

**Table 1 Determination of Slopes  $\alpha$ ,  $S_{50}$  and  $S_{90}$  from Ska-Edeby Sand-drains and Soil Data**

Site and Location	Drain diam. (m)	<sup>1</sup> Drain spacing s (m)	Drain ratio n = D/d	<sup>2</sup> Clay depth H (m)	$c_v$ (m <sup>2</sup> /yr)	$c_r/c_v$	<sup>3</sup> $S_i$	Slopes		
								<sup>4</sup> $\alpha$	<sup>5</sup> $S_{50}$	<sup>5</sup> $S_{90}$
<b>Ska-Edeby sand drains</b>										
AL/V03	0.18	2.2 T	12.8	S	0.22	3	0.0130	0.751	0.035	0.019
AL/V08	0.18	0.9 T	5.25	5	0.16	3	0.0150	0.742	0.041	0.021
AL/V13	0.18	1.5 T	8.75	5	0.16	3	0.0101	0.746	0.027	0.015
AII	0.18	1.5 T	8.75	5	0.16	3	0.0133	0.746	0.036	0.020
AIV	nil	nil	nil	5	0.96	3	0.0192	0.824	0.047	0.026

- <sup>1</sup>Drain spacing, T = triangular (D = 1.05s), S = square (D = 1.135)
- <sup>2</sup>H = clay drainage depth = 1/2 thickness for drain condition top and bottom
- <sup>3</sup> $S_i$  = measured slope of initial linear segment of hyperbolic plot of field data
- <sup>4</sup> $\alpha$  = theoretical slope of initial linear segment determined from Fig. 3
- <sup>5</sup> $S_{50}$  = slope of line from origin to  $U_{50}$  in field hyperbolic plot =  $(1/0.5) (S_i/\alpha)$
- <sup>6</sup> $S_{90}$  = slope of line from origin to  $U_{50}$  in field hyperbolic plot =  $(1/0.5) (S_i/\alpha)$

**Table 2 Comparison of Hyperbolic Settlement Estimates with Observed Primary Ultimate Settlements**

Site and Location	<sup>1</sup> Observed Primary ult sett (cm)	Hansbo Estimates from $C_c$ (cm)	<sup>2</sup> Measured Slopes		Hyperbolic Estimates of Ult Sett			
			$S_i$	$S_r$	$\alpha/S_i$ (cm)	$1/S_r$ (cm)	$2\delta_{50}$ (cm)	$1.11\delta_{90}$ (cm)
<b>Ska-Edeby sand drains</b>								
AL/V03	59	50(-15)	0.0130	0.0146	58(-2)	69(+17)	56(-5)	59(0)
AL/V08	50	63(+26)	0.0150	0.0182	50(0)	55(+10)	54(+8)	53(+6)
AL/V13	74	70(-5)	0.0101	0.0125	74(0)	80(+8)	80(+8)	79(+7)
AII	61	55(-10)	0.0133	0.0157	56(-8)	64(+5)	58(-5)	59(-3)
AIV	nil	43	0.0192	nil	43(0)	nil	44(+2)	42(-2)

- <sup>1</sup> Observed ultimate primary settlement is based on complete dissipation of mid-plane excess pore pressures as measured by piezometers
  - <sup>2</sup> Measured slopes,  $S_i$  = slope of initial linear portion of field hyperbolic plot (between  $U_{50}$  and  $U_{90}$ ), and  $S_r$  = slope of final linear portion (beyond  $U_{90}$ )
- Bracketed values are difference in percentage from observations

The power of the hyperbolic procedure for estimating ultimate primary compression is that the 50% and 90% consolidation points can be located once sufficient data becomes available to define the initial linear portion of the field hyperbolic plot as illustrated by the data of Area IV in Fig. 9b, which is still in primary consolidation after 14 years. For the case without vertical drains,  $T_{50}$  and  $T_{90}$  is 0.196 and 0.848. From Fig. 9b, the hyperbolic procedure defines  $t_{50}$  and  $t_{90}$  and 4.89 and 20 years, which implies (from  $T_v = c_v t/H^2$ ) that  $c_v$  should be 1.00 and 1.06 m<sup>2</sup>/yr, respectively.

## HYPERBOLIC METHOD

**Table 3 Comparison of Estimates with Observed Ultimate Settlements**

Site and Location	<sup>1</sup> Observed Ult Sett after 14 yrs (cm)	Hyperbolic Estimates of Ult Sett			
		$\alpha/S_i$ (cm)	$1/S_f$ (cm)	$2 \delta_{50}$ (cm)	$1.11 \delta_{90}$ (cm)
<b>Ska Edeby sand drains</b>					
ALV03	61	58(-5)	69(+13)	56(-8)	59(-5)
ALV08	55	50(-9)	55(0)	54(-2)	53(-4)
ALV13	80	74(-8)	80(0)	80(0)	79(-1)
AII	65	56(-14)	64(-1)	58(-11)	59(-9)

Bracketed values are difference in percentage from observations

These agrees very well with Holtz (1972) estimate of  $c_v$  for Area IV as  $0.96 \text{ m}^2/\text{yr}$ , as obtained from  $\sqrt{t}$  fitting of the field settlements of that test area. For the areas treated with vertical drains, both  $t_{50}$  and  $t_{90}$  cannot be obtained from the conventional  $\log t$  and  $\sqrt{t}$  plots, as the influence of radial drainage removes the parabolic behavior of the initial settlement data which is the basis of these time fitting methods. Nevertheless, the hyperbolic method can locate these two points for the combined flow problem.

### SUMMARY AND CONCLUSIONS

The hyperbolic method of settlement analysis had been extended to the practical case of vertical drains and surcharge. The characteristics of field settlement data studied indicate that the first straight-line portion of the hyperbolic plot encompasses the 50% to the 90% points of the settlement records. The inverse of the slope of this linear portion multiplied by the theoretical slope value,  $\alpha$  (that is  $\alpha/S_i$ ) gave good estimates of primary ultimate settlement. On the other hand, the inverse of the slope for data beyond the 90% consolidation point gave excellent estimate of the total ultimate settlement, inclusive of secondary compression. These are implied from a careful examination of the long-term settlement data of the Ska-Edeby test fills.

However, when the hyperbolic method is used to locate the 50% and 90% points on the settlement records, primary ultimate settlements obtained from these points also agree well with the measurements at Ska-Edeby to within 10%, and they agree reasonably well with the direct compression calculations based on the soil compression properties as reported by Hansbo (1960). This method has the advantage of allowing the prediction of ultimate settlement once the initial straight-line portion (between 50% and 90% consolidation) of the field hyperbolic plot becomes discernible. Thus, the method will provide a useful and practical means of monitoring progress of consolidation in field applications using drains and surcharge, and help to determine the appropriate time for surcharge removal if required. Further,

## TAN

the method can provide a means to validate the designed ultimate settlements and allow for subsequent modifications to be made in design, particularly when deficiency in the soil compressibility calculations is found.

### LIST OF SYMBOLS

$\alpha$	= slope of the initial linear portion of $T_v\sqrt{U}$ vs $T_v$ plot
$\beta$	= intercept of the initial linear portion of $T_v\sqrt{U}$ vs $T_v$ plot
$\delta_{50}$	= settlement at the 50% consolidation point (L)
$\delta_{90}$	= settlement at the 90% consolidation point (L)
$c_h$	= radial consolidation coefficient ( $L^2/T$ )
$c_v$	= vertical consolidation coefficient ( $L^2/T$ )
$C_c$	= compression index = $\delta e / \delta (\log p)$
$d$	= drain diameter (L)
$D$	= drain influence diameter (L) = 1.05s for triangular spacing or 1.13s for square spacing
$H$	= clay drainage depth = 1/2 thickness of clay if drained top and bottom
$s$	= drain spacing (L)
$n$	= $D/d$ = drain spacing ratio
$S_i$	= slope of initial linear segment of $t/\delta$ vs $t$ plot between 50% and 90% consolidation points (1/L)
$S_f$	= slope of final linear segment of $t/\delta$ vs $t$ plot beyond 90% consolidation points (1/L)
$S_{50}$	= slope of line from origin to 50% consolidation point on $t/\delta$ vs $t$ plot
$S_{90}$	= slope of line from origin to 90% consolidation point on $t/\delta$ vs $t$ plot
$T_h$	= time factor for radial consolidation = $c_h t/D^2$
$T_v$	= time factor for vertical consolidation = $c_v t/H^2$
$U$	= degree of consolidation of combined vertical and radial drainage
$U_h$	= degree of consolidation for radial drainage only
$U_v$	= degree of consolidation for vertical drainage only

### REFERENCES

- BARRON, R.A. (1948). "Consolidation of fine-grained soils by drain wells." Trans. ASCE: Paper No. 2346, ASCE, New York, N.Y., 718-754.
- CARRILLO, N. (1942). "Simple two and three dimensional cases in the theory of consolidation of soils." J., of Mathematics and Physics, Vol. 21, pp. 1-5.
- CHIN, F.K. (1971). "Estimating the final total settlement - a theoretical analysis." Proc. 2nd Southeast Asian Conf. on Soil Engrg., Singapore, pp. 81-90.
- HANSBO, (1960). "Consolidation of clay, with special reference to the influence of vertical sand drains." Swedish Geotechnical Institute Proceedings 18, Stockholm, Sweden.

## HYPERBOLIC METHOD

- HANSBO, S. (1981). "Consolidation of fine-grained soils by prefabricated drains." Paper 12/22 : Proc. 10th Intl. Conf. Soil Mech. Found Engrg., Stockholm, Sweden, 3, pp. 677-682.
- HOLTZ, R.D. & BROMS, B. (1972). "Long-term loading tests at Ska-Edeby, Sweden." Proceedings ASCE Specialty Conference on Earth and earth Supported Structures, Purdue Lafayette Indiana, pp. 435-464.
- SRIDHARANA, A. & SREEPADA RAO, A. (1981). "Rectangular hyperbola fitting method for one-dimensional consolidation." Geotech. Testing J., 4(4), pp. 161-168.
- TAN, S.A. (1993). "Ultimate settlement by hyperbolic plot for clays with vertical drains." J. of Geotechnical Engineering, ASCE. Vol. 119, No. 5, pp. 950-955.
- TAN, T.S., INOUE, T. & LEE, S.L. (1991). "Hyperbolic method for consolidation analysis." J., Geotech. Engrg. ASCE, 117(11), pp. 1723-1737.
- YOSHIKUNI, H., INOUE, T., SUMIOKO, N. & HARA, H. (1981). "On the characteristics of settlement prediction methods by monitoring." (in Japanese), Tsuchi to Kiso, Tokyo, Japan Vol. 29, No. 8, pp. 7-13.

# UNIAXIAL COMPRESSIVE STRENGTHS OF MARBLE FROM THE KUALA LUMPUR LIMESTONE

J.K. Raj<sup>1</sup>

## SYNOPSIS

Marble cores from the Kuala Lumpur Limestone show uniaxial compressive strengths ranging from 79 to 140 Mpa; this range reflecting variations in textures and inherent structural features of tested specimens. Coarse grained specimens show uniaxial compressive strengths of 124 to 140 MPa, with a mean value of 131 MPa, whilst medium and fine grained specimens show strengths of 110 to 119 MPa, with mean values of 113 MPa, and 115 MPa, respectively. This difference in strengths is due to the greater number of inter-granular contacts in the medium and fine grained specimens which allows initiation of fracturing (and failure) at lower values of compressive stress. Specimens containing secondary structural features as healed, and non-continuous, fracture planes furthermore, all show low values of uniaxial compressive strength.

## INTRODUCTION

The uniaxial compressive strength is the most commonly determined property of rock material and is determined by loading a cylindrical or prismatic specimen to failure in a compression machine. The uniaxial compressive strength ( $C_o$ ) is then given by  $C_o = F_c/A$ , where  $F_c$  is the applied compressive load at failure and  $A$  is the cross-sectional area of the specimen. Although the concept of the test is deceptively simple, there are several factors that significantly affect the test results, including the flatness of the bearing surfaces, the specimen shape and size, the rate of loading, the moisture content of the specimen and the alignment of the swivel head (Obert and Duvall, 1967). The effects of these factors cannot be eliminated, though they can be minimized through adoption of standard testing procedures as described in ASTM (1977) or ISRM (1985).

Apart from the test procedures and conditions, inherent features of test specimens can also significantly influence determination of the uniaxial compressive strength. These inherent features mainly involve the homogeneity, isotropy and continuity of the rock material of the test specimens (Farmer, 1968). Homogeneity is a measure of the physical continuity of a material and in an homogeneous rock material, the constituents are so distributed that a minute fragment cut from any part of it will have constituents, and hence properties, representative of the whole. Isotropy is a measure of the directional properties of a material, with rock material usually being anisotropic as it often shows a preferred particle and/or crystal orientation. Continuity can be considered to refer to the amount of fracture and pore space in a material and

---

<sup>1</sup>Associate Professor, Department of Geology, University of Malaysia, Kuala Lumpur, Malaysia.



can vary considerably from specimen to specimen of a similar homogeneous and isotropic rock material.

In this paper are presented the results of uniaxial compressive strength determinations of borehole specimens of marble from the Kuala Lumpur Limestone. The specimens, although homogeneous in terms of chemical and mineralogical composition, show variations in texture as well as continuity, and the influence of these inherent features on the uniaxial compressive strength is discussed.

### KUALA LUMPUR LIMESTONE

In the Sungai Way area of Selangor State in Peninsular Malaysia (Fig. 1) are found marbles (recrystallized limestones) that have been mapped as a part of the Kuala Lumpur Limestone (Yin, 1976). This Formation consists almost entirely of carbonates with relatively little impurity, though regional metamorphism, and a superimposed contact metamorphism close to Mesozoic granite intrusions, has caused marmorization and largely obliterated the original sedimentary features (Gobbett, 1964). The Formation is of a Middle to Upper Silurian age, and over most of its mapped area, is a crystalline calcitic limestone, frequently containing a small percentage of magnesium, while dolomitic limestone and dolomite are locally dominant. Surface outcrops are limited to a few localities and the Formation is mostly only found in mine pits and subsurface quarries beneath a cover of alluvial sediments of variable thickness.

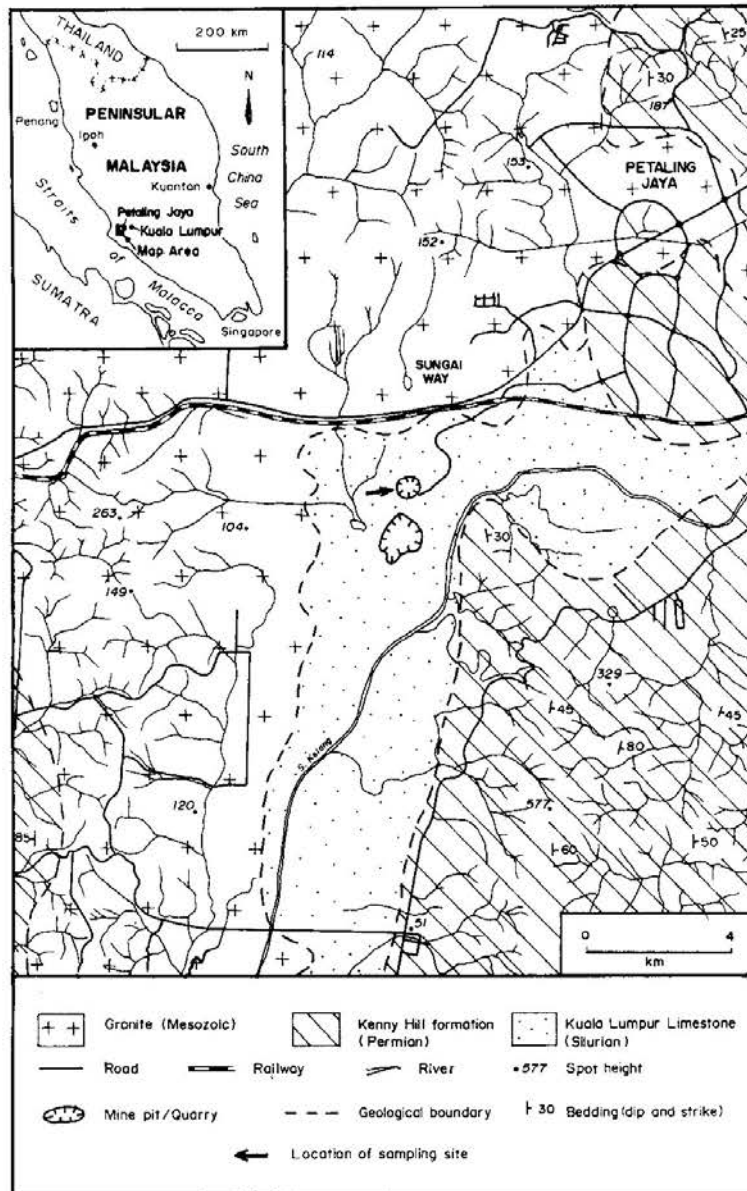
### SAMPLING SITE

In the Sungai Way area, the marble bedrock forms an irregular, pinnacle and trough topography beneath gravelly to sandy and clayey alluvial sediments of some 5 to 35 m in thickness. The pinnacles, which are of various shapes and sizes, are often pock-marked with cavities and are separated by troughs of sinuous and elongate shape. The tops of the pinnacles furthermore, show an approximately accordant surface which dips eastward at about 5°.

The bedrock is variously coloured from white to light and dark grey and is fine to coarse grained. These colours and textures are patchily distributed in the area, though a thin inter-banding of light and dark grey layers is often seen. Secondary calcite veins are also found within the bedrock which is cut by several joints and faults of variable strikes and dips. Along these structural discontinuity planes, which show very irregular to smooth faces, secondary iron oxide and hydroxide stains are sometimes found.

In thin-sections, the bedrock shows effects of both recrystallization and deformation, though these effects are variably distributed in the area. The thin-sections also show that the bedrock consists exclusively of recrystallized calcite, though secondary iron oxide grains are sometimes seen in slightly weathered samples.

## COMPRESSIVE STRENGTHS OF MARBLE



**Fig. 1 Bedrock Geology of The Sungai Way Area, Peninsular Malaysia (After Yin, 1976). Note - Alluvial deposits are not shown.**

### METHOD OF STUDY

In the course of a rock slope stabilisation program at an old mine pit/quarry in the Sungai way area, several orientated (dipping  $30^\circ$  towards North), and vertical, boreholes were drilled some 10 m apart over an area of about 2,000 m<sup>2</sup>. Continuous cores of some 0.5 to 1 m long from several of these boreholes were made available for laboratory tests. These cores of 47.35 mm (1.865 in) diameter were sawn into smaller specimens of 95 to 100 mm length, and their ends polished. All specimens for compression testing had a length to diameter ratio of between 2.0 and 2.1 to conform with the recommendations of the ASTM testing procedure (1977).

Prior to the compression testing, visible textural and structural features of each of the individual test specimens were described, whilst thin-sections were prepared from representative specimens. It is to be noted that no visible signs of any alteration due to weathering were detected in all the specimens which are considered to represent fresh and unweathered samples of the marble rock material. Bulk unit weights, as well as ultrasonic pulse velocities, of each of the individual specimens were also determined prior to the compression tests. The specimens were then air dried for three days before being tested in an ELE 1100 kN compression machine, with a loading rate of some 10 to 15 MPa per minute.

**Table 1 Uniaxial Compressive Strengths of Orientated Borehole Specimens**

Sample Number	Bulk Unit Weight (kN/cu.m.)	Uniaxial Compressive Strength (lb/sq.in.)	Uniaxial Compressive Strength (MPa)	Mode of Failure (after Hawkes and Mellor, 1970)
1a	26.580	17,197	119.11	Cleavage
1b	26.591	16,831	115.70	Cataclasis/cleavage
1c	26.590	17,014	117.97	Cataclasis/cleavage
1d	26.595	16,466	113.44	Cataclasis/cleavage
2a	26.611	15,734	108.90	Cleavage
2b	26.591	11,709	79.41	Shear
2c	26.621	20,308	138.96	Cataclasis/cleavage
2d	26.600	18,661	127.05	Cataclasis/cleavage
2e	26.611	20,490	140.09	Cataclasis/cleavage
2f	26.619	19,393	132.72	Cataclasis/cleavage
2g	26.620	15,917	110.60	Cleavage
3a	26.609	16,831	115.70	Cataclasis/cleavage
3b	26.595	16,283	111.17	Cataclasis/cleavage
3c	26.596	17,197	119.11	Cleavage
4b	26.624	19,027	132.15	Cataclasis/cleavage
4c	26.622	17,929	123.65	Cataclasis/cleavage
5b	26.619	15,734	108.90	Cataclasis/cleavage
5c	26.619	15,551	107.76	Cataclasis/cleavage
5d	26.615	16,100	111.17	Shear
11c	26.619	13,904	96.42	Cataclasis/cleavage
11d	26.617	15,551	107.76	Cataclasis/cleavage
11e	26.619	16,649	115.70	Shear

# COMPRESSIVE STRENGTHS OF MARBLE

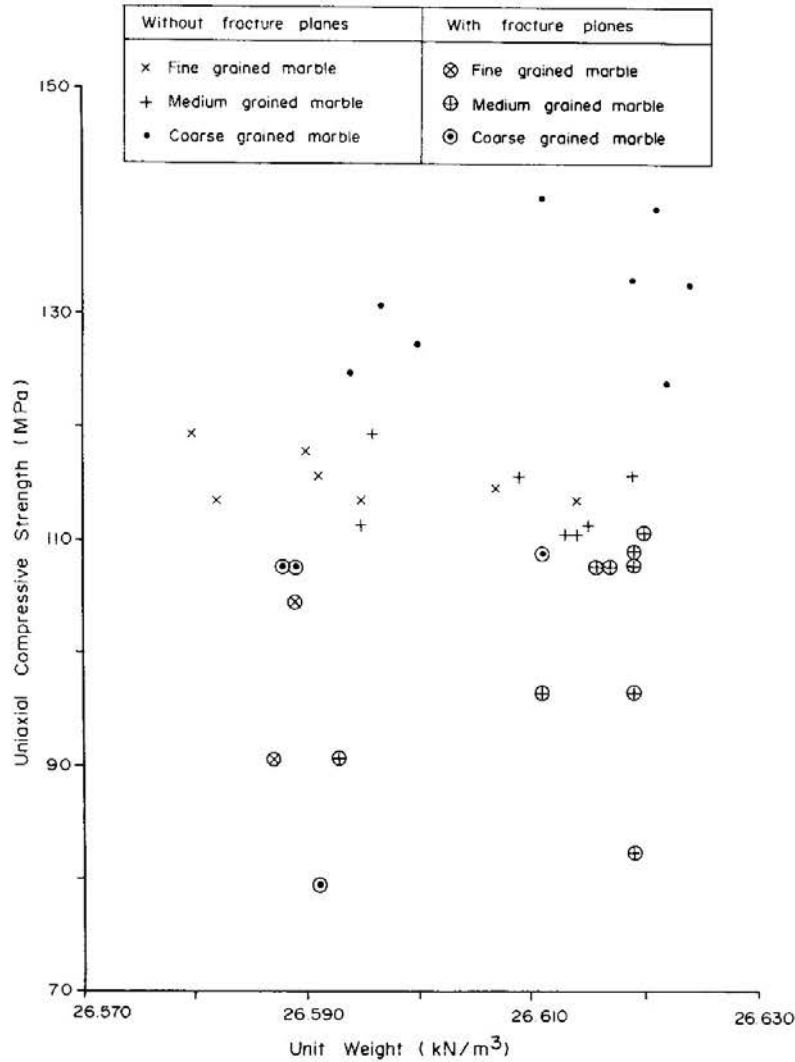
## RESULTS AND DISCUSSION

Results of the uniaxial compression tests of specimens from the orientated and vertical boreholes (Tables 1, and 2, respectively) show a wide range of values with no apparent pattern. When the results are grouped according to inherent textural and structural features of the individual specimens, however, a distinct pattern emerges, with the coarse grained specimens showing higher values of strength than the medium and fine grained specimens (Fig. 2 and Table 3).

The coarse grained specimens show a mean uniaxial compressive strength of 131.2 MPa, with a standard deviation of 6.1 MPa, whilst the medium grained, and fine grained, specimens, show mean uniaxial compressive strengths of 113.4 MPa, and 115.4 MPa, with standard deviations of 3.4 MPa, and 2.3 MPa, respectively. These values are comparable with published data on the uniaxial compressive strengths of other marbles, though little published data is available on the influence of texture on the uniaxial compressive strength of marble. Other marbles with comparable strengths include those from Star Lake (Windes, 1949) and Carthage (Hoskins and Horino, 1969) in the United States with mean uniaxial compressive strengths of 126.86 MPa, and 106.0 MPa, respectively, and those from Tennessee for which a

**Table 2 Uniaxial Compressive Strengths of Vertical Borehole Specimens**

Sample Number	Bulk Unit Weight (kN/cu.m.)	Uniaxial Compressive Strength (lb/sq.in.)	Uniaxial Compressive Strength (MPa)	Mode of Failure (after Hawkes and Mellor, 1970)
21c	26.587	12,989	90.75	Cataclasis
21d	26.582	16,466	113.44	Shear
21e	26.607	16,831	114.57	Cataclasis/cleavage
21f	26.614	16,466	113.44	Shear
21r	26.589	15,368	104.36	Shear
24h	26.616	15,368	107.76	Cataclasis/cleavage
24i	26.619	11,892	82.24	Cleavage
24m	26.611	13,904	96.42	Cleavage
25d	26.597	18,844	130.45	Cataclasis/cleavage
25e	26.588	15,551	107.76	Cleavage
25f	26.589	15,551	107.76	Cleavage
25g	26.594	18,112	124.78	Cataclasis/cleavage
26b	26.614	15,917	110.60	Cataclasis/cleavage
26c	26.613	15,734	110.60	Cataclasis/cleavage
26e	26.593	10,977	90.75	Cataclasis



**Fig. 2 Plot of Uniaxial Compressive Strengths versus Bulk Unit Weights.**

mean uniaxial compressive strength of 105.8 MPa has been quoted (Haimson and Fairhurst, 1970). Medium to coarse grained marbles from Tennessee are also reported to have a mean uniaxial compressive strength of 120.0 MPa (D'Andrea and Condon, 1970), while fine grained marbles have a value of 124.11 MPa (Haimson and Fairhurst, 1969).

The difference in uniaxial compressive strengths between the coarse grained, and medium to fine grained, specimens is in a sense to be expected in view of the textural differences. The medium to fine grained specimens contain a greater number of inter-granular contacts in comparison with the coarse grained specimens, for they (the medium to fine grained specimens) have experienced more granulation as a result of deformation. The greater number of these inter-granular contacts thus leads to lower values of compressive strength, as the contacts serve as the cracks that initiate fracturing (and failure) during compression testing (Hawkes and Mellor, 1970).

## COMPRESSIVE STRENGTHS OF MARBLE

**Table 3 Uniaxial Compressive Strengths, Lithological and Structural Features of Marble Core Specimens**

Specimen Number	Uniaxial Compressive Strength lb/sq.in.	Uniaxial Compressive Strength MPa	Lithological and Structural Features			
			Hand Specimen	Thin-Section		
1a	17,197	119.11				
1b	16,831	115.70	Crystalline, fine grained marble with sub-vertical, thin (< 3 mm wide), light and dark grey bands.	Heterogranular - Granoblastic texture. Mainly fine grained calcite crystals (0.02-0.06 mm size) with some coarser (0.2-0.6 mm size) grained ones. Coarse grained crystals <30% of all crystals.		
1c	17,014	117.97				
1d	16,466	113.44				
21d	16,466	113.44				
21e	16,831	114.57				
21f	16,466	113.44				
MEAN	16,753	115.38				
STD.DEV.	296	2.33				
21c	12,989	90.75	One vertical, healed fracture plane			
21f	15,368	104.36	One moderately dipping, healed fracture plane			
3a	16,831	115.70				
3b	16,283	111.17	Crystalline, medium grained marble with sub-vertical, thin (<5 mm wide), light and dark grey bands.	Heterogranular-granoblastic texture. Fine grained (0.02 - 0.1 mm size) and coarse grained (0.2-0.8 mm size) calcite crystals. Coarse grained crystals about 50% of all crystals.		
3c	17,197	119.11				
5d	16,100	111.17				
11e	16,649	115.70				
26b	15,917	110.60				
26c	15,734	110.60				
MEAN	16,387	113.44				
STD.DEV.	526	3.39				
5b	15,734	108.90	One moderately dipping, healed fracture plane			
5c	15,551	107.76	One moderately dipping, healed fracture plane			
11c	13,904	96.42	One sub-vertical, non-continuous fracture plane			
11d	15,551	107.76	One moderately dipping, healed fracture plane			
24th	15,368	107.76	One moderately dipping, healed fracture plane			
24l	11,892	82.24	One vertical, healed fracture plane			
24m	13,904	96.42	One vertical, healed fracture plane			
26e	10,977	90.75	One sub-vertical, non-continuous fracture plane			
2c	20,308	138.96				
2d	18,661	127.05	Crystalline, coarse grained marble with sub-vertical, thin (< 5 mm wide), light and dark grey bands.	Heterogranular-granoblastic texture. Mainly coarse grained calcite crystals (0.2-1.5 mm size) with some finer grained ones (0.02-0.1 mm size). Coarse grained crystals > 70% of all crystals.		
2e	20,490	140.09				
2f	19,393	132.72				
4b	19,027	132.15				
4c	17,929	123.65				
25d	18,844	130.45				
25g	18,112	124.78				
MEAN	19,096	131.23				
STD.DEV.	933	6.08				
2a	15,734	108.90			One moderately dipping, healed fracture plane	
2b	11,709	79.41	One moderately dipping, open fracture			
2g	15,917	110.60	One moderately dipping, healed fracture plane			
25e	15,551	107.76	One moderately dipping, non-continuous fracture plane			
25f	15,551	107.76	One moderately dipping, non-continuous fracture plane			

One of the surprising features of the results is the absence of a significant difference in the uniaxial compressive strengths of the medium, and fine, grained marble specimens. The absence of this difference suggests that the total number of intergranular contacts in both these varieties is about the same, leading to fracture (and failure) initiation at closely similar levels of compressive stress.

Apart from the influence of textures, the results also show that where structural discontinuity planes are present in the tested specimens, there is a reduction in the uniaxial compressive strength. In most cases furthermore, the orientation of the discontinuity planes influences the compressive strength, for specimens with vertical and sub-vertical discontinuity planes show lower strengths than those with moderately dipping planes. There does not, however, appear to be any influence of texture on the uniaxial compressive strength of specimens with inherent structural discontinuity planes, for all such specimens, regardless of texture, show lower values of strength in comparison with specimens devoid of discontinuity planes.

## CONCLUSIONS

Arising from the above discussion, it is concluded that coarse grained marble of the Kuala Lumpur Limestone shows a mean uniaxial compressive strength of 131 MPa, whilst medium and fine grained marble shows mean strengths of 113 MPa, and 115 MPa, respectively. This difference in strengths results from differences in the number of inter-granular contacts, with the greater number of such contacts in the medium and fine grained marbles leading to lower values of the uniaxial compressive strength. Inherent structural features within individual test specimens furthermore, lead to low values of uniaxial compressive strength.

## ACKNOWLEDGEMENTS

This study forms part of an on-going research project supported by IRPA Grant 04-07-04-172 from the Malaysian Government. Equipment used for the tests was purchased with a grant provided by Projek Lebuh raya Utara-Selatan Sdn. Bhd. (PLUS). Mr. Roshdy drafted the figures.

## REFERENCES

- ASTM (1977). Standard test method for unconfined compressive strength of intact rock core specimens. *American Soc. For Testing And materials*, ASTM Designation D 2938-71a. ASTM Standards, Part 19, p. 389-390.
- D'ANDREA D.V. and CONDON, J.L. (1970). Dye penetrant studies of fractures produced in laboratory cratering. *Proc. 12th Symp. Rock Mech., Rolla, Missouri, 1970*, p. 547-559.

## COMPRESSIVE STRENGTHS OF MARBLE

- FARMER, I.W. (1968). *Engineering Properties of Rocks*. E & F. N. Spon Ltd., London. 180 p.
- GOBBETT, D.J. (1964). The Lower Palaeozoic rocks of Kuala Lumpur. Malaysia. *Fed. Museums Jour.*, No. 9, p. 67-79.
- HAIMSON, B.C. and FAIRHURST, C. (1969). Insitu stress determination at great depth by means of hydraulic fracturing. Proc. 11th Symp. Rock Mech., Berkley, California, 1969, P. 559-584.
- HAIMSON, B.C. and FAIRHURST, C. (1970). Some bit penetration characteristics in pink Tennessee marble. Proc. 12th Symp, Rock Mech., Rolla, Missouri, 1970, p. 547-559.
- HAWKES, I. and MELLOR, M. (1970). Uniaxial testing in rock mechanics laboratories. *Engng. Geol.*, No. 4, p. 177-285.
- HOSKINS, J.R. and HORINO, F.G. (1969). Influence of Spherical Head Size and Specimen Diameters On The Uniaxial Compressive Strength of Rocks. Res. Inst., U.S. Bureau of Mines, No. 7234, 16 p.
- ISRM (1981). Suggested methods for determining the uniaxial compressive strength and deformability of rock materials. In Brown, E.T. (Ed), *Rock Characterization, Tsting And Monitering*. Int. Soc. Rock Mechanics. Pergamon Press. p. 111-116.
- OBERT, L. and DUVALL, W.I. (1967). *Rock Mechanics And The Design Of Structures In Rock*. John Wiley & Sons Inc., New York, 650 p.
- WINDES, S.L. (1949). *Physical Properties of Mine Rock*. Res. Inst., U.S. Bureau of Mines, No. 4459, 79 p.
- YIN, E.H. (1976). *Geological Map Of Kuala Lumpur*. Map Sheet No. 94, New Series, Pen. Malaysia, Scale 1:63, 360. Director-General, Geological Survey Of malaysia.



## ANNOUNCEMENTS

### **a) Dr. Alister D. Burnett - 1993 Engineering Geology Group Award**

Dr Alister D. Burnett has been awarded the 1993 Engineering Geology Group Award by the Engineering Group of the Geological Society (of London). This annual award is essentially for professionals who have given notable and meritorious service to the profession of Engineering Geology. As a member of our society, Dr Burnett, who has carried out considerable work over the last 25 years in Africa, UK, Hong Kong, the Middle East and now in America, is to be congratulated and encouraged to continue his work from his current position as Professor of Engineering Geology and Chairman of the Department of Geology at Florida Atlantic University, Boca Raton, USA.

### **b) Dr. Dennes T. Bergado - 1993 Shamsheer Prakash Research Award**

The Shamsheer Prakash Foundation has announced the 1993 SHAMSHER PRAKASH RESEARCH AWARD which will be shared by Dennes T. Bergado, Associate Professor, Asian Institute of Thailand, Bangkok and Shobha K. Bhatia, Associate Professor, Syracuse University, Syracuse, New York, USA.

Dr. Bergado is expert in probabilistic modeling of soil properties, geotechnical analysis, ground subsidence and improvement, and insitu testing. He has published 35 papers in journals and approximately 90 papers in conferences.

Dr. Bhatia is expert in earthquake engineering, geosynthetics and image processing. She has published 36 papers in refereed publications. She has received the Certificate of Achievement from the American Society of Civil Engineers, 1992, and the Faculty Achievement Award from the National Science Foundation, 1991-1997. Dr Bhatia was Chairperson of the Soil Dynamics Committee of the ASCE for six years.

The previous "SHAMSHER PRAKASH RESEARCH AWARD" winners were Professor George Gazetas, University of New York, Buffalo, New York, and Professor R. Kerry Rowe, University of Western Ontario, London, Ontario, Canada.